

**Controlling porosity and pore size
distribution in green ceramics bodies via
Freeze-casting method**



DISSERTATION

**zur Erlangung des akademischen Grades
Doktor-Ingenieur (Dr.-Ing.)**

genehmigt durch die

**Mathematisch-Naturwissenschaftlich-Technische
Fakultät (Ingenieurwissenschaftlicher Bereich)
der Martin-Luther-Universität Halle-Wittenberg**

**von Herrn Dipl.-Ing. Danail Donchev
geb. am 24.05.1974 in Kazanlak / Bulgarien**

Dekan der Fakultät: Prof. Dr. habil. Altenbach

Gutachter:

- 1. Prof. Dr. habil. Ulrich**
- 2. Prof. Dr. König**

18.08.05 Halle (Saale)

urn:nbn:de:gbv:3-000010045

[<http://nbn-resolving.de/urn/resolver.pl?urn=nbn%3Ade%3A3Agbv%3A3-000010045>]

Acknowledgments

My grateful appreciation to my supervisor, Prof. Dr-Ing. habil. Joachim Ulrich for his help, guidance and a continued encouragement, which not only account for a major part of my knowledge but also strongly fuel my interest in direction crystallization and ceramic materials as this thesis shows.

I would like to thank Prof. König for serving and helpful referring on my thesis.

I would also like to thank Prof. Rogendorf for serving as the Chairman of the Ph.D. defense committee.

I am grateful to Martin-Luther-University Halle-Wittenberg, especially Engineering Department, for admitting me as a graduate student in 2001. To me, M.L.U. is a very special place, and I thank all those who contribute to and are in stewardship of this unique and friendly environment.

I acknowledge the DFG Fellowship for providing financial support during my Ph.D. study.

I would like to thank Dr. L. Andresen, Dr. D. Koch and Prof. G. Grathwohl for their hospitality during my visits to the Bremen University, where I learned the techniques of Freeze-casting.

I would like to thank Dr. Diter Möring for his support, fruitful discussions and camaraderie.

I would like to thank Dr. Jung-Woo Kim, Dr. Tero Tahti and Dr. Jun-Jun Lu, you are all wonderful friends. I will always remember the many happy occasions and what I learned from you.

I would like to thank all previous and present members of TVT group for their help during my studying.

I must thank my dear wife Venelina who has supported me during the years. Special thank to my two kids Simona and Pavlin for their obedience during my study.

I thank my mother, father, sister and grandmother for their fortitude and encouragements that helped build my character and stimulated my interest in science since childhood.

Table of contents

1 Introduction	1
2 Technical background and theory	3
2.1 Nucleation	3
2.1.1 Homogeneous Nucleation	4
2.1.2 Heterogeneous Nucleation	6
2.1.3 Active Site Nucleation	8
2.2 Crystal growth	11
2.2.1 Theory of crystal growth	11
2.2.2 Crystal growth kinetics	13
2.3 Porosity and pore size distribution	14
2.3.1 Open, close, and total porosity	14
2.3.2 Pores characteristics	15
2.3.3 Methods and techniques for production of porous ceramics	16
2.3.4 Methods for characterizing porous ceramic materials	18
2.4 Freeze-casting. Bases and principles	20
2.4.1 Colloidal systems. Introduction	20
2.4.2 Freeze-casting	21
3. Materials and Experimental Setup	25
3.1 Materials	25
3.2 Experimental procedure and setup	26
4 Instrumentation	29
5 Results	30
5.1 Rheology	30
5.1.1 Density	30
5.1.2 Viscosity	32
5.2 Nucleation and Crystal growth	37
5.2.1 Nucleation	37
5.2.1.1 Roughness of the cooling plates	37
5.2.1.2 Contact angle	39
5.2.1.3 Surface tension of suspensions	42
5.2.1.4 Interfacial tension, suspensions-cooling plate	43

5.2.1.5 Nucleation kinetic	48
5.2.1.6 Determination of freezing and melting temperatures	56
5.2.1.6.1 Cooling curves	56
5.2.1.6.2 Melting points	57
5.2.2 Crystal growth rate	59
5.2.2.1 Influence on crystal growth rate in dependence of the volume fraction of solids	61
5.2.2.2 Influence on crystal growth rate in dependence on cooling plate materials and properties	63
5.2.2.3 Influence on crystal growth rate in dependence of moulding form materials and properties	64
5.3 Porosity and pore size distribution	66
5.3.1 Porosity	67
5.3.1.1 Porosity dependence of solids load content	67
5.3.1.2 Porosity dependence of freezing temperature	68
5.3.1.3 Porosity in dependence of cooling plate materials	70
5.3.1.4 Porosity in dependence of moulding form materials	71
5.3.2 Pore size distribution	72
5.3.2.1 Pore size distribution in dependence of solid load content	74
5.3.2.2 Pore size distribution in dependence of freezing temperature	76
5.3.2.3 Pore size distribution in dependence of cooling plate materials	78
5.3.2.4 Pore size distribution in dependence of moulding form materials	79
6. Discussions	81
6.1 Discussions of rheological properties on the starting slurries and the dependence on porosity as well as the pore size distribution	81
6.2 Discussions on contact angle, interfacial tension and nucleation kinetics	86
6.3 Porosity and pore size distribution	95

7. Conclusions	100
8. Zusammenfassung	102
9. List of Symbols	103
10. Appendix	107
11. References	

1 Introduction

Porous ceramics have attracted very high interests of the scientific and industrial parties during the past two decades. This is especially true for forming techniques that offer great flexibility and trustworthiness. The efforts have been invested because of the necessity of porous ceramic materials as filters, dust collectors, absorbers, dielectric resonators, thermal insulation, bioreactors, bone replacement, hot gas collectors, automobile engine components. There could be named many other applications.

Several methods have been tried to produce ceramic materials with an open pore structure such as injection moulding, acid leaching etc. One of the most common ways is to add to ceramic powder an organic material that is burning out during sintering. However, the problem with these methods is, that they are harmful to the environment, and the pore structure cannot be controlled.

This thesis concentrates on the properties of highly porous ceramics and one of the most promising methods to create them. Microstructural features are the most determining factor of that technology. It is the freeze-casting method that has been employed. The products, the ceramic green bodies, produced by this method are of high porosity and uniformity concerning size and morphologies as well as pore structure. Specific characteristics that distinguish the freeze-casting route from conventional fabrication processes are to offer great possibilities to control porosity and pore size distribution and its simplicity. Furthermore, this method is applicable to many types of ceramics. However, on this technology is rarely reported concerning the preparation of macroporous ceramics.

Freeze casting is based on phase separation during freezing. It requires preparation of aqueous ceramic slurry which is poured into a mould, and then been frozen. After a complete freezing the samples are subject to ice sublimation and water removing. The pore structure, morphology and size, which are gained and remain, are the negative image of the ice crystals. A good knowledge and control of the crystallization process is, therefore, needed.

The aim of the presented work is to achieve simple, systematic and effective ways to control porosity and the pore size distribution. Therefore, this work aims for an in depth understanding of the factors and parameters effecting ice crystallization.

The experimental work is divided in to two major parts. The first part deals with the factors affecting and controlling nucleation, are furthermore, ice crystal growth. Solid load content and its consequence on the crystallization process are studied. Factors such as cooling plate and moulding form materials and their physical properties have been exanimate, too. To attain a deeper insight in real structures, the main objective of this thesis is to evaluate experimentally the characteristics of the obtained pores such as porosity, pore morphology and pore size distribution in dependence of the crystallization process. These results are given in the second part. Since suspension characteristics, especially, solid load contents are known to be very important in practical situations and have been found to be one of the major parameter to manage porosity and pore size distribution, they have also been studied and discussed intensively.

In this thesis are presented results of successful attempts to develop porous ceramic products with well controlled of porosity and pore size distribution.

2 Theoretical backgrounds

2.1 Nucleation

When a liquid is cooled, there exists a temperature at which it turns to solid. The first formed solid embryos or nuclei, which can only be a few nanometres in size, appear when the system is supersaturated [Jon02]. Supersaturated solutions exhibit a metastable zone in which all crystallization processes take place. Even when a solution is supersaturated nucleation do not start always spontaneously. Whenever the upper limit of the metastable zone of the supersaturation is reached nucleation will occur spontaneously. This happens when the system reaches the metastable limit $\partial^2 G / \partial x^2 = 0$ [Mye02].

Frequently nucleation can be promoted by agitation, shearing action, crystal breakage or abrasion, and pressure changes [Mul01].

There are different kinds of nucleation processes:

If a solution contains no foreign particles or crystals of it's own type, nucleus can only be formed by homogeneous nucleation. If foreign surfaces (particles) are present in the system, it is possible for a liquid to form on those surfaces nuclei at less supersaturation compared to the case of homogeneous nucleation. This process is called heterogeneous nucleation [Mer01]. It has been observed that nuclei occur even at very low supersaturations. This is the case when crystals of the same material exist and act as attrition agents or seed crystals [Mul01]. Such nuclei are known as secondary nuclei.

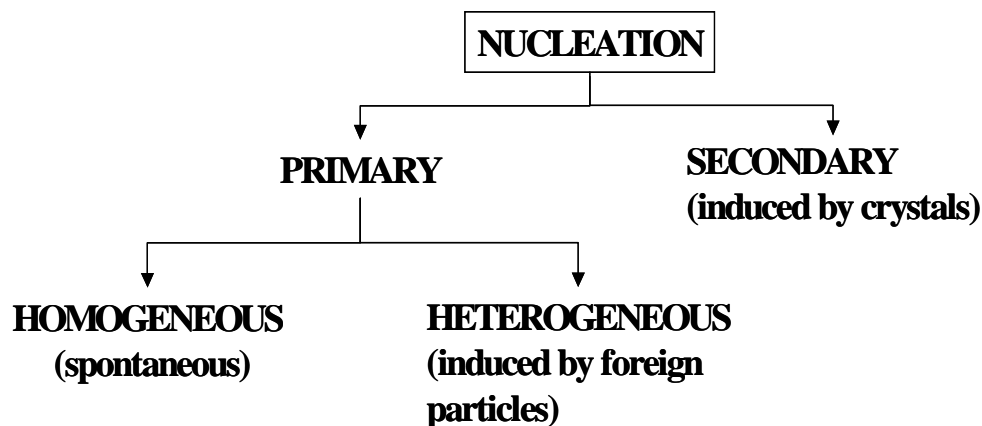


Fig. 2-1: Mechanisms of nucleation, according to [Mul01]

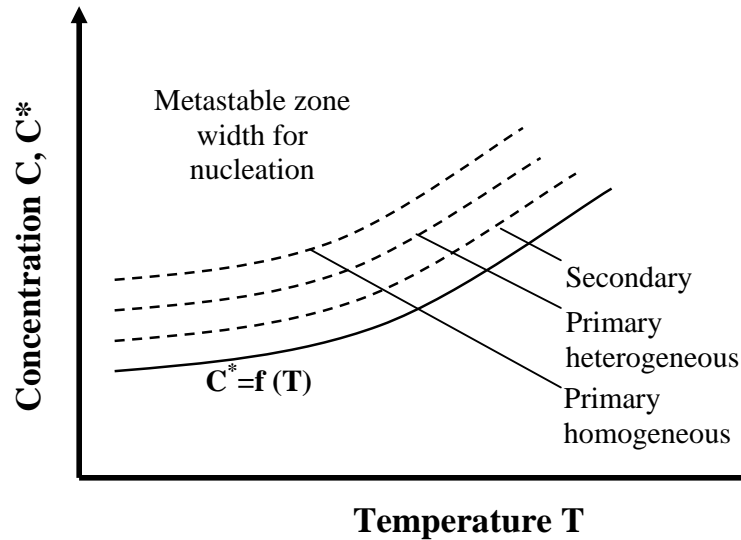
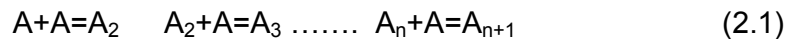


Figure 2-2: Concentration against temperature for several types of nucleation processes [Mer01]

2.1.1 Homogeneous Nucleation

Exactly how stable nuclei and crystals are formed within a homogeneous fluid is not known with any degree of certainty. The theories for homogeneous nucleation processes are communicated by Becker and Döring [Bec35], Volmer [Vol39] and Gibbs [Gib48]. The classical theories of nucleation suppose that the clusters are formed by an additional mechanism until the critical size is reached.



The classical theory of nucleation is based on a condensation of a vapour to liquid, and can be extended to crystallization from melts and solutions.

The change of the free energies associated with the process of homogeneous nucleation may be considered as follows:

$$\Delta G = \Delta G_s + \Delta G_v = 4\pi r^2 \sigma + \frac{4}{3} \pi r^3 \Delta G_v \quad (2.2)$$

where ΔG_s is the excess free energy between the surface of the particle and the bulk. ΔG_v is excess free energy between a very large particle and the solute in

solution. For homogeneous nucleation the volume free energy for supercooling can be expressed by:

$$\Delta G_v = \frac{\Delta H_f \Delta T}{T^*} \quad (2.3)$$

The two terms on the right-hand side of equation (2.2) have an opposite effect on the system and they depend differently on the radius of the nucleus r . Therefore the free energy of formation ΔG passes through a maximum value ΔG_{crys} , which corresponds to the nucleus critical size. From Fig. 2-3 it can be seen that ΔG_s is a positive quantity, proportional to r^2 . ΔG_v is a negative quantity proportional to r^3 .

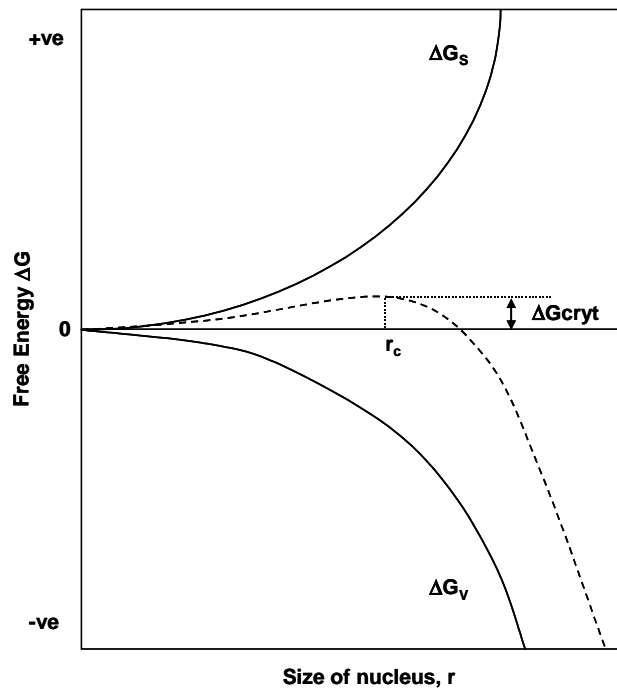


Fig. 2-3: Free energy diagram for nucleation explaining the existence of a critical nucleus (according to [Mul01])

With respect to r the critical size for a spherical nucleus can be obtained from equation 2.2 as follows:

$$\frac{d\Delta G}{dr} = 8\pi r \sigma + 4\pi r^2 \Delta G_v = 0 \quad (2.4)$$

or

$$r_c = \frac{-2\sigma}{\Delta G_v} \quad (2.5)$$

The r_c represents the minimal size of a nucleus which needs to be gained before the new phase is formed. If the cluster size is smaller than the critical size they can easily be dissolved back in the liquid or evaporate. From Fig. 2-3 it can be seen that nuclei with sizes larger r_c will reduce the energy necessary to get a stable nucleus which can continuously grow into crystals [MUL01].

Combining the equations 2.2 and 2.5 it leads to:

$$\Delta G_{cryt} = \frac{16\pi\sigma^3}{3(\Delta G_v)^2} = \frac{4\pi\sigma r_c^2}{3} \quad (2.6)$$

The nucleation rate can be expressed as follows:

$$J = A \exp\left[\frac{-16\pi\sigma^3 v^2}{3k^3 T^3 (\ln S)^2}\right] \quad (2.7)$$

The nucleation process is strongly depending on the interfacial tension. This is one of the most difficult parameters concerning the measurements, when trying to calculate nuclei critical size.

There are a lot of theories [Kash00], [Mer01], [Mul01], trying to explain physically and mathematically the mechanism for homogeneous and heterogeneous nucleation but even with lot of research performance there is no general theory, which can explain and calculate experimental data in good agreement.

2.1.2 Heterogeneous Nucleation

It has been known for many years that different heterogeneities, motes, inclusions, etc. can encourage phase transformations (by reducing formation energies), mainly condensation and crystallization.

Nucleation in heterogeneous systems normally occurs at lower supersaturations compared with homogeneous nucleation (see Fig. 2-2). Therefore a correction factor is needed which, must be less than a unit and can be explained as follows:

$$\Delta G_{het} = f\Delta G_{hom} \quad (2.8)$$

where

$$f = \frac{(2 + \cos \theta)(1 - \cos \theta)^2}{4} \quad (2.9)$$

where θ is the contact angle between liquid and solid surface. The contact angle θ is determined by Young's relation [Youn55].

$$\cos \theta = \frac{\sigma_{sl} - \sigma_{cs}}{\sigma_{cl}} \quad (2.10)$$

where σ_{sl} is the solid-liquid interfacial tension, σ_{cs} is crystal-solid interfacial tension and σ_{cl} crystal-liquid interfacial tension (see Fig. 2-4).

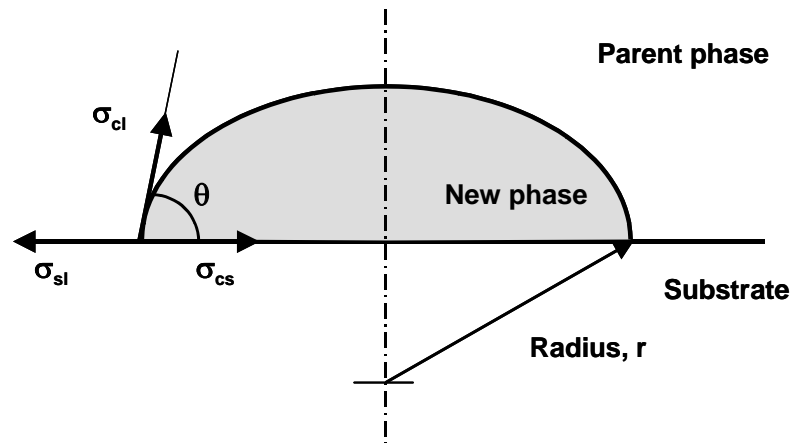


Fig. 2-4: Contact angle and interfacial tension

It is assumed that a free liquid drop automatically takes the shape that minimizes the free energy of the entire system. A surface with cluster contact angle of zero is known as wetting while a surface with cluster contact of more than 90° is known as non-wetting [Ada97]. When the contact angle is between 0° to 90° a system is known as partially wetting. A surface will also be known as hydrophilic if liquid wets the surface and as hydrophobic if a water cluster has a contact angle greater than 30° on the surface. In general, there appears to be only a limited number of places at which nuclei can form. Nuclei are always formed on a surface [Gar55] (see Fig. 2-5).

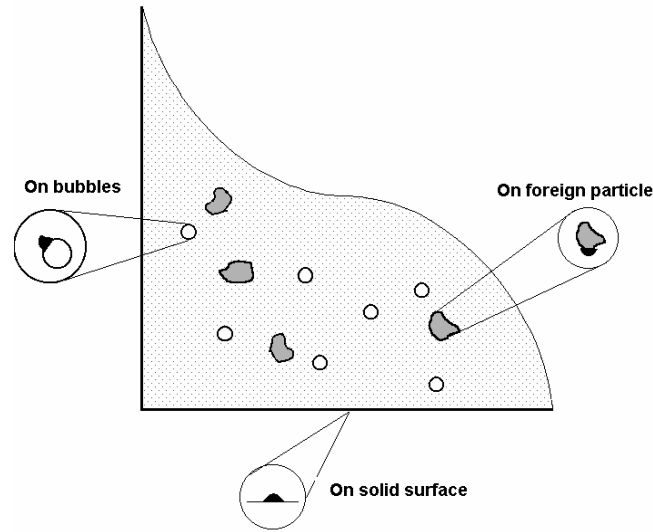


Fig. 2-5: Heterogeneous nucleation occurs on foreign surfaces or interfaces

2.1.3 Active Site Nucleation

If geometric or chemical inhomogeneities are added to the liquid, nucleation may occur on the surface of these inhomogeneities at lower supersaturations. In this case the inhomogeneities are known as active sites.

Formation of stable clusters on inhomogeneities or active sites has recently received growing experimental and theoretical interest. Several authors have published theoretical and experimental work [Gor01, Gor82, Fle58, Fle62, For03, Lee98, Meg02, Pad01, Smo87, Ylee98]. Although many theories have been developed as shown in Fig. 2-5 the cluster formation can occur on bubbles or on foreign particles. Therefore a cluster on a special convex surface as shown in Fig. 2-6 the volume is given by:

$$V = \frac{4}{3}\pi r^3 g(\cos\psi) - \frac{4}{3}\pi R^3 g(\cos\phi) \quad (2.11)$$

The critical free energy of the cluster is given by (see [Fle58])

$$G^* = \frac{16\pi\sigma^3}{3(\Delta G_v)^2} f(m, x) \quad (2.12)$$

where

$$2f(m,x) = 1 + \left(\frac{1-mx}{k}\right)^3 + x^3 \left[2 - 3\left(\frac{x-m}{k}\right) + \left(\frac{x-m}{k}\right)^3 \right] + 3mx^2 \left(\frac{x-m}{k} - 1\right) \quad (2.13)$$

with, $k = (1 + x^2 - 2mx)^{\frac{1}{2}}$, $m = \cos \theta$, $x = \frac{R}{r^*}$ where r^* is given by Eq. 2.5.

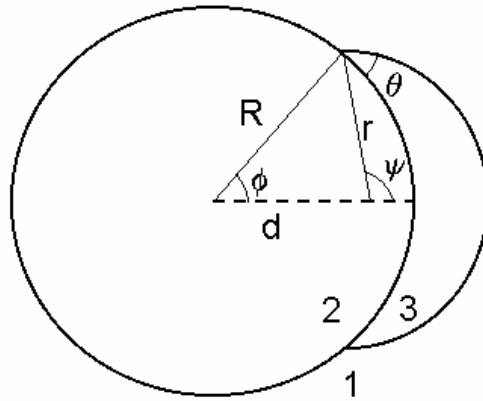


Fig. 2-6: Cluster formation on spherically convex surface (see [Fle58])

Fletcher [Fle62] observed the conditions, which are required for nucleation in a conical cavity at a spherical particle. He assumed that ice completely filled the cavity and that the surface curvature of the vapour-ice interface is the same as that of the curved surface (see Fig. 2-7).

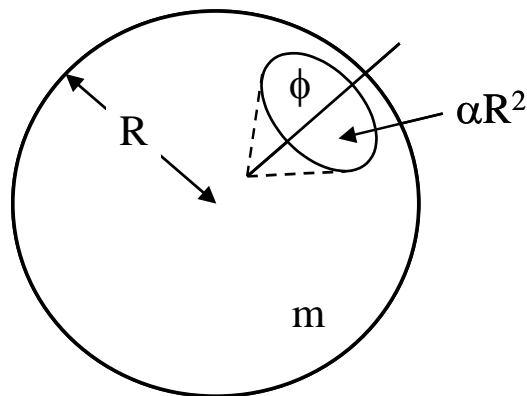


Fig. 2-7: A spherical particle of radius R and surface parameter m containing a conical cavity of semi-angle f and surface area αR^2 (see [Fle62])

Fletcher gave the nucleation rate per particle as

$$J \approx 4\pi R^2 J_o \exp(-G_{crys} / kT) \quad (2.14)$$

with

$$G_{crys} = \frac{16\pi\sigma^3}{3(\Delta G_v)^2} f(m, x) - \alpha R^2 (1-m)\sigma \quad (2.15)$$

where αR^2 is the surface area of cavity (see Fig. 2-7).

Contrasting with Fletcher, Gorbunov and Kakutina [Gor82] take different stages into account during the formation of stable clusters on active sites [see Fig. 2-8].

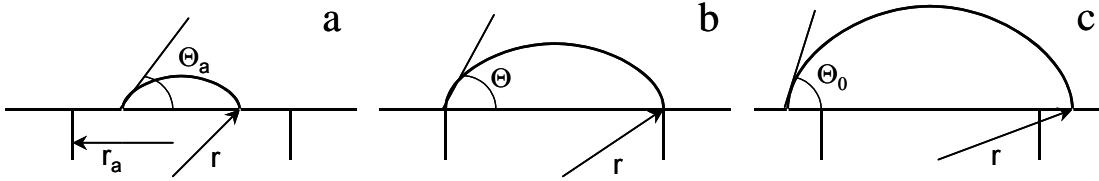


Fig. 2-8: Stages of cluster growth on an active site

For the first stage (Fig. 2-8a) the free energy of a cluster is given as:

$$G_1 = V\Delta G_v + S_{lv}\sigma + S_{lv}(-\sigma \cos \theta_a) \quad (2.16)$$

After the cluster reaches the active site boundaries (Fig. 2-8b), the contact angle changed from Θ_a to Θ . Therefore the energy in this stage is given as:

$$G_2 = V\Delta G_v + S_{lv}\sigma + S_a(-\sigma \cos \theta) \quad (2.17)$$

In the third stage (Fig. 2-8c) cluster grow beyond active sites and the contact angle is changed from Θ to Θ_0 .

$$G_3 = V\Delta G_v + S_{lv}\sigma + S_{lv}(-\sigma \cos \theta_0) + S_a(-\sigma \cos \theta_a + \sigma \cos \theta_0) \quad (2.18)$$

A lot of efforts have been carried out to investigate nucleation on active sites. Different models and theories have been developed but the nucleation process is very complex and has not been well understood up to now.

2.2 Crystal growth

2.2.1 Theory of crystal growth

After the nucleus reaches the critical size it begins to grow by adding and incorporating of units. This stage of the crystallization process is known as crystal growth [Mye01, Mul01]. Nucleation and crystal growth are the primary particle formation processes during crystallization and have large effects in determining product crystal size distributions [Jon02].

Crystal's growth and habit have for long been in the centre of the interest of scientists, but are still not well understood up to now.

Many theories dealing with crystal growth have been developed. But none has succeeded to be generalized for the growth mechanism. This is due to the fact that many varieties of mechanisms needs to be considered before growth units, from the solution, reach and incorporated in to the crystal surface.

According to Garside [Gar90] there are three main ways to express the growth rate of a crystals or population of crystals:

1. Face growth rate, v_{hkl} . This is the rate of advance of the crystallographic face, measured perpendicular to the face. It means the individual crystal face needs to be observed and measured. The illustration of these theories can be taken from Burton, Cabrera, Frank (BCF model) [Bur51], or "birth and spread" (BS) model, purposed by O'Hara and Reid [Oha73].
2. Overall mass growth rate, best expressed as the total mass flux to the crystal surface, R_G . This is the growth rate over the whole crystal.

$$R_G = \frac{1}{A_c} \cdot \frac{dM_c}{dt} \quad (2.19)$$

If the face growth rates, v_{hkl} , and areas A_{hkl} of all the faces on a crystal

are known, RG can be related to the different values of v_{hkl} by the expression:

$$R_G = \frac{\rho_c}{A_c} \sum v_{hkl} * A_{hkl} \quad (2.20)$$

The overall mass growth rate is mainly used for calculations in batch systems.

- Overall linear growth rate, which is defined as the time rate of change of a characteristic dimension, L, of the crystal.

$$G = \frac{dL}{dt} \quad (2.21)$$

The overall linear growth rate is widely used in population balance theory for calculating continuous and batch crystallizers.

Reviews on crystal growth theories can be found e.g. in the works of Ohara and Reid [Oha73], Strickland-Constable [Str68], Nyvlt et al. [Nyv85] and [Shö92]. Table 2.2.1 provides a summary of these growth models.

Table 2.2.1: Growth rate models (according to [Oha73])

<u>Two-dimensional growth models</u>	
<i>PN model</i>	$v_{PN} = \frac{D_{AB}}{3d_m} \left(\frac{\Delta C}{C_C} \right)^{2/3} \exp \left(-\pi \frac{[K \ln(C_C/C^*)]^2}{v \ln S} \right)$
	$\text{With } v = \frac{\dot{n}\tilde{M}}{\rho_C}$
<i>B+S model</i>	$v_{B+S} = K_{B+S} \left(\frac{\Delta C}{C^*} \right)^{5/6} \exp \left(\frac{K'_{B+S} C^*}{T \Delta C} \right)$
<u>BCF surface diffusion model</u>	
<i>BCF Model</i>	$v_{BCF} = K_{BCF} T \left(\frac{\Delta C}{C^*} \right)^2 \tan \cdot h \left(\frac{K''_{BCF} C^*}{T \Delta C} \right)$

Diffusion layer model

Only convection and diffusion $\dot{n} = k_d(C - C_i)$

Only surface integration $\dot{n} = k_r(C_i - C^*)$

with $k_r = k_{r0} \exp(-\Delta E_r/RT)$,

Elimination of C_i $\dot{n} = k_r \left(\Delta C - \frac{\dot{n}}{k_d} \right)^r$

Special case $r = 1$ $\dot{n} = \frac{\Delta C}{\frac{1}{k_d} + \frac{1}{K_r}}$

Special case $r = 2$ $\dot{n} = k_d \Delta C + \frac{k_d^2}{2k_r} - \sqrt{\frac{k_d^4}{4k_r^2} + \frac{k_d^3 \Delta C}{k_r}}$

2.2.2 Crystal growth kinetics

Design of industrial crystallizers and crystallization processes is based on calculations of crystal growth kinetics. Such calculations can be obtained if the data on crystal growth kinetics are available.

One of the main parameters for controlling the crystal growth is supersaturation, which can be expressed in a simplified form as follows:

$$\Delta C = C_c - C^* \quad (2.22)$$

From here the equations for linear and mass growth rate can be rewritten:

$$G = k_g \Delta C^g \quad (2.23)$$

and

$$R_G = K_g \Delta C^g \quad (2.24)$$

The constants K_g and k_g are related to each other through the expression:

$$K_g = 3 \frac{\lambda}{\beta} \rho k_g \quad (2.25)$$

Both constants K_g and k_g are temperature dependent and can be fitted to the Arrhenius equation, which can be rewritten, for growth rates, as a function of temperature as follows:

$$k_g = A \exp(-E_G / RT) \quad (2.26)$$

The activation energy can be used to obtain information of whether the rate-controlling step is diffusion or surface integration [Nýv85]. Therefore the equation (2.23) can be written as:

$$G = A \exp(-E_G / RT) \Delta C^g \quad (2.27)$$

In this equation both parameters temperature and supersaturation are taken into account.

The techniques used to measure crystal growth rates can be divided into two main groups. In the first group are methods using data obtained from single crystals and in the second group are methods using suspension of crystals. Reviews and information about crystal growth rate measurements and techniques can be found in [Gar90], [Mul01] [Nýv85] and [Ulr89]

2.3 Porosity and pore size distribution

2.3.1 Open, close, and total porosity

Many solids and powder materials, natural or manufactured contain a certain volume of voids and empty spaces. This is distributed within the solid form of pores, cavities and cracks of various shapes and sizes. The total sum of this voids volume is called porosity. Porosity is defined as the ratio of the void volume V_v to the total volume V_{tot} of the specimen.

$$\varepsilon = \frac{V_v}{V_{tot}} \quad (2.28)$$

There are three different porosities that must be distinguished [Pus04]:

- *Total porosity*, this is the sum of open and closed porosity, Eq. 2.29.
- *Open or effective porosity*, which may be defined continuous, channels involving connecting the interior of the specimen with the surrounding gas or liquid phase. Effective porosity is less than total porosity.
- *Closed porosity* contains pores, which are completely isolated from the external surface, not allowing access of external liquids or gaseous phases (see Fig. 2-9), [Rav97, Som00]. This closed porosity is impossible to be measured directly. Data about it can only be gained with measurements of the apparent density.

The sum of effective and closed porosity gives the total porosity.

$$\varepsilon_{tot} = \varepsilon_e + \varepsilon_{cl} \quad (2.29)$$

Closed porosity has a great influence on physical parameters like density, mechanical or thermal properties. Open pores are connected with the external specimen surface and therefore allowing liquids or gases to flow through or into the porous article. Open pores can be further divided in dead-end or interconnected pores. Dead-end pores have access to external specimen surface at one of the ends while the other one is closed. Interconnected pores have an access with external surface with the both ends or one of the ends is connected with other pores. The type and nature of porosity in natural materials depend on their genesis while in synthetic materials it depends on their manufacturing and generally it can be controlled.

2.3.2 Pores characteristics

The characterization of solids in terms of porosity can be determined by the parameters of the pores:

Pore size is the dimension, which classified the pores up to their sizes (see Fig. 2-10) to micropores, mesopores and macropores. Several techniques are on hand to examine pores depending on their size and nature. They will be discussed in section 2.3.3.

Specific pore volume and porosity: The internal void space in a porous material can be measured. It is generally expressed as a void volume (in cc or ml) referred to the mass unit (g).

Pore size distribution: The pore size distribution represents the pore volume in function of pore size and commonly is given as percentage or a derivative

Percentage porosity: Corresponding to the ratio between the total pore volume and the external sample volume.

Specific surface area: This is the total surface area of the sample, which is in contact with the external environment. This parameter is mainly dependable to the pore size and the pore volume. The smaller the pore size is the higher is the surface area [Por02].

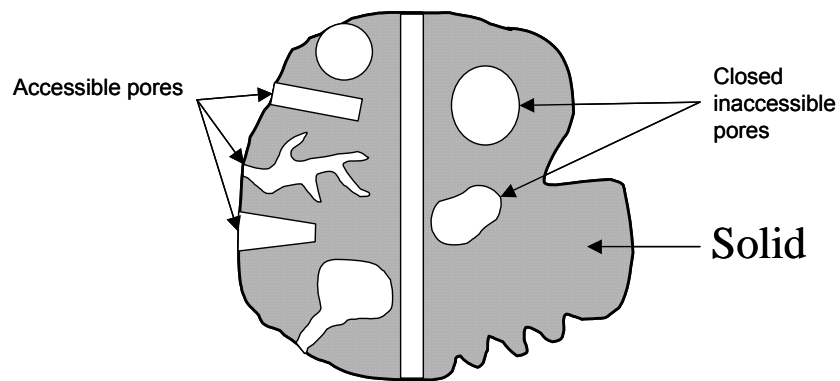


Fig. 2-9: Structure of open and closed pores

2.3.3 Methods and techniques for production of porous ceramics

Methods and techniques of creating porosity depend on the wanted porosity or on the techniques and devices to obtain it. More information about different techniques can be found e.g. in the following books Segal [Seg89] and Liu [Liu96, Liu97].

All fabrication techniques and methods lead to a variety of microstructure. As discussed in the previous section most of the macro properties such as density, thermal expansion, electrical conductivity, melting points, Young's modulus and thermal expansion are to a large extent microstructural dependent [Bar03]. However, all microstructural properties are in consequence based on used manufacturing procedure and the starting materials characteristics.

Methods and techniques used to obtain porosity may be categorized as follows [Liu97]:

- Porosity formers by gas development give rise to a reaction of chemical scission of the constituting molecules activated by heating, with development of one or more gaseous components. Among them are the classical CaCO_3 , NH_4NO_3 , $(\text{NH}_4)_2\text{CO}_3$, and other can be taken into account. Developing of gas involves its outlet along radial directions in respect to the site of emission. Since the sites of emission are distributed homogeneously, the obtained porosity is distributed randomly. The functionality of such agents may be expressed only if the temperature of chemical scission occurs just slightly below the one at which the sintering begins, a step in which the small channels are created as a result of gas outlet can be maintained for the stiffening due to sintering for the join of the grains.
- Volume preserver agents involve substances like NaCl, grains of sugar, etc. which are able to resist chemically the increase of temperature at least until the start of ceramic sintering. Such agents preserve the volume, which they occupied. In this way the body on the way to be ceramized actuate remarkably well a sufficient number of intergranular linking's. After the sintering, when the body becomes ceramics cold, the preserver agents are taken away by simple immersion in a liquid medium (mostly H_2O) in which they are soluble. The volume occupied by the disappeared agents is set free, so obtaining the desired porosity.
- Thermounstable porosity formers are agents constituted by organic substances, which disappear during heating, leaving empty volume, which they occupied. Their disappearance must happen just below the consolidation temperature or, at least, over specific threshold temperatures. The formation of gas, if any, along the formed and preserved meanders contributes to the preservation of the porous volume. The nature of the involved processes of disappearance can be chemical and/or physical
 - sublimation (e.g. naphthalene, camphor, etc.)
 - oxidative pyrolysis (e.g. polystyrene, nylon, carbon, sawdust, etc.)

- Agents for replamineform process are porous substances, generally natural, the porous structure of which is considered for serial reproduction. The process consists in reproducing in negative or in positive (terms taken from photographs) the porous network of such porous substances. These are generally natural (e.g. porites, corals, Madreporas, etc.). If the starting material is easily dissolvable chemically with specific substances, as in the case of acids for the calcium phosphates of the natural corals, its natural porosity is filled with substances not affectible by them.
- Agents at cryoscopic action are liquids at very low temperature. These are used in particular to obtain porous granules. The process that requires them consists in plunging spheroidal bodies constituted by polymeric slurry of the starting powder into liquid nitrogen. The immersion of granulates into the freezing liquid produce fast decreases of their temperature with the consequence of the strong shrinkage of the volume of each granulate. This leads to the formation of microcracks, which the liquid nitrogen penetrates. The later becomes warm at contact with the warmer granule until overcoming the boiling temperature of nitrogen, becoming vapor with an expansion of volume.

2.3.4 Methods for characterizing porous ceramic materials

Many techniques have been developed for characterizing porous materials. Here can be noted methods such as gas adsorption, fluid penetration, NMR, ultrasonic technique or other. The most popular and widely used methods are the gas adsorption and mercury intrusion porosimetry. To characterize mesopores and surface area the Brunauer, Emmett and Teller (BET) method is applied, and for macropores mercury porosimetry. Any condensable vapor can be used for BET. For this purpose the vapor molecules should be small and approximately spherical. Mainly liquid nitrogen is used. The measurement is based on the adsorption isotherms. For more details see [Bru44]. In this study mercury porosimetry will be used. This method is based on the physical properties of mercury. It is interacting with most of the solids as non-wetting liquid (contact angle, greater then 140°) and having a surface tension over 480dyne/cm [Was22, Por02]. This high surface tension

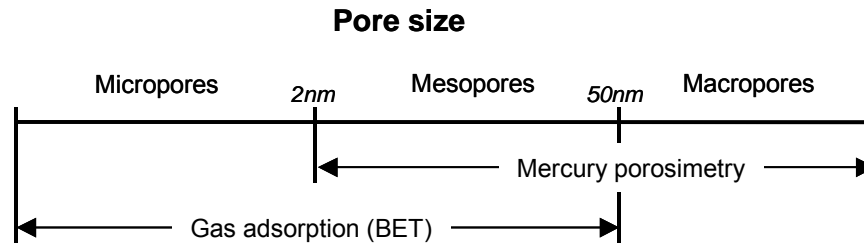


Fig. 2-10: Pore sizes and methods for their characterization

can be passed by applying external pressure. This external pressure is needed for the mercury to penetrate into small pores. Under this conditions the pore radius in which the mercury intrudes at a given external pressure can be calculated by the Washburn equation:

$$r_p = \frac{2\sigma_m \cos \theta_m}{P_e} \quad (2.31)$$

where θ_m is the contact angle between mercury and measured solid, P_e is the external pressure, r_p is the pore radius and σ_m is mercury surface tension. This equation is applicable for cylindrical pores. For pores with other shapes a shape factor for corrections should be taken into account.

In this study a Mercury intrusion Porosimeter serial Pascal 140+440 is used. The sample is placed in a special holder (dilatometer) with known volume and put forward to vacuum. After an indispensable vacuum level is reached mercury is dropped in the holder. So the volume of the macropores of the sample can be found, with respect to the large cavities, which can be filled by mercury at low pressure. The porosity of the sample is defined as the ratio between the samples voids volumes (inter and intra porosity) and its external volume [Por02].

$$\varepsilon[\%] = \frac{V_{\max}}{1/\rho_{BD}} - 100 \quad (2.32)$$

The apparent density is defined as the density of the sample referred to the real sample volume. The apparent density is very close to the real density (or true density) in the following cases:

- The sample is not compressed by the high pressure

- The sample is not collapsed by the high pressure
- The sample has no pores smaller than the mercury porosimetry lower limits

The apparent density can be calculated as follows:

$$\rho_{AD} = \frac{1}{(1/\rho_{BD}) - V_{\max}} \quad (2.33)$$

where ρ_{AD} is the apparent density, ρ_{BD} is the bulk density and V_{\max} is the total mercury penetrated into the sample at the end of measurements referred to the sample mass (cumulative volume) and can be calculated as follows:

$$V_{\max} = V_c / S_m \quad (2.34)$$

where V_c is the cumulative volume and S_m is the sample mass.

2.4 Freeze-casting. Bases and principles

2.4.1 Colloidal systems. Introduction

The colloidal systems are defined as comprising a disperse phase with at least one dimension between 1nm and 1 μm in a dispersion medium [Seg89]. Examples of such a systems can be found in Tab 2.4.

One of the most important attributes of all colloidal systems is that the contact area between the phases is very large, and interparticle forces strongly influences the system behaviour.

Ceramics have been produced by different colloidal routs and techniques for several millennia. But in the last decades the research has been mainly focused on so-called “clay- based” systems. Colloidal processing offers a great potential for producing thin ceramic films and bulk forms through careful control of initial suspension “structure” and its evolution during fabrication [Lew00]. Five steps are involved for this purpose:

- ✓ Powder synthesis
- ✓ Suspension preparation
- ✓ Consolidation into desired component shape

- ✓ Removal of the solvent phase
- ✓ Densification to produce the final microstructure required for optimal performance

Table 2.4 Classification of colloidal systems [Seg89]

System	Disperse phase	Dispersion medium
Dispersion (Sol)	Solid	Liquid
Emulsion	Liquid	Liquid
Solid emulsion	Liquid	Solid
Fog, mist or aerosol (of liquid particles)	Liquid	Gas
Smoke or aerosol (of solid particles)	Solid	Gas
Alloy, solid suspension	Solid	Solid

The forces responsible for the colloid systems stability and interparticle potential can be summarized in the follow equation:

$$F_{Total} = F_{vdW} + F_{elect} + F_{steric} + F_{structural} \quad (2.35)$$

where F_{vdW} is the attractive potential energy due to long-range van der Waals interactions between particles, F_{elect} the repulsive potential energy resulting from electrostatic interactions between like-charged particle surfaces, F_{steric} the repulsive potential energy resulting from steric interactions between particle surfaces coated with adsorbed polymeric species, and $F_{structural}$ the potential energy resulting from the presence of nonadsorbed species in solution that may either increase or decrease suspension stability.

More information and very deep investigation on colloidal processing of ceramics and sol-gel science and technology can be found e.g. by Lewis [Lew00], Segal [Seg89], Sigmund et al. [Sig00] and Lopez et al. [Lop03].

2.4.2 Freeze-casting

Colloidal processing techniques are typically used in complex-shape forming for ceramics. Colloidal processing contains methods such as slip casting, injection moulding [Nov92], gelcasting, [Mor99, Oma91, You91] and freeze- casting [Don04,

Jon00, Koc03, Sof01]. Among these colloidal processing techniques, freeze-casting is one of the simplest techniques.

First Smith-Johannsen [Smi61] reported a method for producing metallic and ceramic bodies by using freeze sensitive colloidal silica. Furthermore, Mahler [Mah78] and Mahler and Bechtold [Mah80] upgraded the existing method and used it for the production of Silica fibbers. A lot of investigations have been done in the past decade observing operating conditions [Don03, Don04, Don04a, Koc03], sintering [Fuk01, Sta98] and the effect of additives [Sof01] on the microstructure of produced specimens by the freeze-casting route.

Freeze-casting is a technique, which takes ceramic slurries into a form of a nonporous mould. The ceramic slurries containing freeze sensitive liquids (water or silica-sol), which can be frozen under extremely cold temperatures followed by demolding and liquid phase removal by sublimation. Polymerization occurs because of the concentration of silica particles within the interspaces between ice crystals [And03]. The polymerization process is schematically exposed in Fig. 2-11.

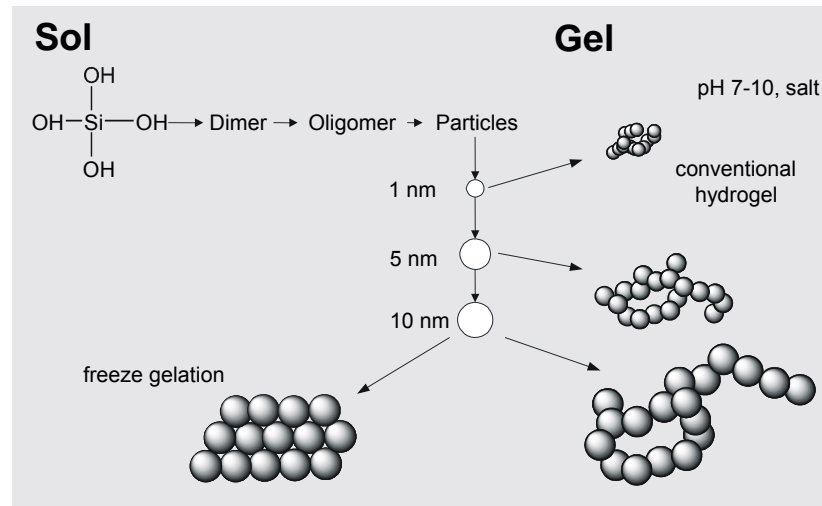


Fig. 2-11: Polymerization process for Silica-Sol (Adopted from Andresen et al. [And03])

The important steps of the freeze-casting process are graphically shown in Fig. 2-12. The freeze-casting technique is based on a phase separation as a pore forming principle of aqueous suspensions with simultaneous growth for the ice crystals in one direction (see Fig. 2-13). After a complete freezing the samples are warmed to melt

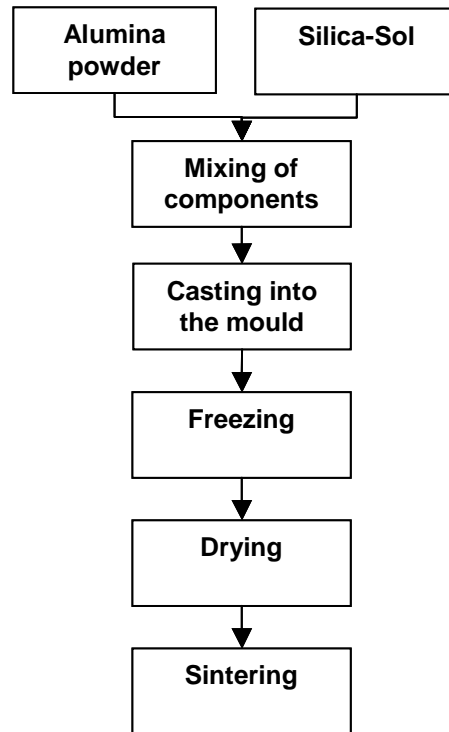


Fig. 2-12: Flow chart of the freeze-casting process

or sublimate the ice crystals and then to dry the sample. The freezing agent acts temporary as binder. The result is a formation of rigid bodies [Sof01]. Therefore no binder agents are needed.

After drying the formed green body has a relatively high degree of overall porosity, where the pores reproducing the morphology and dimensions of the ice crystals formed during the freezing process [Sta98]. The pores are the negative images of the ice crystals. A control of pore size, shape and morphology of the ice crystals can be achieved by controlling nucleation and growth rate of the ice during the freezing [Don04, Don04a] and dependence of solid load content (filler) amount. Removing of the liquid phase by sublimation minimizes the possibility of stresses, which can occur due to the drying process [Lau92].

The freeze- casting route has many advantages such as a fast manufacturing cycle, no drying cracks, essentially zero-shrinkage [Sta98] and no troublesome binder burnout process [Ara04]. Also one of the advantageous of the freeze- casting process is a preparation of a highly concentrated suspensions [Hua01,Sta98]. Such a great additions of solid loads (over 70wt.%) can be a good enhancement of mechanical and thermal properties.

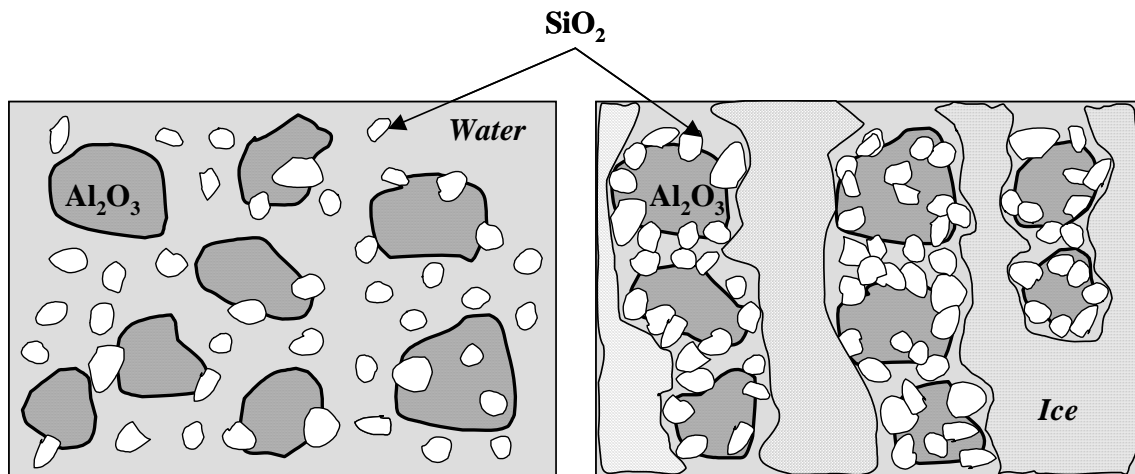


Fig. 2-13: Phase separation of water and solid particles during freezing (Adopted from [Don04a])

3. Materials and Experimental Setup

3.1 Materials

As aqueous sol in this study Nyacol 1440, (EKA-Chemicals, Sweden) with 17 vol.% SiO_2 suspended in water has been used, with a particle size $d_{50}=14\text{nm}$ and alumina powder (99,99 wt.% Al_2O_3 , CT 3000 SG, Alcoa, Germany) having an average particle size of 700 nm and a surface area of 10,4 m^2/g . Suspensions were prepared by mixing of known amount of dry powder (Al_2O_3) with silica sol to obtain the desired volume fraction. The components were mixed by stirring and prepared at different solid loads in order to investigate the effect of the solid load content on the overall porosity and pore size distribution (see Fig. 3-1). After the alumina powder was added to the silica-sol the slurries were treated with an ultrasonic buster (Sonoplus HD220, Bandelin electronics, Germany) for about 5 min to prevent uncontrolled agglomerates formation and high densities zones. As dispersing agent Polyacrylic acid (35 wt.% solution in water $M_w\sim 100,000$, Aldrich Chemicals Company Inc., Milwaukee, USA) has been used influencing the electrostatic stability of the suspensions and the surface charge of the particles.

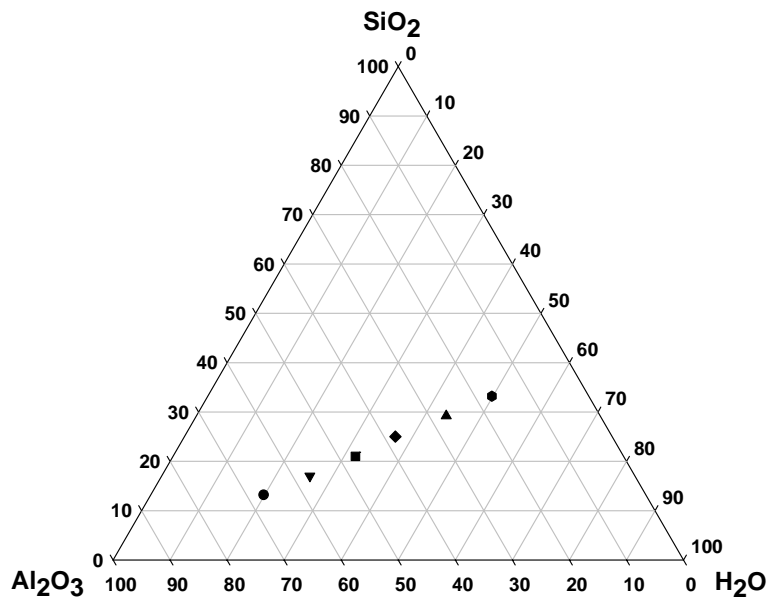


Fig. 3-1: Ternary plot of materials mixture

3.2 Experimental procedure and setup

The suspensions were poured into the polyethylene or glass moulding form, which were subsequently frozen from the bottom to the top (see Fig.3-2). A cooling device in which the temperature was controlled by a thermostatic bath provided the cooling from the bottom face. The top of the moulding form was always open, so the upper face of the suspensions was exposed to ambient conditions and a temperature gradient between the faces was generate. Therefore the ice crystals formed due to the freezing were encouraged to grow only in vertical direction. Different freezing temperatures have been utilized in order to examine closely ice crystals growth. The growth of ice crystals was observed using a CCD camera and a microscope. A connection of the camera to a computer allows getting on-line pictures for the calculation of the linear ice growth rate. While freezing the phase separations occurs. The water forms during freezing ice crystals, which compact surrounding solid particles (see Fig. 2-13). When the freezing begins and phase separation occurs columns of formed ice piled up between the surrounding ceramic particles. After complete freezing the samples were removed from the cooling device. Melting of the ice and then evaporation of the water was allowed to occur in the dryer for 24 hours.

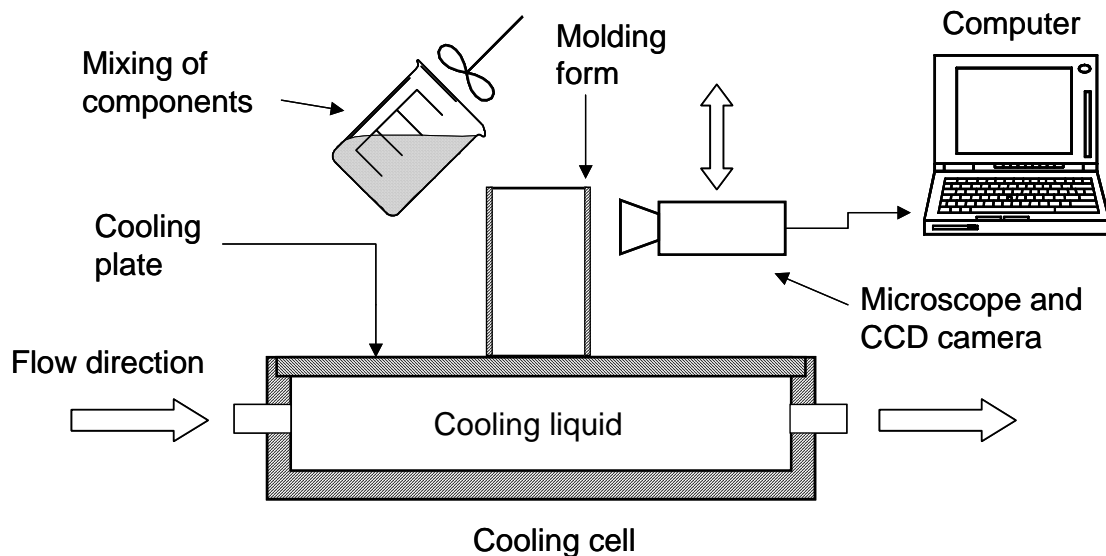


Fig. 3-2: Experimental setup

The moulding forms, which have been used, had always the same dimensions, diameter 2cm and height of 5cm. To observe the influence of material properties

respectively interfacial energies on nucleation and ice crystals growth different materials (glass and polyethylene) for the moulding form have been used. Furthermore, different shapes of the moulding forms have been examined. The second experimental setup is called “diffusion chamber” and consists of two reservoirs and five steel disks (see Fig. 3-3). Each disk has a thickness of 8mm and is insulated from the others and the reservoirs by teflon gaskets (see Fig. 3-4). Every teflon gasket has a thickness of 2mm.

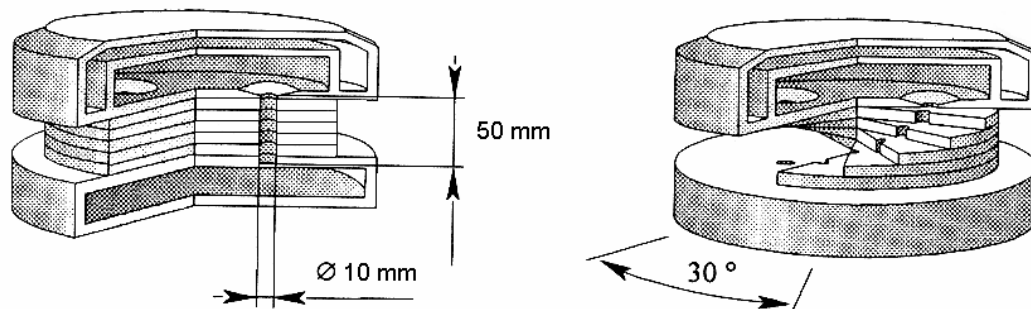


Fig. 3-3: Diffusion cell (Adopted from [Neu95])

The disks, teflon gaskets and the bottom reservoir are fixed by a swivelling on an axle. Through the disks and the teflon gaskets 3 openings with a diameter of 1,5 cm are available. The upper reservoir was constructed that way that it allows to be removed. On this way the suspensions to be investigated can be mould into the disks openings. All the disks are routable against each other by 30°. By rotating of the disks the samples placed into the openings can be separated into different sections. All sections represent a part of the moulding form. The teflon gaskets are fixed on one of the disks so that the sections can be completely locked from each other.

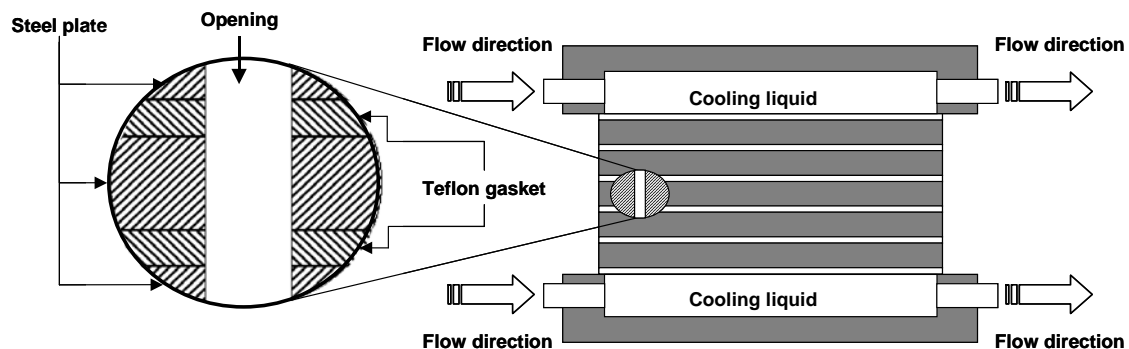


Fig. 3-3: Schematic of diffusion cell

The top and the bottom reservoirs are double-jacketed. By the connection with thermostats different temperature gradients can be applied. Even a freezing procedure of the samples from both sides is possible.

4 Instrumentation

ViscoTester 550 (VT550 DIN/ISO Cylinder Package, HAAKE) rotational viscosimeter was used to investigate the suspensions viscosity. Suspensions density measurements have been carried out by using Density/ Specific Gravity/ Concentration Meter - DMA 4500 (Anton Paar, Switzerland). The cooling plates roughness measurements were done using Perthometer S3P (Mahr, Göttingen, Germany). Optical Stereo Microscope Stemi 2000- C (Zeiss, Germany) was used to observe samples microstructural evolution and measurements for crystal growth. Ceramic particle surface and cooling plates microstructure have been observed with ESEM, Model XL30ESEM-FEG, XL Series (Philips). The contact angle measurements were made using an Optical Contact Angle Measuring System OCA 20 (Krüss, Germany). Drop Shape Analysis System G10/DSA10 (Krüss, Germany) was used for determining surface energies of used suspensions. Thermostats FP 50 and FP 81 from Julabo (Julabo, Germany) were used for controlling of temperature and temperature gradients on cooling and diffusion cells. The measurements on overall porosity and pore size distribution were carried out by using system of mercury intrusion porosimeters Pascal 140 (low pressure) and Pascal 440 (high pressure), from Porotec, Germany. All samples have been dried, after freezing in a convection oven (AX60, Carbolite, Germany). Using DSC 12E Device from Mettler Toledo has done DSC measurements of suspension melting temperatures to describe metastable zone. Phase transformation temperatures have been measured to find the temperatures at which consolidation start. For this express purpose has been utilized thermocouples Typ K NiCrNi (ZA9020-FS Ahlborn) and data logger ALMEMO 8990-8 (Ahlborn) connected with computer

5 Results

The majority of the experiments in this study were conducted using the illustrated (in Chapters 3.1 and 3.2) experimental setups. In this chapter, the results of measurements and tests will be given. The presentation of results for various suspension densities and operating temperatures and their relationship with the major properties in focus (overall porosity and pore size distribution) will follow. Chapter 4.1 deals with rheological properties of the used suspensions. In Chapter 4.2 data of the ice crystallization process will be given. Finally, the investigations on the overall porosity and pore size distribution are presented in Chapter 4.3.

5.1 Rheology

The rheological properties of suspensions are extremely important for the processing. The particle size distribution, interparticle forces and solid filler content can in close relation to their temperature dependence determine those properties. In this chapter density and viscosity measurements of investigated ceramic suspensions (see Chapter 3.1) will be presented.

5.1.1 Density

The slurry densities have been investigated in a temperature range of 5 to 25°C. Temperatures below 0°C has not been examined because a potential freezing of the water and thereby the volume expansion might damage the device. The relative density measurements are shown in Fig. 5-1. The relative density (RD) is the density of the slurries related to the density of the liquid phase (water). This value is always greater than unity because of the presence of solid particles in the suspension.

$$RD = \frac{\text{density} \cdot \text{of} \cdot \text{slurry}}{\text{density} \cdot \text{of} \cdot \text{liquid} \cdot \text{phase}} \quad (5.1)$$

The density is a temperature dependent function therefore it needs to be reported at exact temperature. The increase of density by decreasing temperature, Fig. 5-1, is related to a density incensement of the liquid phase (water). Density changes due to temperature of the solid particles in this temperature region are insignificant and can

be neglected.

From Fig. 5-1 it is obvious that an increase of the density depends on the solid loading. Higher solid loads correspond to less water in the slurries and therefore an increasing of the slurry density.

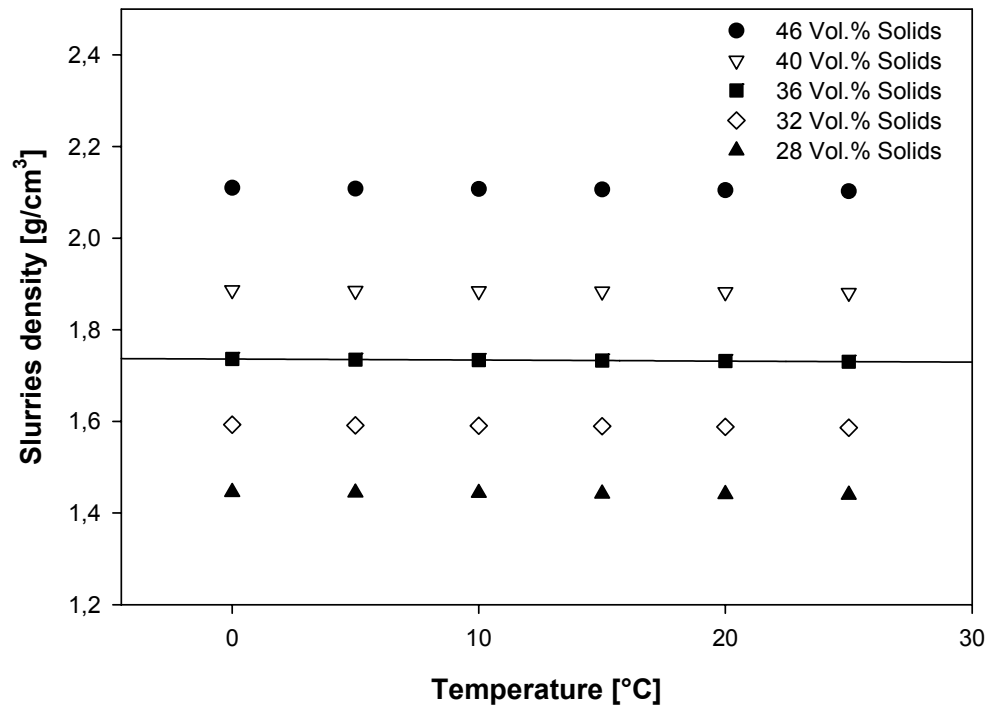
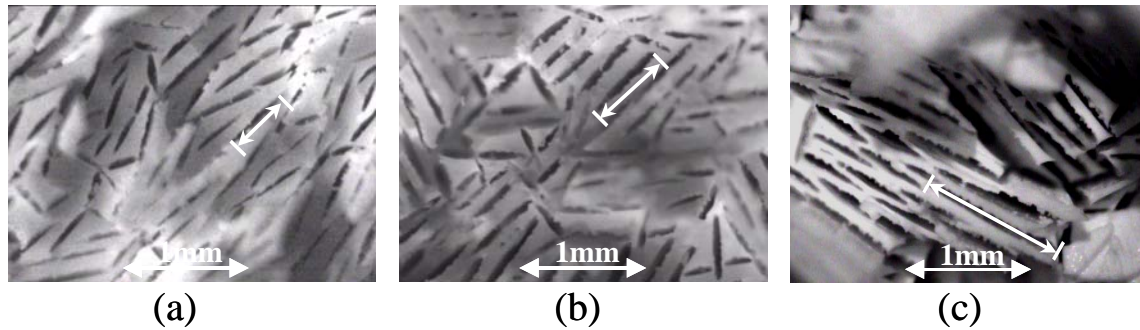


Fig. 5-1: Slurries density measurement

The maximal amount of solid in the slurries was 46 Vol.%. A further increase of the solid load has not been reported because the slurries become too dense and not castable any more. Increasing the solid load leads to a formation of high-density zones and agglomerates. Such zones do not allow the ice crystals to grow continuously during freezing and results in microstructural evolution of the final samples.

The effect of increasing density on the microstructural evolution on the final samples is shown in Fig. 5-2. In Fig. 5-2 the freezing temperature and the distance from the cooling plate is the same for all samples. The increase of solid loads will decrease the final porosity of the samples and therefore will have an effect on the mechanical properties of the sample.



*Fig. 5-2: Microstructure evolution of slurries with different solid loads
(a) 46 (b) 40 and (c) 36 Vol.%*

5.1.2 Viscosity

The viscosity is one of the most important factors in the freeze casting process. The temperature dependence of the viscosity strongly effects the suspension quality and the time required for the homogenisation as well as the required cooling rate.

Therefore temperature and solid content dependence have been examined.

Suspensions were prepared according to the procedure described in Chapter 3.1.

The measurements were performed over a wide range of shear rates (between 10 to 1000 s^{-1}). The temperature effect was observed in the range of 5 to 25°C by connecting the beaker of the device with the thermostat and so allowing an adjustment of wanted temperature.

The relations between shear rate and shear stress are shown in Fig. 5-3.

The slurries with 46 and 40 Vol. % solids display an orderly shear thinning behaviour observed with a small yield stress from the hysteresis between ascending and descending curves. With decreasing solid load content shear thinning is decreasing this effect as is also reported by Zhu [Zhu02] and Rao [Ram99]. At 28 Vol.% the shear rate is almost proportional to the shear stress. This slurry exhibits almost Newtonian behaviour (which can be observed from Fig. 5-4) with only a small deviation at small shear rates. The change in suspension behaviour is clearly related to the volume fraction of the solids. In case of high solid loads and low shear rates the particles form big agglomerates. Therefore their mobility becomes limited. An increase in shear rate affects the suspension structure. A beginning in breaking agglomerates and big particles due to increasing viscosity forces results in only a small deviation in viscosity.

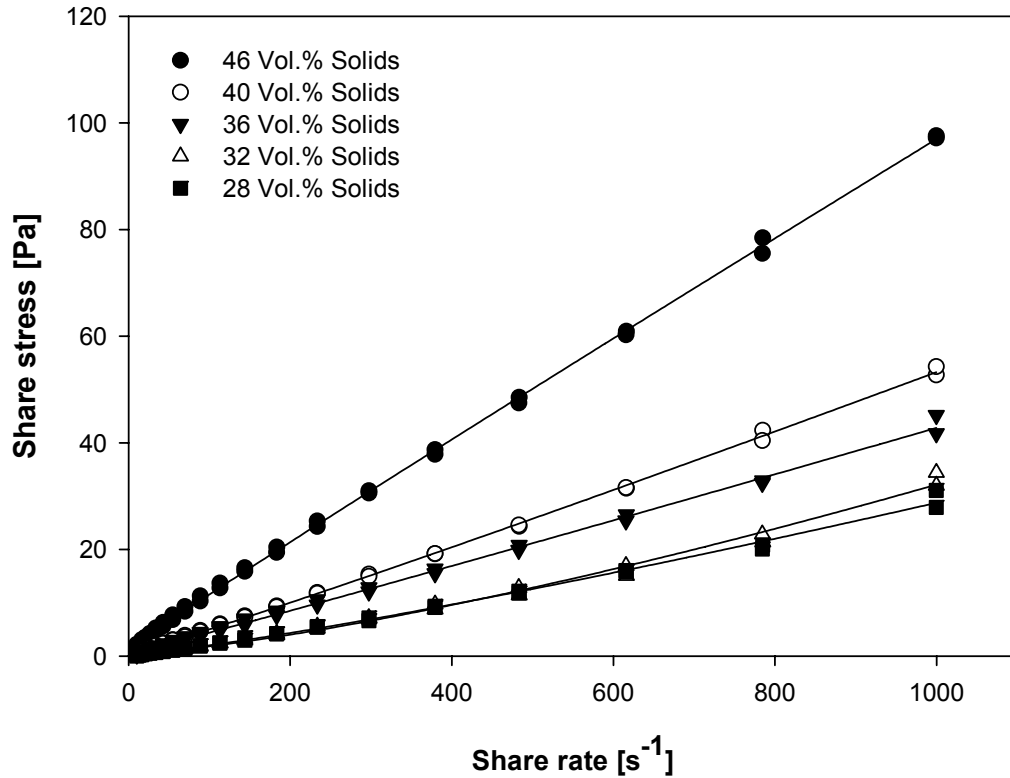


Fig. 5-3: Share rate versus share stress of slurries with various solid contents at 10°C

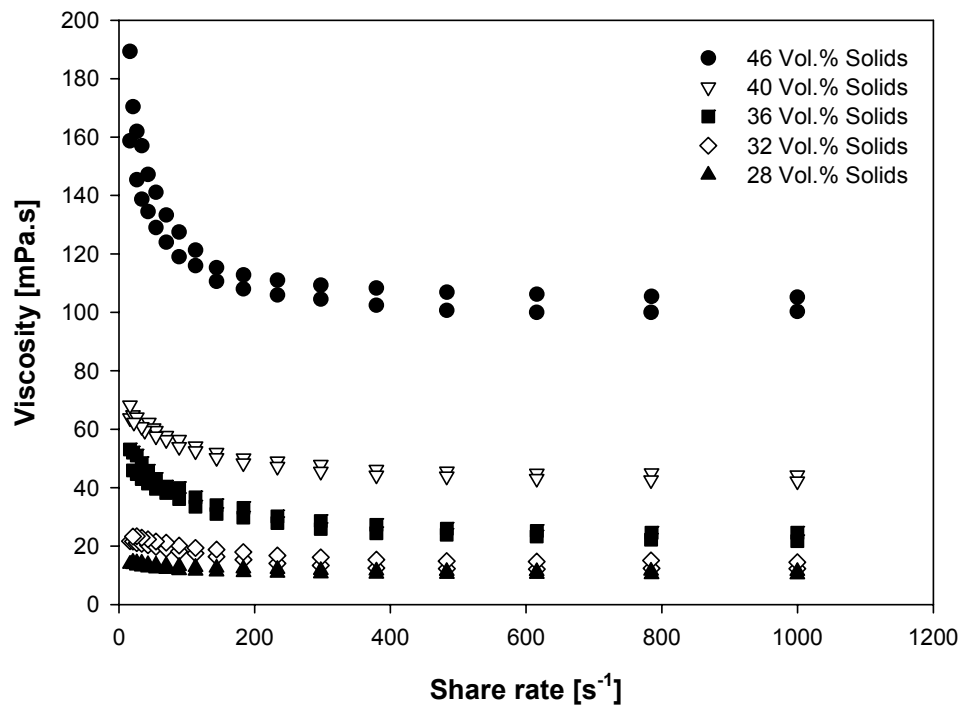


Fig. 5-4: Viscosity versus share rate for slurries with various solid content at 10°C

Fig. 5-5 shows the viscosity dependence on temperature. The data show obviously that with decreasing temperature viscosity increases. This can be explained by a decrease in viscosity of the liquid medium and decreasing of Brownian movement of ceramic particles. By reducing Brownian movement of the particles the forces avoiding agglomerates formation become smaller.

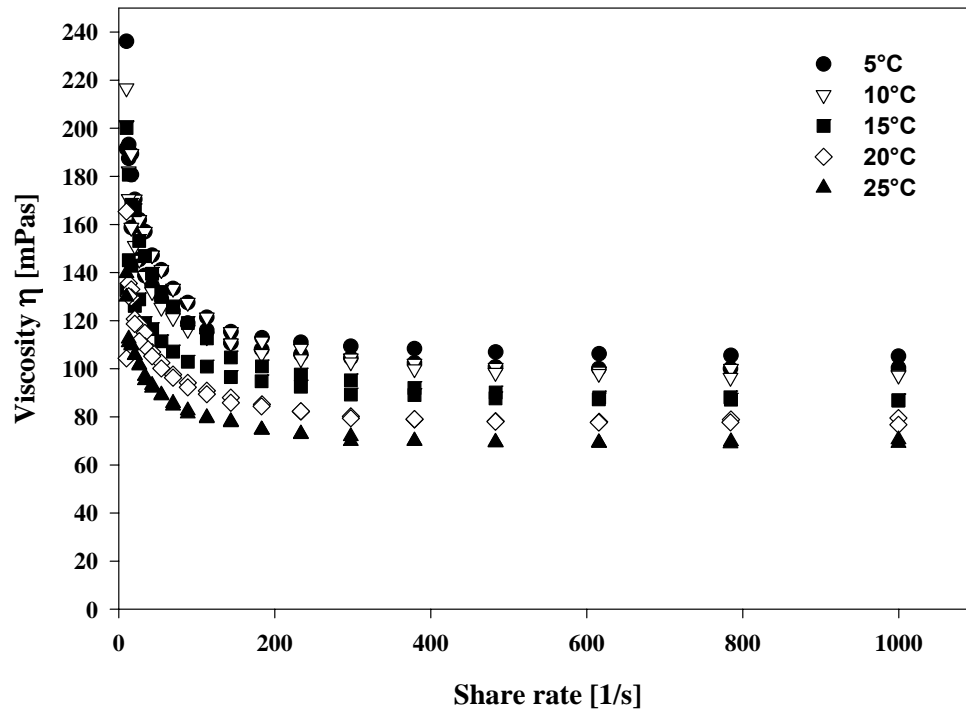


Fig. 5-5: Viscosity temperature dependence for slurries with 46 Vol.% solid loads at various temperatures

For the shown experimental data the best regression was obtained by using Cross's model [Cro65].

$$\frac{\eta_s - \eta_\infty}{\eta_0 - \eta_\infty} = \frac{1}{1 + b \dot{\xi}^p} \quad (5.2)$$

In this model η_0 is a low share viscosity, η_∞ is a high share viscosity, b and p are constants. The constant p has a recommended value of $2/3$. η_s is the suspension viscosity at a specific share rate. The common way to express the suspension viscosity η is to present it as a relative viscosity which is defined as:

$$\eta_r = \frac{\eta}{\eta_l} \quad (5.3)$$

were η_r is the relative viscosity and η_l is the viscosity of the liquid phase.

Table 5.1: Fitting parameters obtained from the Cross regression for steady share rates of Fig. 5-3

Volume Fraction [Vol.%]	η_∞	b	p	R²
0,46	105,3	0,9195	2/3	0,9986
0,40	41,3	0,6761	2/3	0,9997
0,36	20,7	0,3328	2/3	0,9825
0,32	8,1	0,0775	2/3	0,9897

The data for 0,28 Vol.% is not included in Table 5.1 because the slurry does not sufficiently behave like a concentrated suspension and exhibits almost Newtonian behaviour.

Fig. 5-6 shows the extrapolated values of the viscosity calculated by Cross's regression. The relative viscosity data are plotted as a function of the volume fraction of solids. The best fit of the data was obtained using the modified Krieger-Dougherty model [Kri59].

$$\eta_{sr} = \left(1 - \frac{\phi_{sl}}{\phi_{sl}^*} \right)^{-n} \quad (5.4)$$

were η_{sr} is the highest share rate viscosity, ϕ_{sl} is the volume fraction of solids, ϕ_{sl}^* and n are fitting parameters. In this Figure 5-6 the relative high share viscosity is defined as η_∞ from the Cross model normalized by the viscosity of the slurry with no solids (water in this case 1mPa.s at 25°C), as a function of the volume fraction of solids. The fitting parameter ϕ_{sl}^* shows the maximum volume fraction of solids were the slurry becomes infinite [Ara04]. The Krieger-Dougherty model yields a maximum solid volume fraction of $\phi_{sl}^*=0,66$ suggesting that higher solids volume fractions should

also be attainable for such a complex suspension. On the other hand the value of 0,66 Vol.% was found to be too high because already at ambient conditions in case of solid contents higher than 48 Vol.% a very fast gelation was found and the suspensions could not be handled anymore. Since it is not known how much water molecules still remain in the slurry, compared with those absorbed on the hydrophilic alumina and silica particles surfaces.

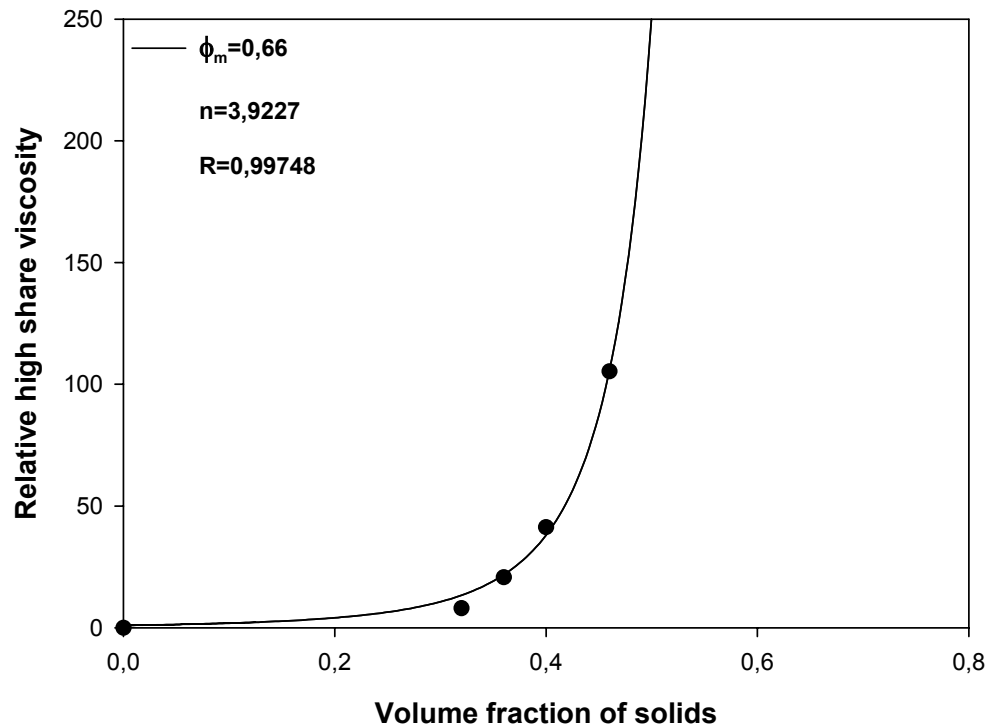


Fig. 5-6: Viscosity at extreme share conditions as a function of volume fraction

5.2 Nucleation and Crystal growth

In this chapter the experiments are presented which are carried out on crystallization of ice. The experimental work is divided into two parts. The first set of data is on nucleation. The second part deals with crystal growth.

5.2.1 Nucleation

5.2.1.1 Roughness of the cooling plates

Two different materials, stainless steel and cooper, have been chosen to prepare the cooling plates in the device presented in Fig 3-2. These materials have been chosen because of their mechanical and thermal properties and their wide application in industry. For each material two plates with different roughness have been tested to observe their effects and influences on interfacial tension compared to ceramic suspensions. Haasner [Haa02] has found a correlation between initial roughness and the control of nucleation conditions.

The data obtained and evaluated are plotted in Fig. 5-7. A perthometer technique was used for the roughness measurements. The instrument was equipped with a diamante needle with a radius of 0,25 mm tip. The needle was driven on the plate surface tracking 2 cm. The needle top follows 2 dimensionally the plate topography and the data are recorded into the device memory. Each measurement has been repeated 4 times and is presented as averaged result. From the measurements following parameters have been achieved: R_z and R_a . The parameter R_z is an averaged roughness depth value from the single measuring sections and R_a is the arithmetic average value of the roughness profile.

The average roughness profile of the used plates was found to be between 0,5 to 0,95 μ m. The “cooper polished” surface shows a very fine structure. However, some scratches and slits have been detected and they can be seen in Fig. 5-8 (SEM micrographs of the plates). The roughest surface was from the “cooper rough” plate were the depth of the scratches was about $7 \pm 0,29\mu$ m. An increasing in roughness profile results in the contact angle and area between suspension and plate because the thermal conduction occurs only through contact regions. In the case of thermal conduction, for example, the roughness can cause distortion in the heat flux but also promote nucleation because of the irregularities.

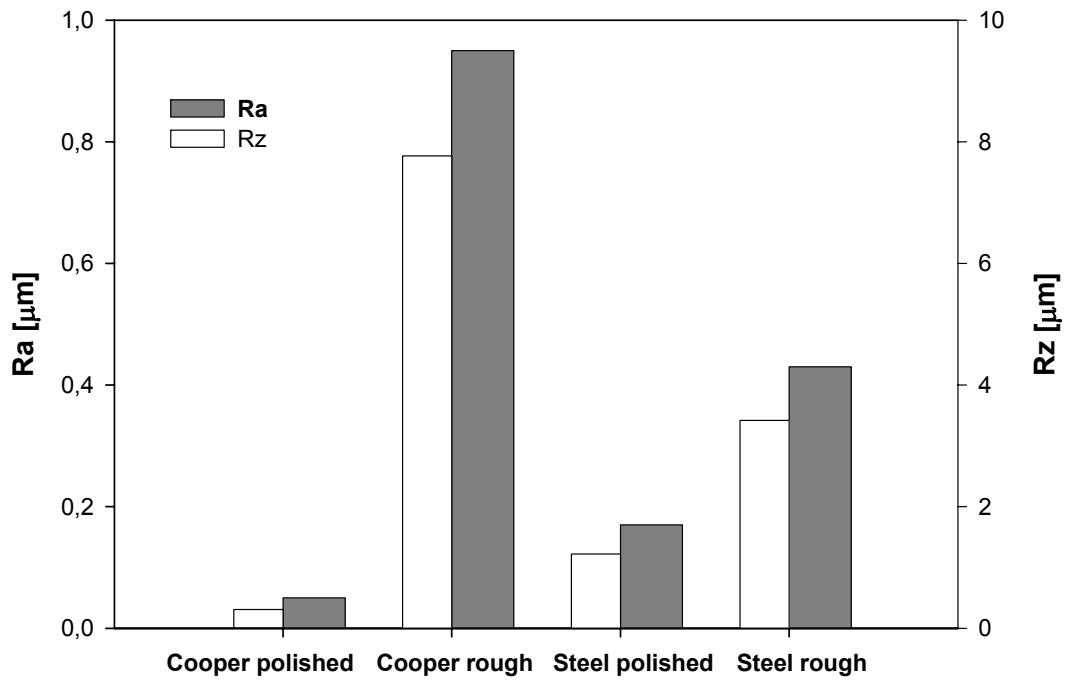


Fig. 5-7: Measurements of the roughness profiles

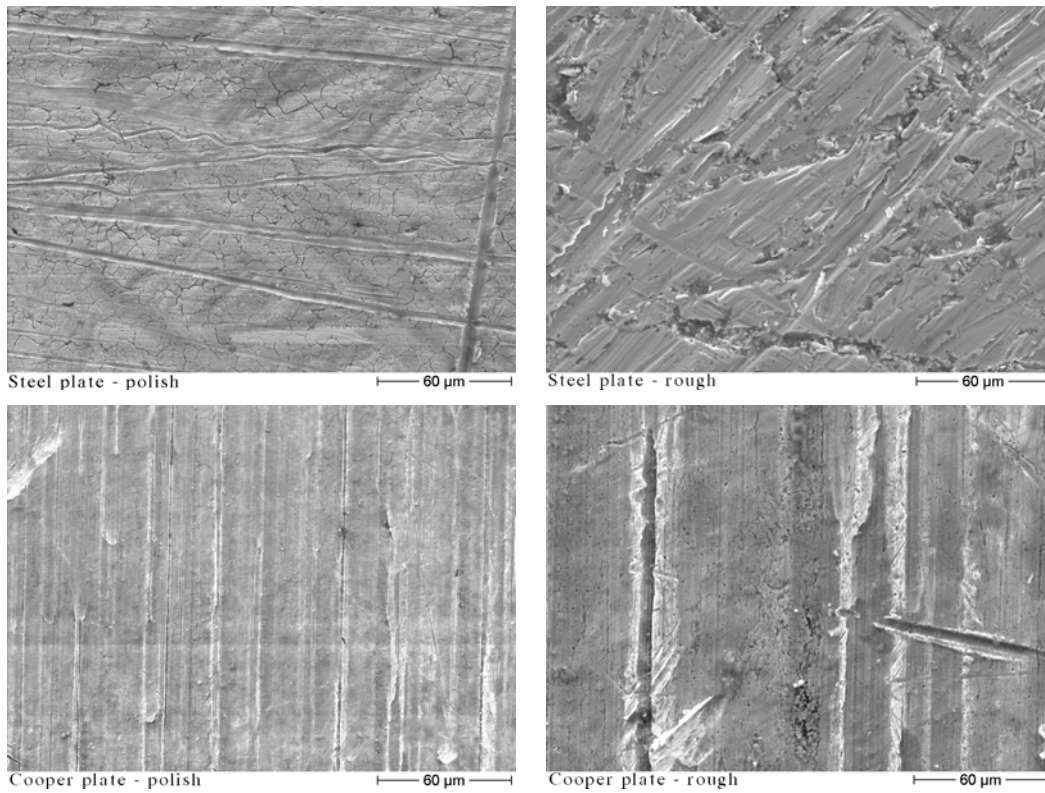


Fig. 5-8: SEM micrographs of the cooling plate surfaces

5.2.1.2 Contact angle

When the liquid is placed on a solid substrate it will wet the surface to a certain degree, therefore droplets with different forms and profiles are formed depending on both the interfacial tension and the contact angle.

The micrographs from the droplet profiles have been recorded by a CCD camera and a microscope connected with a computer. The micrographs have been evaluated using the contact angle measurement device software. In order to separate the droplet profiles from the environment a back light source was used.

A schematic view of the measurement device is shown in Fig. 5-9.

To put droplets on the substrate surface a syringe with a micrometer piston has been used. Such syringe was used in order to control the droplets volume. All presented experiments have been carried out with droplets with a size of $3 \pm 0,1$ mm.

The solid substrate surface was the cooling cell surface, which is in contact with the ceramic slurries to be frozen, as shown in Fig. 3-2. The cooling cell was connected with a thermostat allowing setting the desired temperatures. All investigated suspensions were in the temperature range between $+5$ and -30°C .

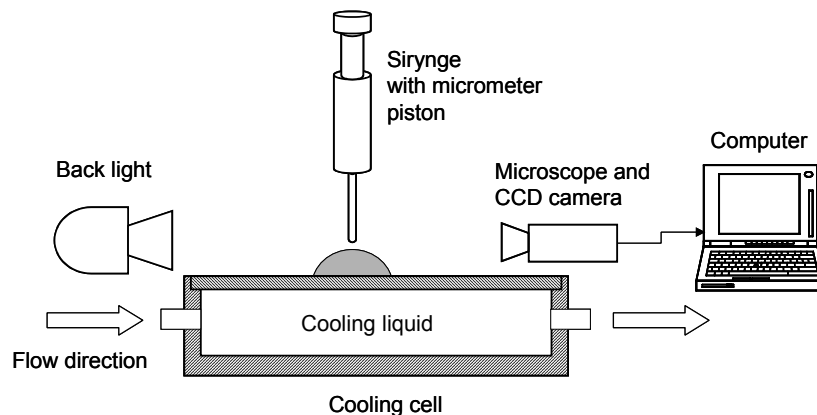


Fig. 5-9: Schematic view of the contact angle measurement system

First the syringe needle was placed as close as possible to the solid substrate surface. After the droplet was formed it was removed. The micrographs have been taken immediately after the syringe needle was removed. That avoiding to gain measurement mistakes of the droplet profiles in dependence with time. Before starting the measurements the used surface was carefully cleaned in order to

diminish results on the contact angle values from inhomogeneities and impurities on the solid substrate surface.

In Fig. 5-10 are micrographs shown of the droplets profiles.

In Fig. 5-11 are the measurement results plotted of investigations on the contact angle in dependence of the substrate surface temperature. For all presented data the substrate was used is a “steel rough” surface. An increase in contact angle results in a decrease in temperature. At least 5 measurements were taken for each pair suspension/substrate surface in order to obtain average values. All presented data show such an average value for the contact angle.

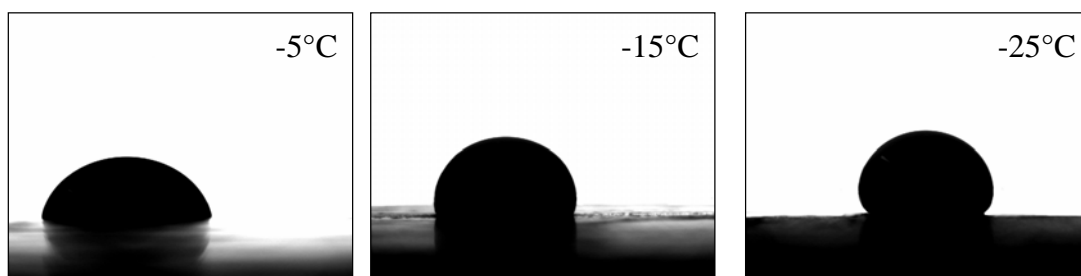


Fig. 5-10: Droplets profiles. Micrographs taken on “Steel polished” surface for 36 Vol.% solid load

From the data in Fig. 5-11 it can clearly be seen that the non-wetting behaviour of suspensions on the steel surface is increasing with decreasing temperature. The data of the other surfaces are shown in Appendix A. (The found behaviour is in principle the same as presented above). Figure 5-12 illustrates the contact angle measurements for suspension drops impacted onto the stainless steel or the cooper surfaces. Figure 5-12 evidently demonstrates that the contact angle is a direct correlation of the pair liquid substrate surface. The variations of the contact angle values have been found significant by varying the substrate material, which can be connected to differences in interfacial tension values. The substrate surface roughness has been found to have little influence on the contact angle in the range of the experimental settings. For example at -20°C for suspensions with 40 Vol.% solid load the difference of contact angle between steel rough and the polished surface is $1,2^{\circ}$ which lies in the error range of the measurement.

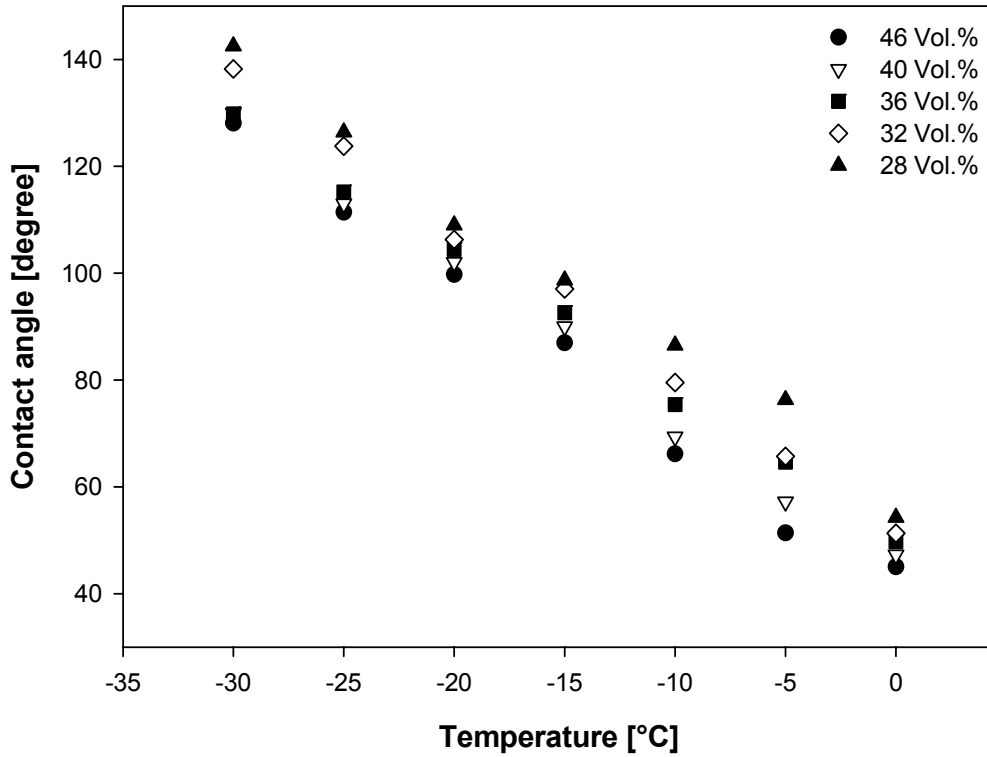


Fig. 5-11: Effect of temperature on contact angle. Measurements of a steel polished surface

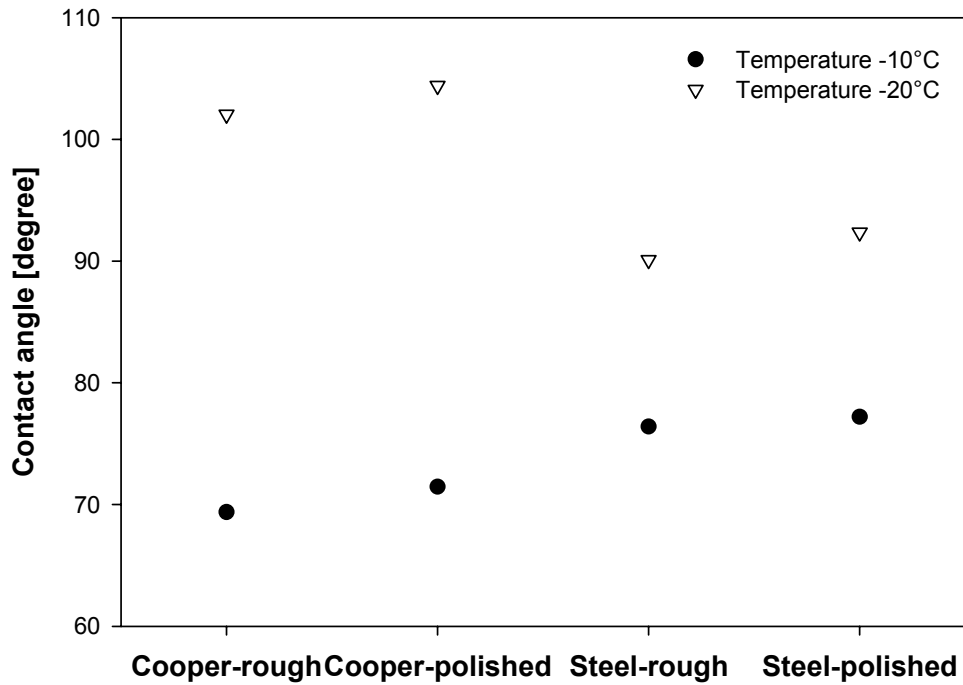


Fig. 5-12: Effect of substrate material and roughness on the contact angle for suspensions with 40 Vol.% solid load

5.2.1.3 Surface tension of suspensions

A Drop Shape Analysis System (DSA) was used to measure the surface tension. A chamber for temperature control was used. Two opposed walls of the chamber were made of glass. The temperature chamber was connected with a thermostat allowing adjustments of the desired temperature. The suspensions were put into the temperature chamber by using a syringe with a micrometer piston. A controlled volume of the suspension droplets was achieved by slowly moving the syringe piston to form a pendant drop hanged on the syringe needle. The syringe and the temperature chamber were placed in such a way that on the one side was a light source and on the other side a CCD camera and a microscope. The microscope was connected with a computer, which allows viewing the droplet profile on-line, recording the pictures and making those available for evaluations by using appropriate software. The formed droplets have different profiles in dependence of solid load content or temperature. The profile is a result of a reached equilibrium between droplet surface forces and its environment, respectively, (in presented data) and the gravitation forces. Drop profiles were recorded and evaluations over time intervals of 0,5 to 60s were carried out. The characteristic suspension densities obtained from density measurements (presented in Chapter 4.1.1) were entered into the software and the surface tension values were determined by analysis based on the Wu [Wu71, Wu82] and the Zisman [Zis64] technique.

The data obtained for suspension surface tensions versus temperature are plotted in Fig. 5-13.

The plot shows that with decreasing temperature the surface tension is slightly increasing. The experimental procedure was repeated at least 20 times and averaged results are presented.

The surface tension has been investigated in a temperature region between 0 and 20°C. Measurements for temperatures below 0°C have not been carried out because the suspensions start to freeze.

The surface tension has increased with increasing solid load content, which shows on the one hand that the ceramic particles become more surface active in aqueous suspension and the interactions between water molecules and ceramic particles is very strong. On the other hand the surface tension increases at high solid concentrations are less pronounced.

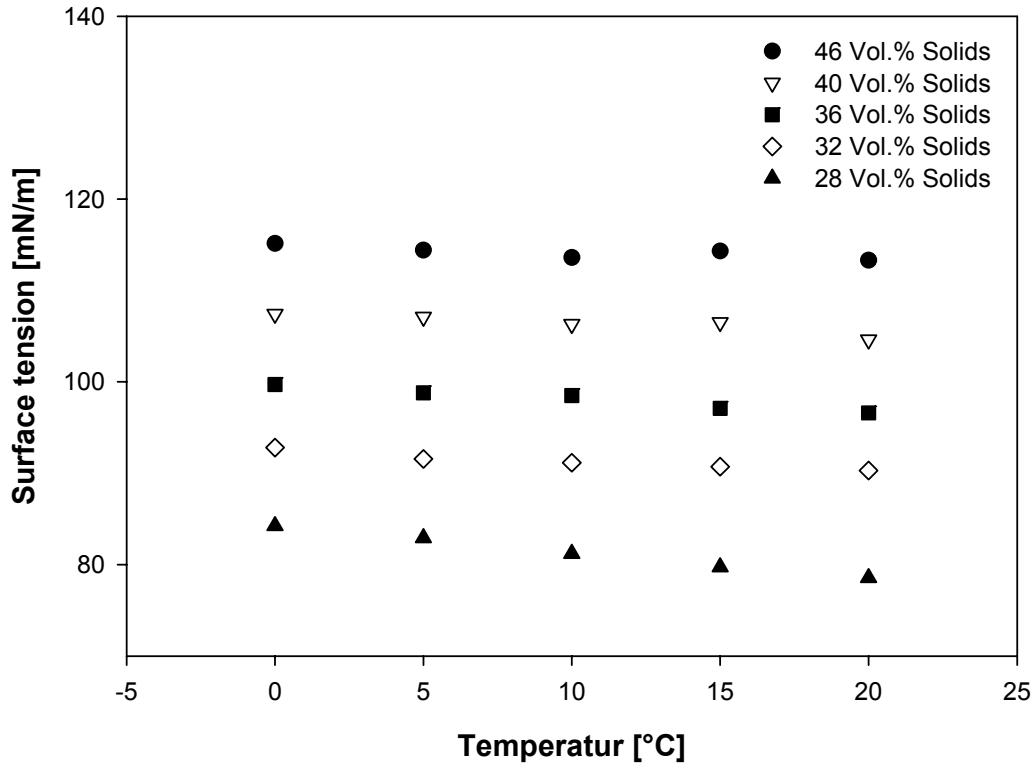


Fig. 5-13: Variations of surface tension as a function of temperature and solids load content

5.2.1.4 Interfacial tension, suspensions-cooling plate

For solid-liquid systems, the interfacial tension plays an important role not only in the stability of suspensions and the adsorption of molecules on solid surfaces but also in the classical description of the shape and kinetics of growth of crystals from solution or suspension [Wu99]. In Young's equation (2.10), which will be rewritten here, two of the parameters can be measured easily as shown in the Chapters 5.2.1.2 and 5.2.1.3, but these still leaves two unknown parameters σ_{sv} and σ_{sl} .

$$\cos \theta = \frac{\sigma_{sv} - \sigma_{sl}}{\sigma_{lv}} \quad (2.10)$$

To solve Young's equation at least one of them should be known. In many cases to measured solid-vapour interfacial tension σ_{sv} is very difficult or even impossible. One

of the most widely used methods to do so is Zisman's approach [Zis64, Sha60]. Zisman noted that by plotting the data for $\cos\theta$ versus σ_{lv} there is an linear dependence. The proposed function is:

$$\cos\theta = 1 - \delta(\sigma_{lv} - \sigma_c) \quad (5.5)$$

where δ is the slope of the curves $\cos\theta$ - surface tension and σ_c is the critical interfacial tension. The value of σ_c can be obtained by intercepting of the $\cos\theta$ - σ_{lv} plot to $\cos\theta=1$ or $\theta=0$. These conditions are corresponding to a complete wetting by a liquid of a substrate surface. The data from Chapters 5.2.1.2 and 5.2.1.3 have been used to attain Zisman's plot. The results for a rough steel plate are plotted in Fig. 5-14.

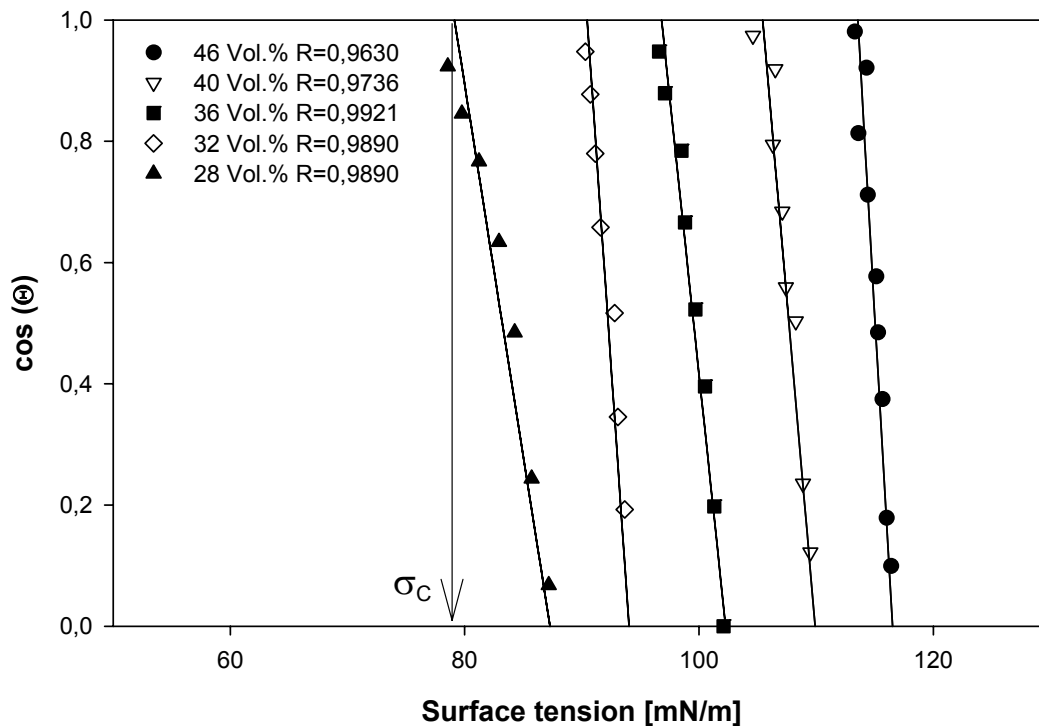


Fig. 5-14: Zisman's plot obtained from contact angle and surface tension measurements for determination of σ_c at steel rough plate

As can be seen from Figure 5-14 the liquid forms on the substrate surface a contact angle at $\sigma_c < \sigma_{lv}$ [Ozk04].

The results for the rest of the substrate surfaces are presented in Appendix B.

The values of critical interfacial tensions obtained from Zisman's plots are accessible in Table 5.2. The suspension surface tensions for low temperatures have been calculated by extrapolating data. It was impossible to obtain surface tension values for temperatures below 0°C, because of the air humidity freezing on the chamber windows and the freezing of the suspensions in the syringe needle.

Table 5.2: Values of critical surface tensions obtained from Zisman's plots for different surfaces

Solid Content\ Surface	Steel rough mN/m	Steel polished mN/m	Cooper rough mN/m	Cooper polished mN/m
46 Vol.% Solids	113,3	113,4	113,9	114
40 Vol.% Solids	105,5	105,3	105,9	106
36 Vol.% Solids	96,7	96,5	97,5	97,5
32 Vol.% Solids	90,3	90,3	90,8	90,9
28 Vol.% Solids	78,9	78,7	79,9	79,9

To obtain data for the interfacial tension between liquids and solid substrate surfaces the Zisman's approach (Eq. 5.5) was used.

The contact angle was measured at +20°C down to -30°C. Therefore the interfacial energy between the substrate and the liquid (suspension) phase at the freezing temperature increased due to the increased surface energy of the substrate. Also the surface tension of water, which is the liquid phase in the used suspensions, is increasing due to decreasing temperature [Wea89]. Therefore incensement of interfacial energies have been supposed and evidently found by calculations. The calculations obtained by the Zisman's approach for solid vapour interfaces are presented in Fig. 5-15. Subsequent calculations using Young's equations have been carried out to attain the interfacial tension between suspensions and substrate surfaces. The above calculations show that the interfacial energy increases as the

surface energy increases. Results from above mentioned calculations are shown in Fig. 5-15.

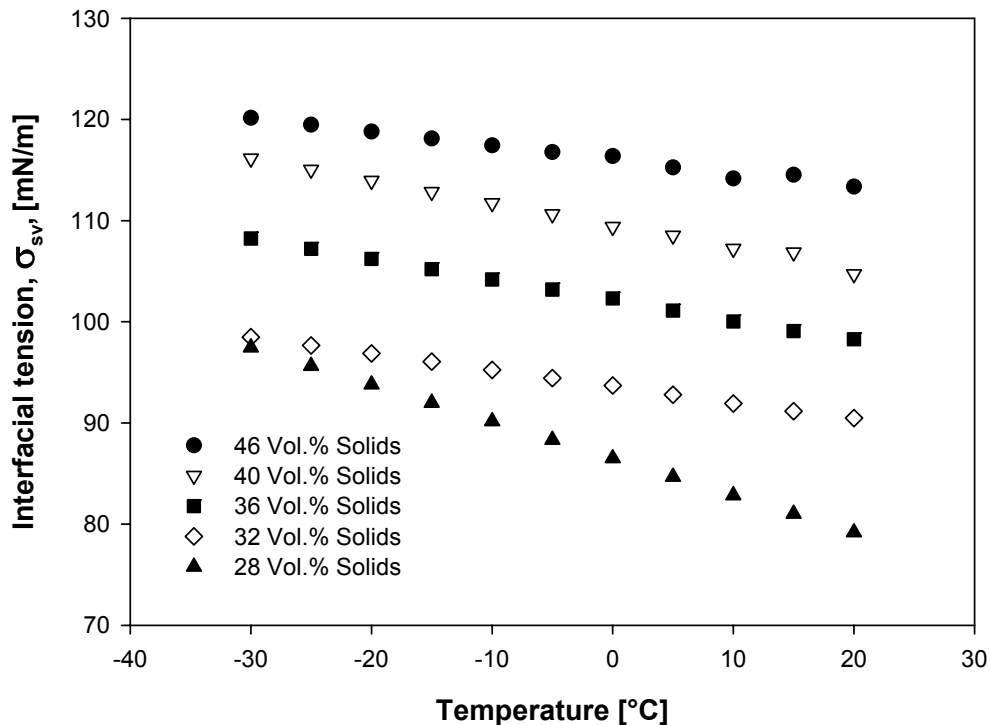


Fig. 5-15: Calculated interfacial tension substrate-vapour σ_{sv} at steel rough plate

In Appendix C results for the other three surfaces are presented, showing in principle the same behaviour as the presented results.

Calculations for interfacial tension substrate-suspension σ_{sl} versus temperature obtained by Young's equation are given in Fig. 5-16. The plot shows that starting from relatively high temperatures, about 20°C, the interfacial tension quickly increases with decreasing temperature.

From Fig. 5-16 it can clearly be seen that with increasing solids content interfacial tension σ_{sl} is also increasing. As the solids concentration increases, the particles in the suspension become more highly packed. Such a packing or agglomerates will effect on the interface resulting as increasing of interfacial tension. The rest of results for the other used plates are presented in Appendix C. All data have the same behaviour as the presented results. In Fig. 5-17 are the results shown for interfacial tension versus temperature for the same solids load contents on different surfaces. As can be seen the dependence of the interfacial tension on substrate (cooling plate) material is clearly noticeable, however, the effect of roughness can be neglected.

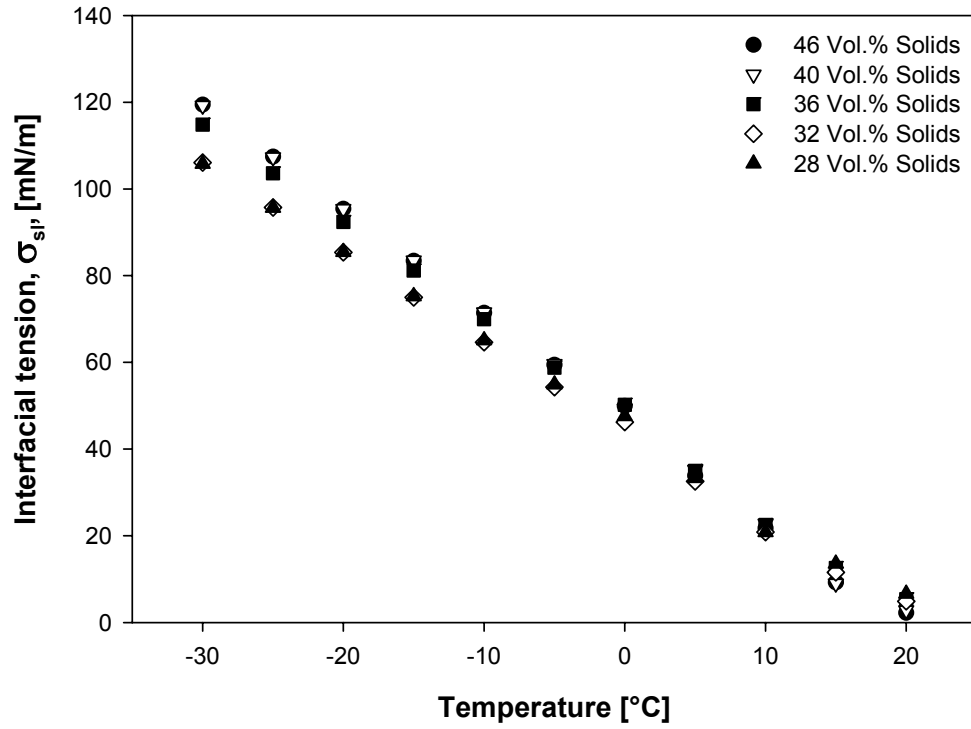


Fig. 5-16: Calculated interfacial tension substrate-suspension σ_{sl} at rough steel plate

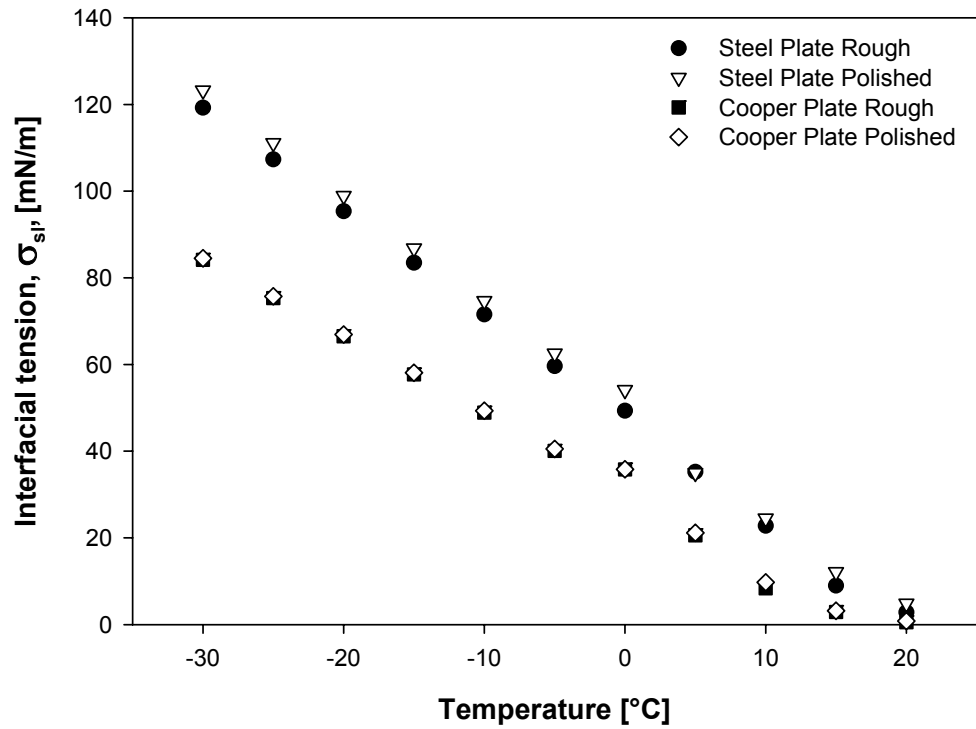


Fig. 5-17: Calculated interfacial tension substrate-suspension σ_{sl} for 40 Vol.% solids at different plates

5.2.1.5 Nucleation kinetic

To calculate the critical nucleus radius the latent heat of fusion is needed (see Eq. 2.5). The latent heat can be described as enthalpy changes associated with the phase change [Mye01].

The measurements of latent heat of fusion are very difficult and not very accurate, therefore here a simple approximation is used for the calculation of standard heats of formation developed by Felder and Rousseau [Fel86], which for inorganic compounds can be expressed as follows:

$$\Delta H_m \approx 0,025T_m \quad (5.7)$$

where ΔH_m is the latent heat of fusion in kJ/mol and T_m is the melting temperature in Kelvin. The melting temperature data for the used ceramic suspensions have been obtain by DSC measurements and will be discussed in Chapter 5.2.1.6.

Calculations for the radius of the critical nucleus have been done by using Eq.4.8 [Mul01]:

$$r_c = \frac{2\sigma_{sl}T^*}{\Delta H_m \Delta T} \quad (5.8)$$

where $\Delta T = T^* - T$ is the supercooling. From this equation it can clearly be seen that the critical radius of the nucleus is very sensitive to interfacial tension and that the key importance is with the supercooling. Such behaviour has been observed in all calculations.

Fig. 5-18 shows the variations of the size of the critical nucleus versus supercooling for different solid loads. The value of the critical radius of the nucleus is decreasing with increasing supercooling. The results show that supercooling has the main influence even the solid loads are less important. The rest of calculated results are presented in Appendix D.

From Fig. 5-19 it can be seen again that the weight of the radius of the critical nucleus given by supercooling and interfacial tension and substrate surface roughness is only of minor importance.

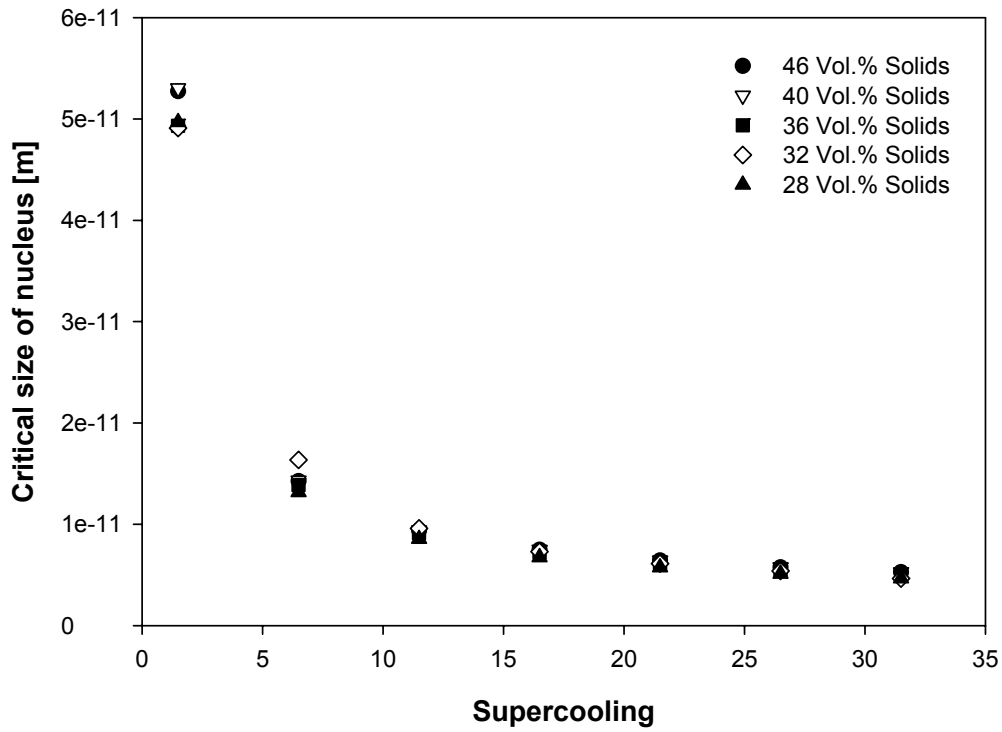


Fig. 5-18: Critical nucleus size for a rough steel plate

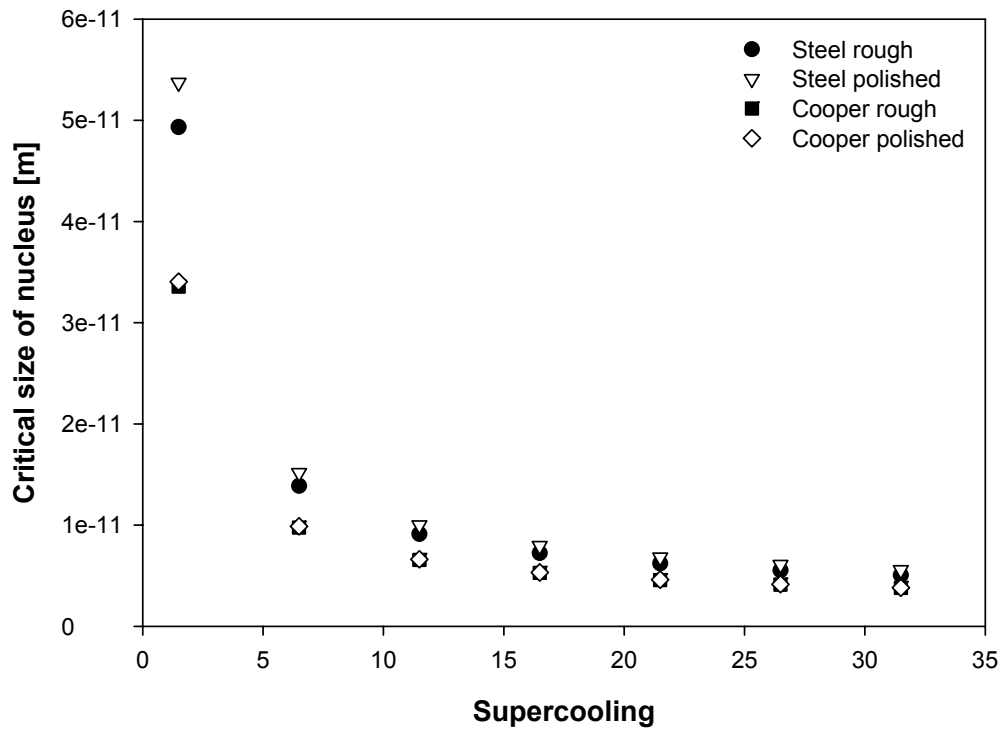


Fig. 5-19: Critical nucleus size for suspension with 36 Vol.% solid loads on different substrate surfaces

Fig. 5-20 shows the data obtained for a critical free energy, ΔG_{crit} this is the energy needed to form stable nuclei with critical size. Once again supercooling comes into view as a main parameter for controlling critical sizes of nuclei, decreasing the critical energy by increasing supercooling.

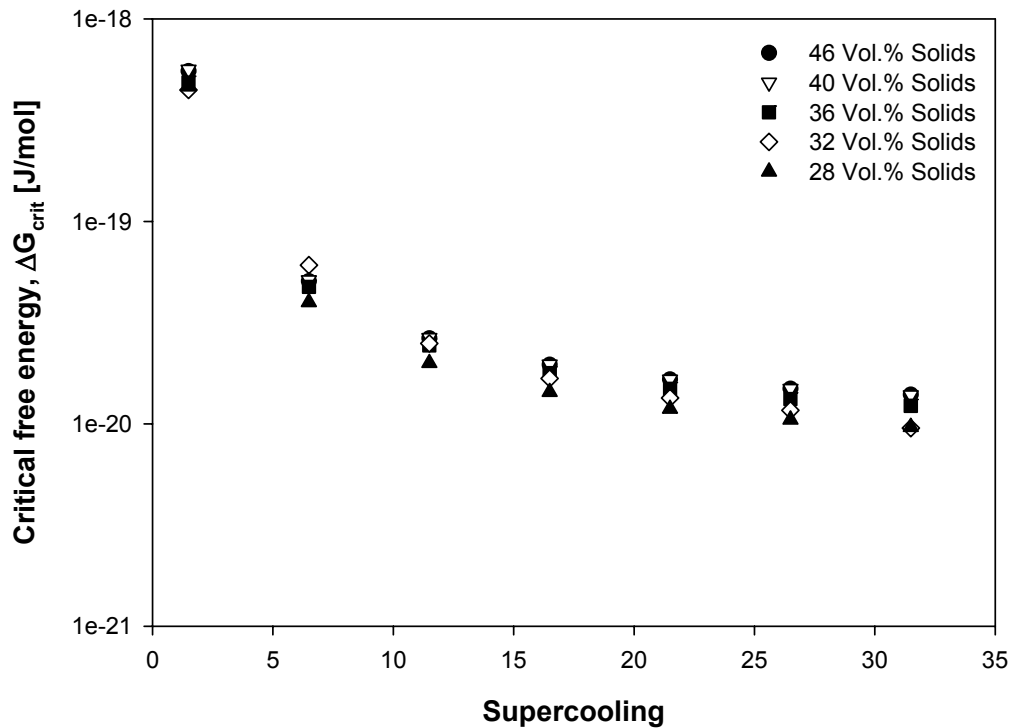


Fig. 5-20: Critical free energy for steel rough surface

In Fig. 5-21 are calculations presented for the volume free energy versus supercooling. From the figure it can be seen that with increasing supercooling the volume free energy is decreasing and the difference is getting smaller. A dependence on solid load contents has only been observed at low supercoolings. In Fig. 5-22 are the data given for the volume free energy for suspensions with 36 Vol.% solid loads at different substrate surfaces. Similar as in the previous results a distinction in volume free energy at high supercoolings cannot be found. At low supercoolings divergences are higher. Cooper surfaces show less divergence on the volume free energy in dependence on surface roughness. Such differences can be found at steel surfaces, which have more inhomogeneous structure (see Chapter 5.2.1.1).

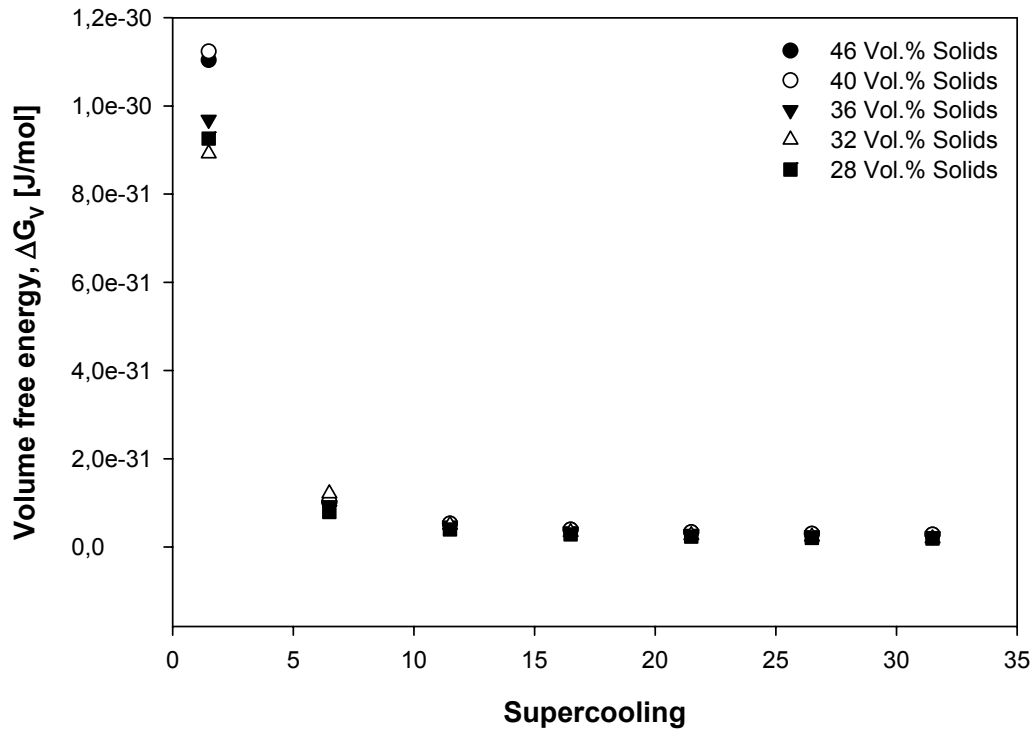


Fig. 5-21: Volume free energy for a rough steel surface

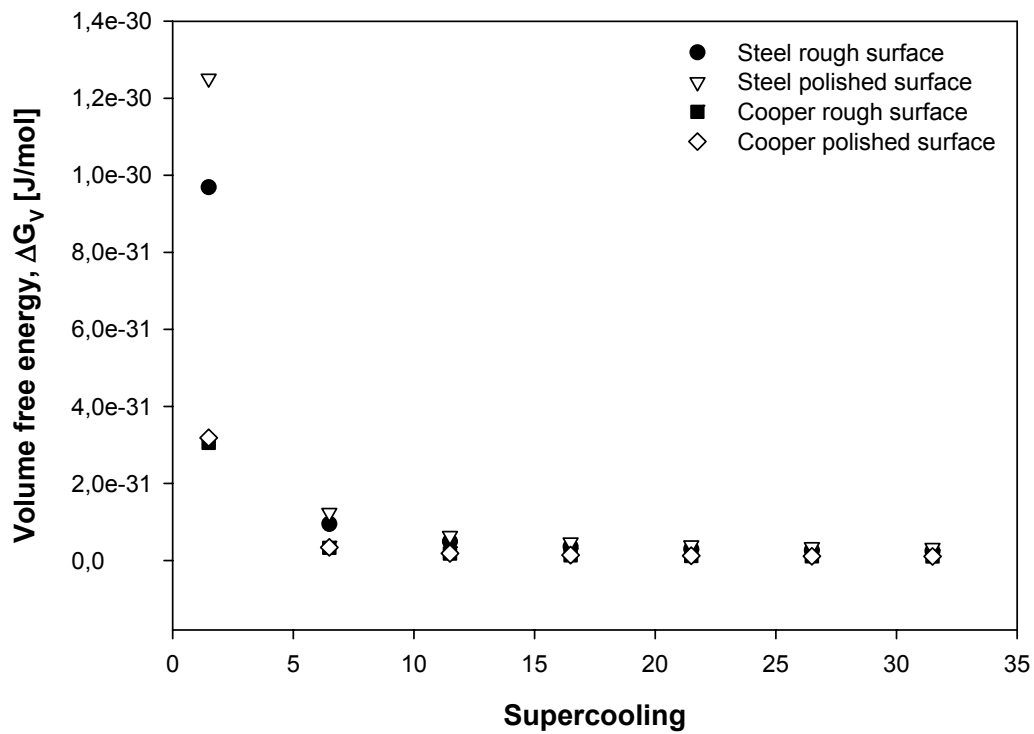


Fig. 5-22: Volume free energy for suspension with 36 Vol.% solids at different surfaces

In Fig. 5-23 are the results of calculations plotted for free surface energy versus supercooling. Similar results have been found for the volume free energy. Surface free energy is decreasing with increasing supercooling.

Differences in the values of surface free energy in dependence of solid load contents can be found only at low supercoolings, but with increasing supercooling it becomes smaller and can be neglected.

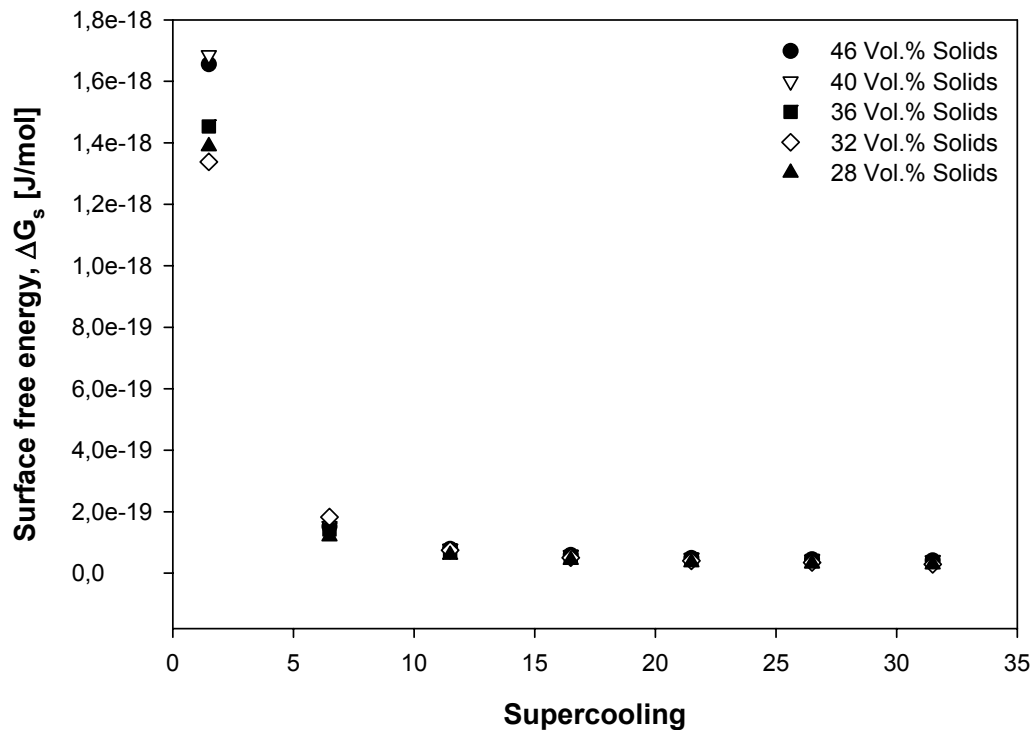


Fig. 5-23: Surface free energy for a rough steel surface

The results for volume and surface free energies for other surfaces are accessible in Appendix D, showing equivalent behaviour as the presented results.

The energetic of the heterogeneous nucleation can be described in terms of homogeneous nucleation, by using a single parameter f , which is a function of the contact angle (see Eq. 2.9). In Fig. 5-24 are results of calculations presented for the Gibbs free energies for homogeneous nucleation versus supercooling which are used to calculate free energies required for heterogeneous nucleation. In general results for free energies show strong dependence on supercooling.

Influences gained from solids concentration have been observed only at low supercoolings. But this effect becomes less pronounced as supercooling increases.

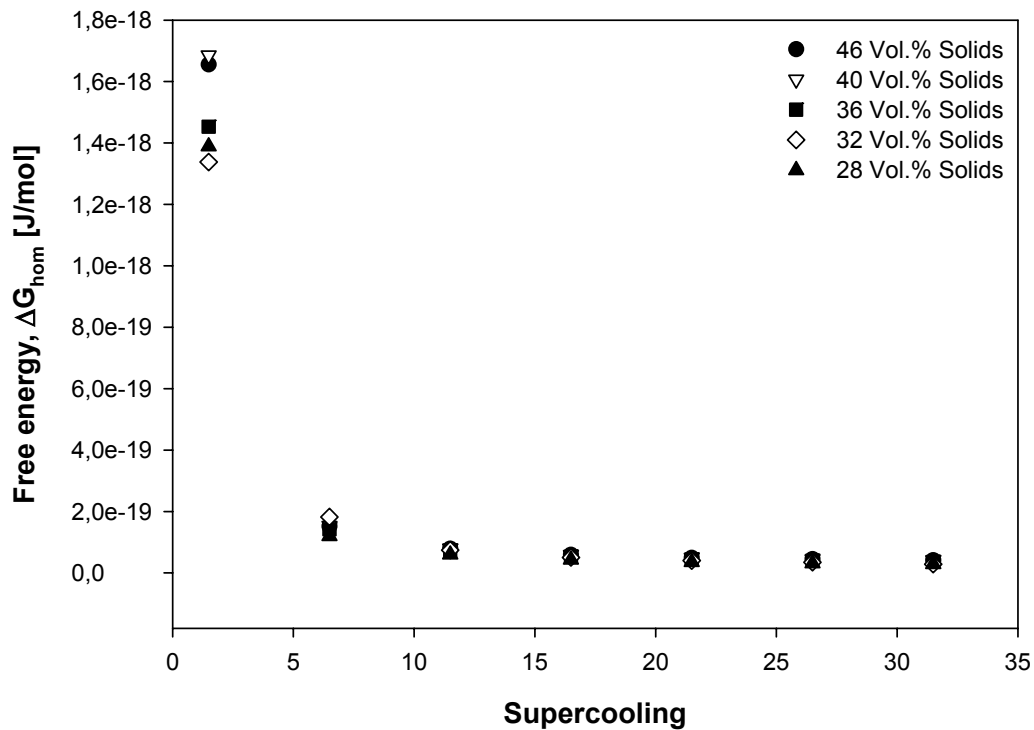


Fig. 5-24: Gibbs free energy for homogeneous nucleation at a rough steel surface

In Fig. 5-25 the factor f is plotted against the contact angle. When $f=1$, corresponding to $\Theta=180^\circ$, or point contact with substrate surface is happening homogeneous nucleation takes place. In case of $f=0$ ($\Theta=0^\circ$) or complete wetting heterogeneous nucleation occurs. In all cases for contact angles between $0 < \Theta < 180^\circ$ partial wetting of substrate surfaces is observed. Smaller contact angles are favourable energetically and the system will easily reach the state of critical conditions. From Figure 5-25 it can be seen that investigations have been done in almost the complete range of the f factor.

The factor f has been found to have strong temperature dependence and a very small dependence on surface roughness. Those statements have the following effect on the Gibbs free energy required for heterogeneous nucleation.

For the completion of the calculations for the heterogeneous nucleation Eq. 2.8 has been used and the data are given in Fig. 5-26. As shown in the Figure 5-26 Gibbs free energy is strongly related to the supercooling.

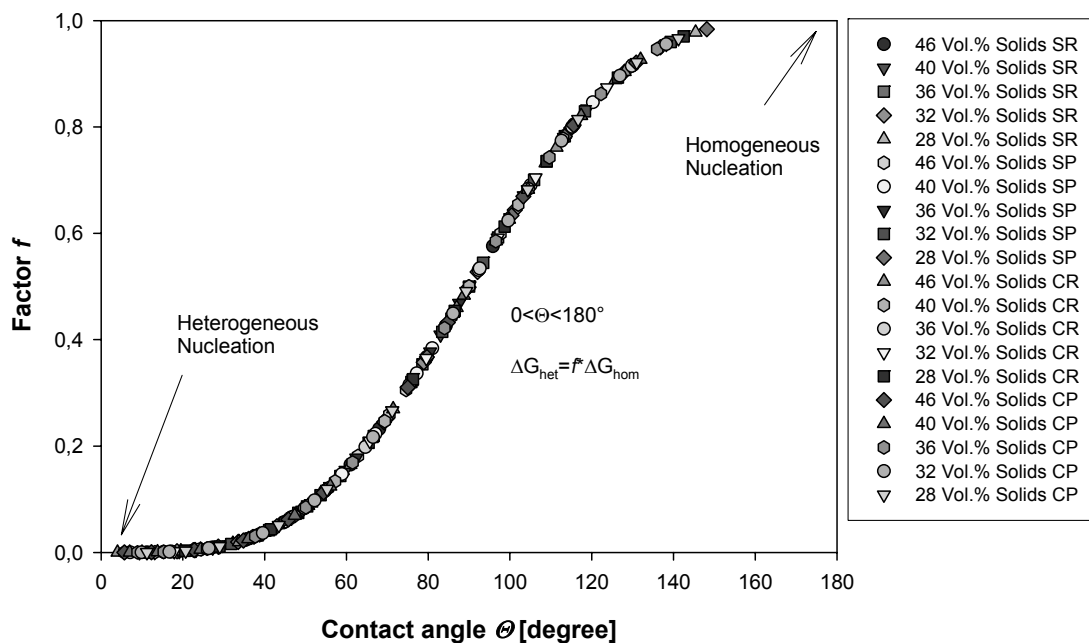


Fig. 5-25: Calculations of f -factor for different surfaces. On the diagram SR is the abbreviation of a rough steel surface, SP- steel polished, CR- cooper rough and CP cooper polished

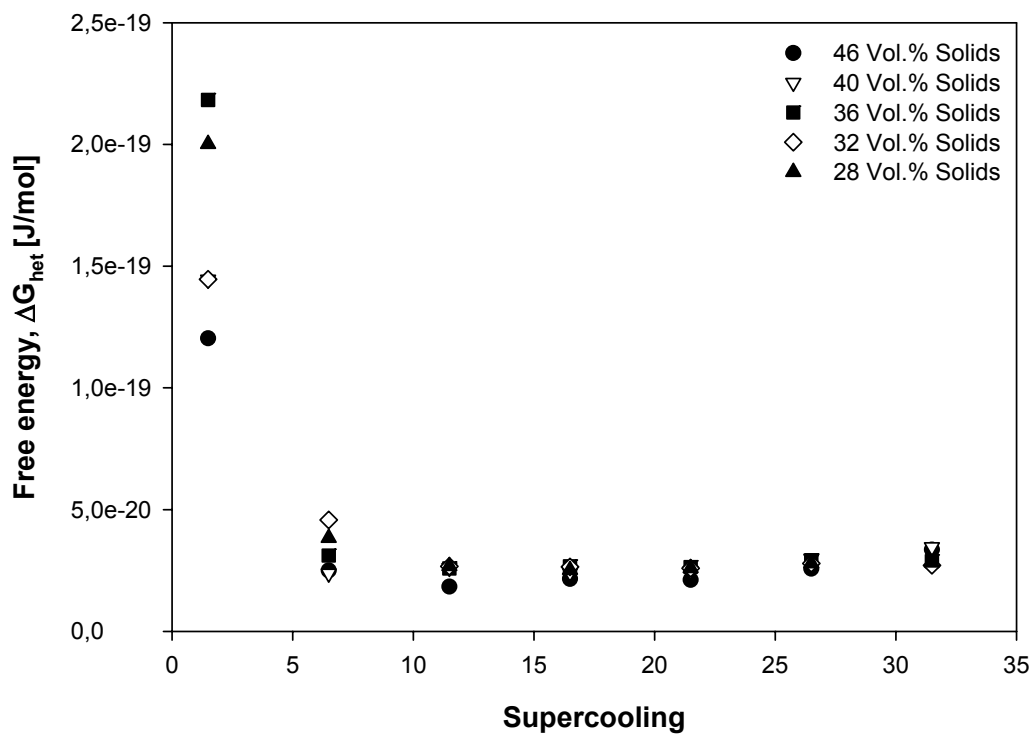


Fig. 5-26: Effect of supercooling on Gibbs free energy for heterogeneous nucleation on a rough steel surface

Most of the investigations on the temperature dependence of the free energy have been focused on relatively low supercoolings and practically no data have been found for high supercooling regimes.

The results for Gibbs free energy for heterogeneous nucleation for the rest of the surfaces are presented in Appendix D showing the same behaviour.

In Fig. 5-27 is the behaviour shown of ΔG_{het} as a function of substrate surface properties. The Gibbs free energy is influenced by the surface energy, which can be well observed at low supercoolings. With increasing supercooling the margin between energies is getting smaller. The free energy changes on a steel surface are much larger than that on a copper surface, however, roughness has been found to be almost of no relevance.

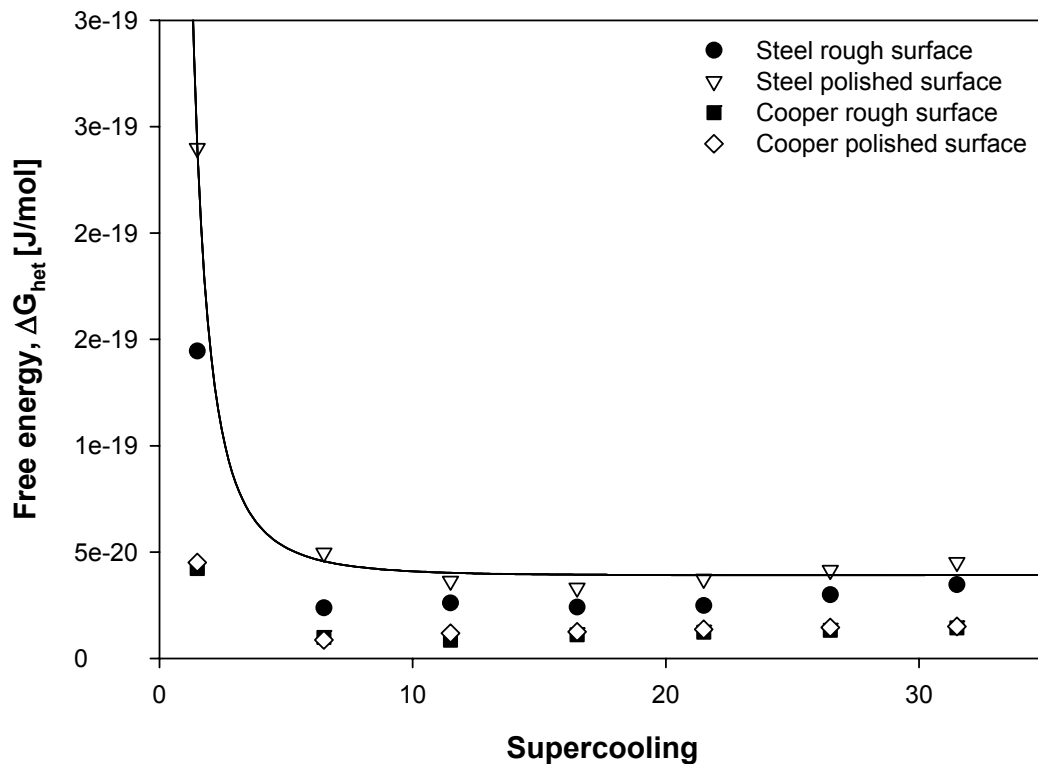


Fig. 5-27: Effect of substrate surface properties on Gibbs free energy for suspension with 36 Vol.% solids

In all the cases the data exhibit the same general temperature dependence behaviour but also indicate the relations with surface characteristics. This is also consistent with the contact angle temperature dependence.

All results reported in this section are in a good agreement with classical nucleation theory. The temperature dependence of Gibbs free energy is very similar to that reported by Mullin [Mul01].

5.2.1.6 Determination of freezing and melting temperatures

5.2.1.6.1 Cooling curves

If a crystalline solid is heated up its building blocks from which it is built start rapidly to vibrate in their positions. At melting temperature these vibrations overcome forces, which keep the lattice, and melting occurs. The temperature remains constant until the material is fully melted. The liquid and solid phase exist in equilibrium only at this temperature. Thereafter, the temperature of the resulting liquid starts to increase. The energy required to melt a solid is known as the heat of fusion. If the same liquid is cooled these processes are reversed. The temperature at which the liquid turns solid (nucleation occurs) is called freezing temperature. When a liquid freezes, energy is released to the surroundings. For pure substances freezing and melting temperatures have the same values at constant pressure. This remains on cooling or heating temperatures allows the melting, respectively freezing points to be identified on a time-temperature curve.

The temperature at which nucleation occurs has been experimentally detected by using the second freezing device, schematically presented in Fig. 3-3. The suspensions were filled into disc openings. The upper reservoir was taken off and in this way the suspension's upper face meets atmosphere at ambient conditions. A programmable thermostat controlled the temperature in the bottom reservoir. Each disc was connected with a thermocouple and the data logger. The data logger was connected with a computer having appropriate software allowing following the temperature changes in-line and saving the data for further estimations. Nývlt et al. [Nýv77] reported that the values of the freezing temperature might vary in dependence of the cooling speed because it takes time until heat removed by cooling is compensated by the latent heat of the phase change. Therefore, two cooling rates have been applied and the freezing behaviour was observed. Cooling of suspensions always has started at room temperature and was completed at -40°C . Only on one position deviation from linearity has been observed. In Fig. 5-28 are cooling curves

presented for suspensions with 36 Vol.% solid loads. The zoomed region represent the deviation from linearity respectively the temperature at which nucleation occurs.

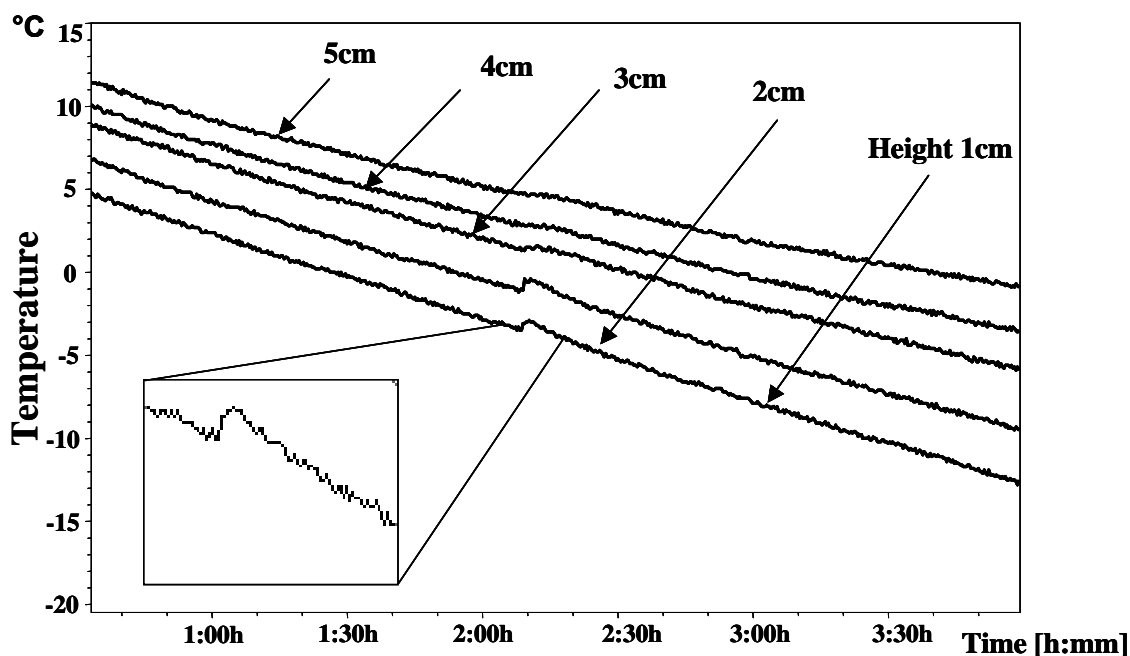


Fig. 5-28: Cooling curves for suspension with 36 Vol.% solids and cooling rate 0,08 K/min

5.2.1.6.2 Melting points

The examination of melting temperatures has been carried out by DSC measurements. Two Al crucibles were used one containing the sample and the other one is used as reference. It is recommended that prior to the scan start the crucibles should be kept at constant temperature for equilibration of temperature.

The measurements are divided in 4 steps. In a first step the temperature was kept constant at 10°C for 2 minutes and the suspensions were cooled down to -30°C in the second step. In the third step samples were heated up to 10°C. At fourth step samples were kept at constant temperature of 10°C for 2 minutes. For second and third step heating respectively cooling rates were set to 1K/min allowing detailed observations of heating- cooling behaviour. The same cooling heating rates were applied in all measured suspensions. The data obtain from the measurements have been recorded by a computer for further evaluations.

In Fig. 5-29 is represented the third part of the measurement steps. Other picks have not been detected in the third step.

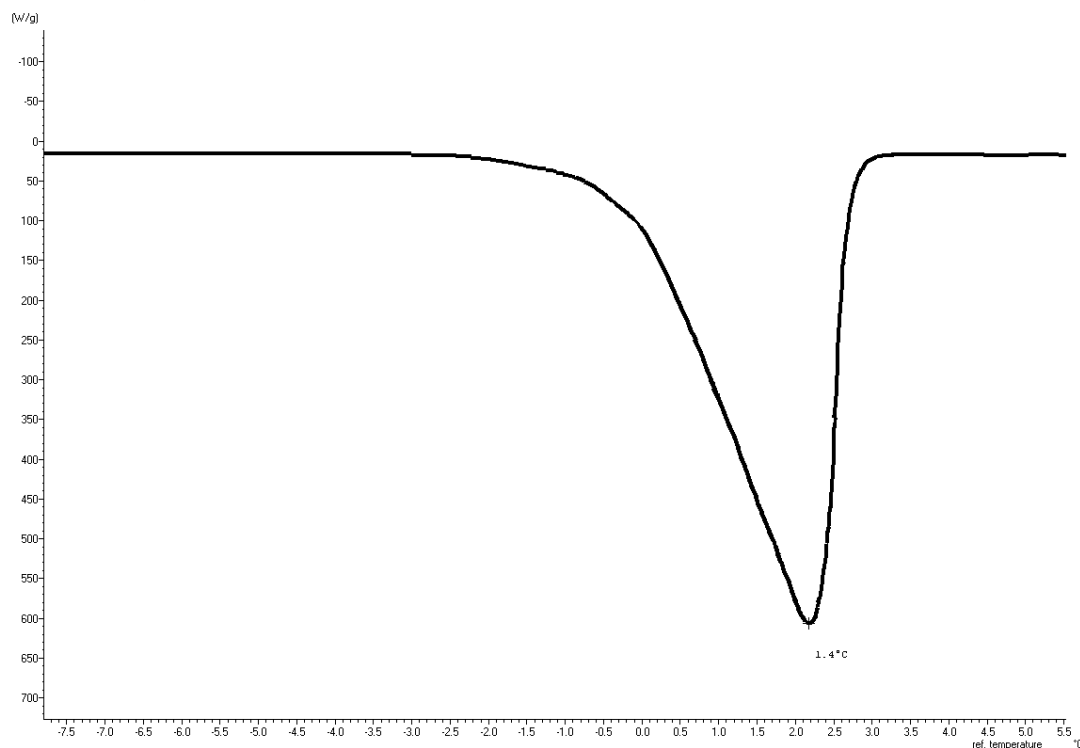


*Fig. 5-29: DSC measurement of suspension with 36 Vol.% solid load
at a heating rate 1K/min*

The data obtained for the melting and freezing temperatures are given in Fig. 5-30. As mentioned above two cooling rates have been utilized but as can be seen from the figure obviously the cooling rate has only a small effect on freezing temperature and can therefore be neglected. Small deviations in the melting temperature have been observed in dependence of solid load content. The presence of solid load amount seems to restrain the melting temperature.

By decreasing the amount of solids the difference between melting and freezing temperature become smaller. All presented results are averaged from several measurements.

The knowledge of the freezing temperature is important in crystallization because it gives assistance in understanding of the nucleation behaviour.

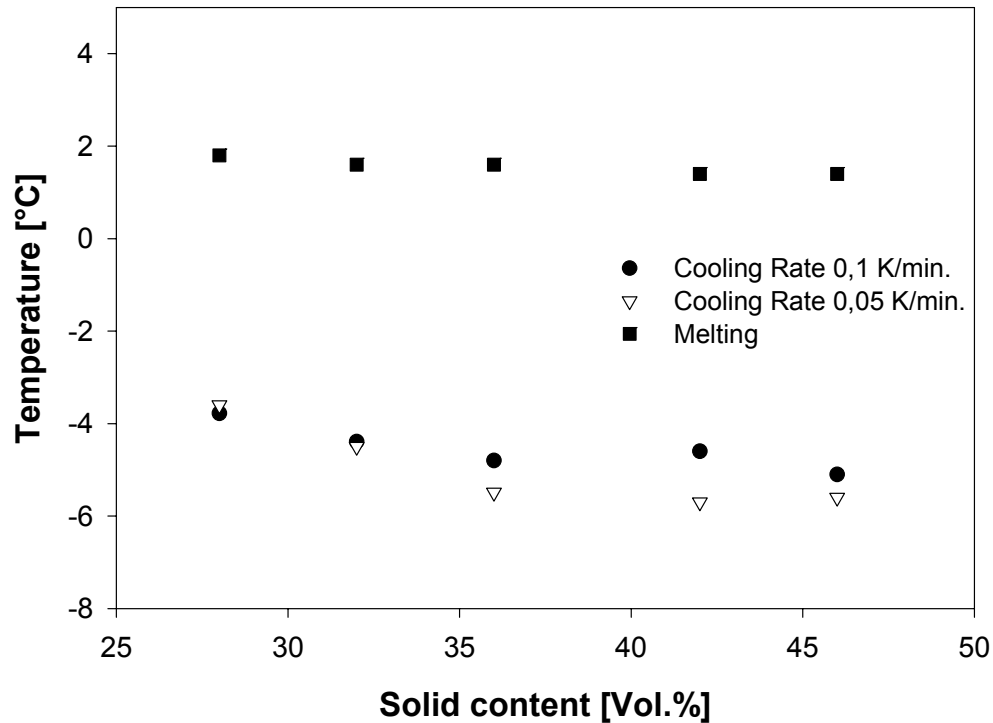


Fig. 5-30: Melting and freezing temperatures for suspensions with various solid contents

5.2.2 Crystal growth rate

When the crystal nuclei reach the critical size they begin to grow. In order to attain the essential properties of the crystals and to operate the process the behaviour of crystal growth should be known.

In the Freeze-casting process ice crystals are used as negative image giving procedure. The ice crystals are therefore determining morphology and size of the pores to be obtained. Therefore a good understanding of crystal growth behaviour is necessary. Good understood data will promote better-defined initial conditions, which would supply better understanding of the correlation between crystal growth rate and the crystal size. A linear growth rate (Eq. 2.21) has been applied to calculate crystal growth. For this purpose the freezing device presented in Fig. 3-2 has been employed. The thermostated cooling cell was fixed stationary and the CCD camera and microscope was positioned in such a way that it can be moved up and down.

This construction enables observing the molding form from bottom to the upper face. The molding form was fixed on the cooling cell. By this way the construction allowed to follow crystal growth, in-line, during freezing by means of microscopic observation. Very little Methylene blue was mixed in the suspensions, before starting the measurements. Making the ice crystals coloured to have them easily to be distinguished them from the frozen surface. The freezing front, respectively the growing ice crystals, has been observed parallel to the growth direction by CCD camera and microscope. By connecting the microscope with computer it is possible to view in-line the freezing process and taking pictures, which can be saved for further investigations (see Fig. 5-31). Pictures were taken frequently, immediately after pouring ceramic suspension into the molding form.

On the molding form wall was pasted a thin colourless film with a millimetre scale from the bottom up to the upper face. This scale was used to calculate the distance from the cooling plate and the distance covered from ice crystals during freezing.

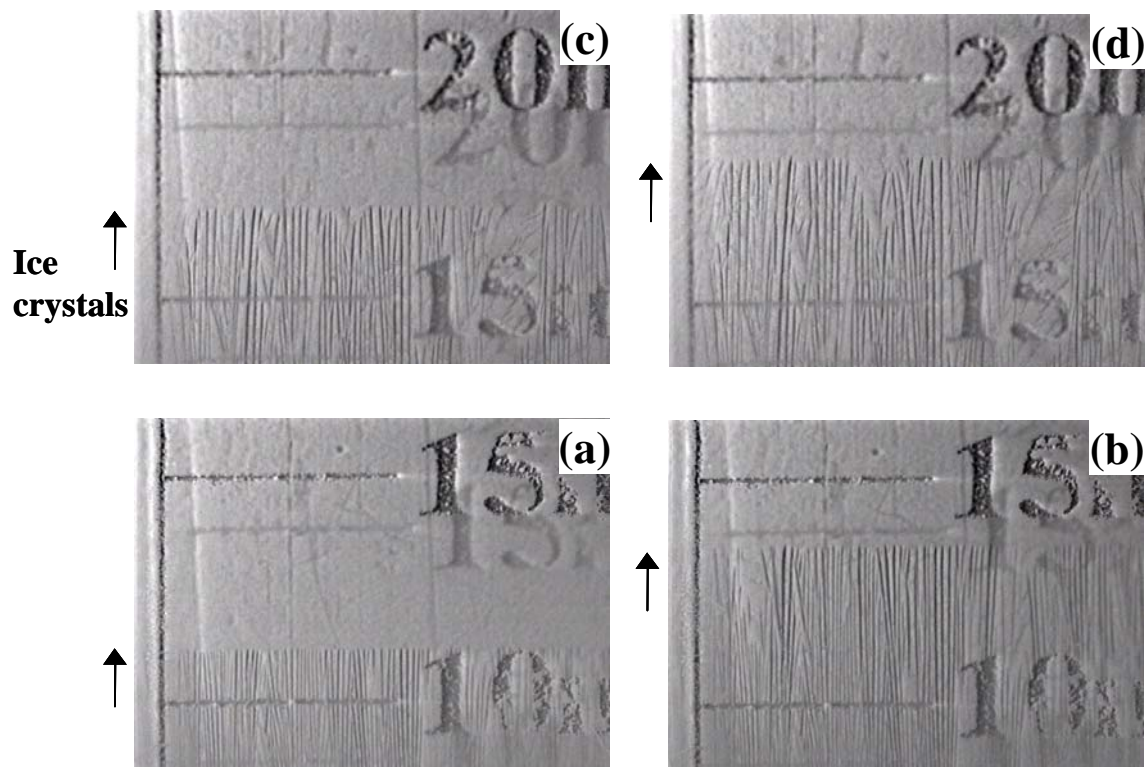


Fig. 5-31: Micrographs taken parallel to the ice crystals growth direction for suspensions with 36 Vol.% at freezing temperature -25°C . (a) 10min. (b) 15min (c) 25min (d) 30min after freezing starts

In Fig. 5-32 are the data given on crystals growth rates for different solid loads versus distance from cooling plate. Here are averaged values presented of several experiments. The experiments yield highly reproducible results for crystal growth rates.

5.2.2.1 Influence on crystal growth rate in dependence of the volume fraction of solids

From Fig. 5-32 it appears that the growth rate is high at a small distance from the cooling plate and then exponentially slows down. This is attributed to a decreasing temperature and to an increase of the thermal resistance obtained from already frozen suspension.

Correspondingly to the volume fraction of solids in suspensions it has been observed a decrease in the growth rate by decreasing solid amounts. This can be associated to enlarge of the water amount, which requires more time and more cooling.

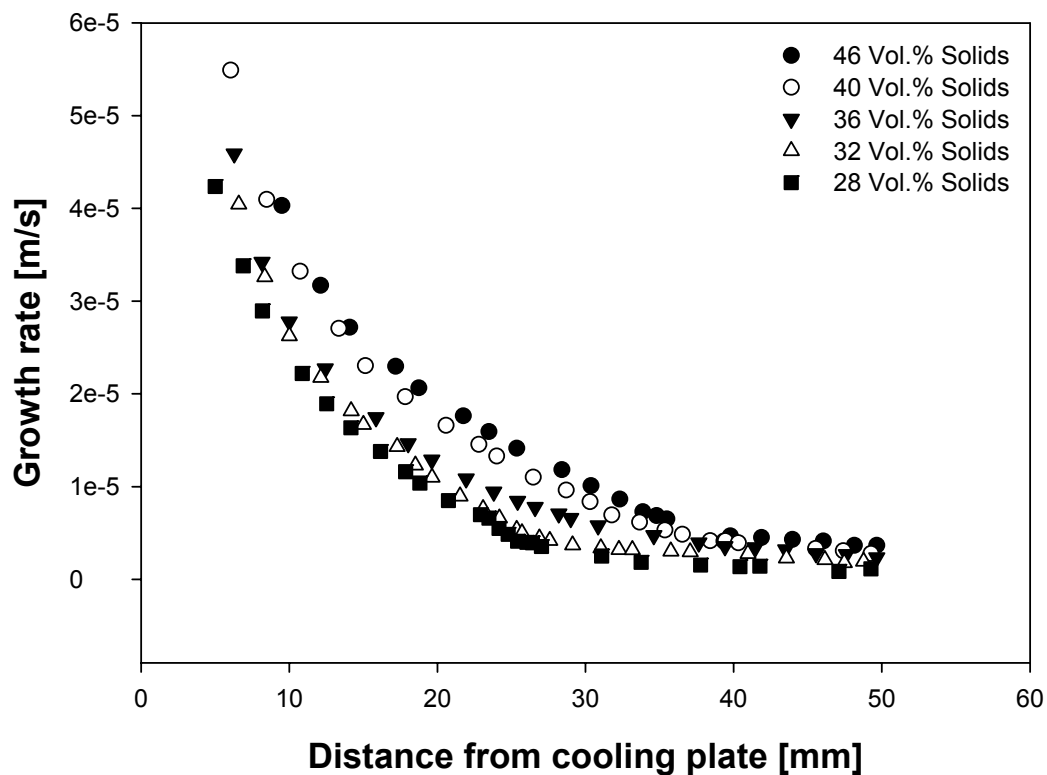


Fig. 5-32: Crystal growth rate for suspensions with different solid loads content frozen at -30°C on a rough steel plate

The effect of freezing temperature on growth rates has been investigated. Experimental data of the crystal growth rates of a suspension with 36 Vol.% solids at different freezing temperatures are plotted in Fig. 5-33. In the figure it is clearly to be seen a relation between freezing temperature and growth rate. By decreasing

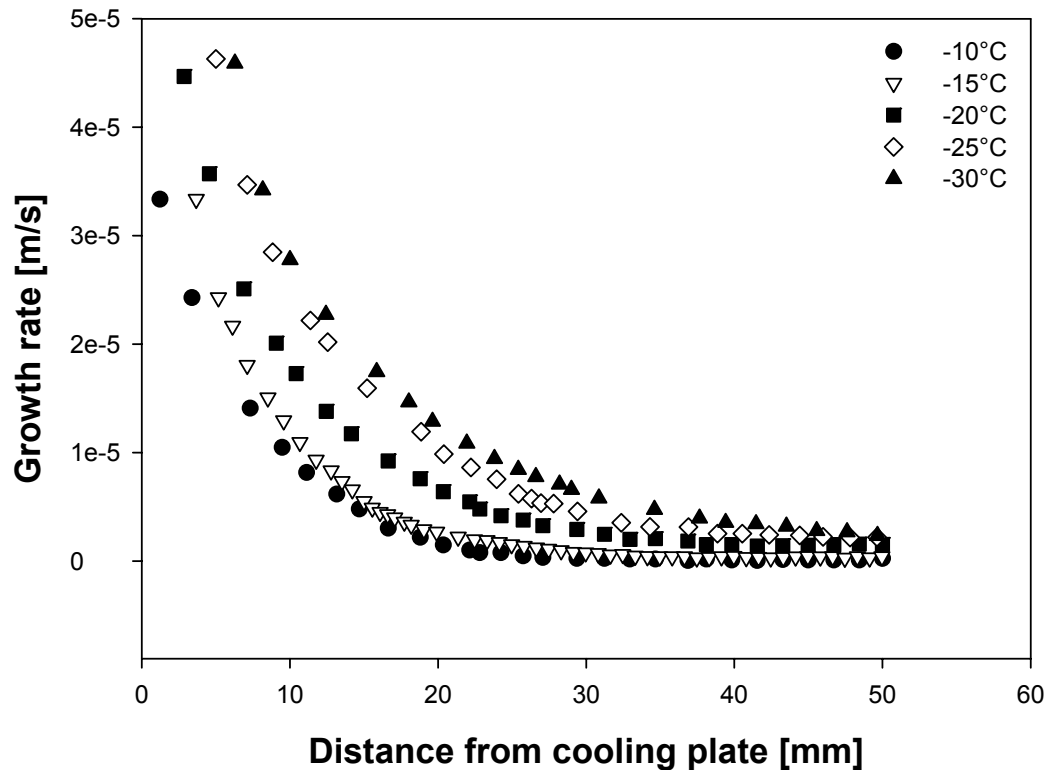


Fig. 5-33: Crystal growth rate for suspensions with 36 Vol.% solid loads at different temperatures on a rough steel plate

temperature the growth rate is increasing. At a small distance to the cooling plate the difference between growth rates is larger and there is a decrease with increasing distance from the cooling plate. In the earlier stage of freezing the driving force for crystallization, the temperature gradient, is very powerful and results in fast growth of the crystals. With increasing distance from the cooling plate the frozen layer act as an insulator and decreases the temperature gradient, therefore the growth rate is decreasing. By increasing the distance from cooling plate the difference between the growth rates is decreasing.

For the rest of the suspensions the data on crystal growth rates are presented in Appendix E. All investigated suspensions show the same growth behaviour as the above presented.

Statham et al. [Sta98] has observed that the cooling rate has a large effect on the size and porosity formed. They found that at rapid cooling of the ice crystals results in a very fine structure. At intermediate cooling rates the ice structure is mainly columnar. A dendritic structure of ice has been found at low cooling rates. The same phenomena have been observed here even the materials of the suspensions are different. In Fig. 5-34 are presented the ice formations at different distances from the cooling plate. In micrograph (a) it can be clearly distinguished a fine columnar structure. (b) shows again a columnar structure but with an increase in crystal sizes. Micrograph (c) shows the beginning of a dendritic growth, which can clearly be seen in micrograph (d).

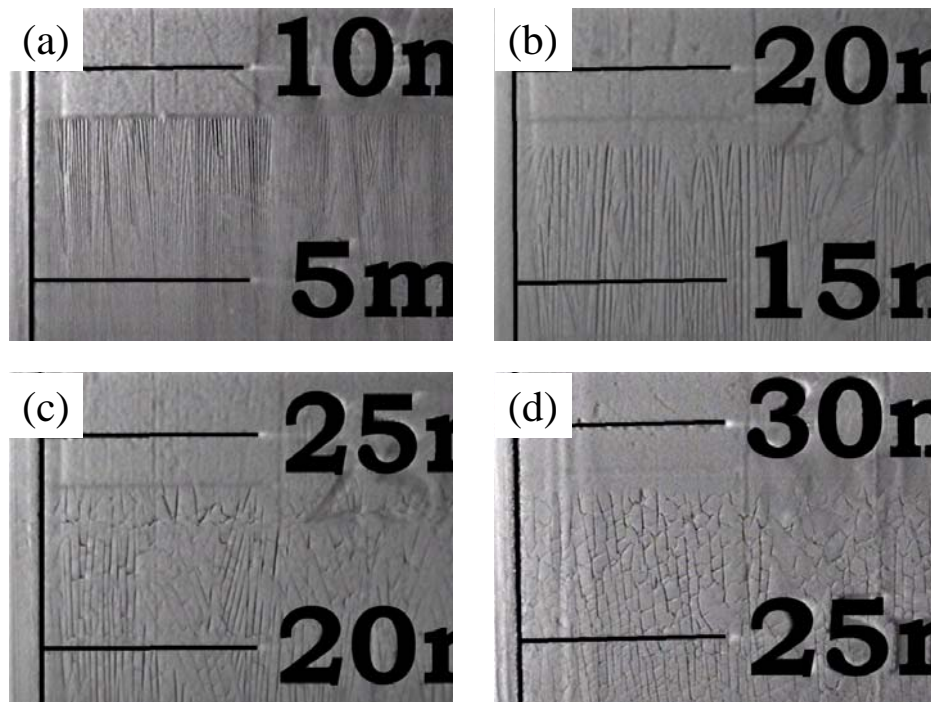


Fig. 5-34: Micrograph taken from the molding form wall for a suspension with 32 Vol.% solid loads, freezing temperature -25°C

5.2.2.2 Influence on crystal growth rate in dependence on cooling plate materials and properties

The influence on growth rate gained from cooling plate materials and their properties has been investigated. In Fig. 5-35 are the experimental results presented from growth rate measurements on the four cooling plates used for the contact angle

measurements. For all utilized surfaces there has been observed the same growth behaviour. It is a fast growth near the cooling surface and exponential decrease by increasing distance from the cooling plate.

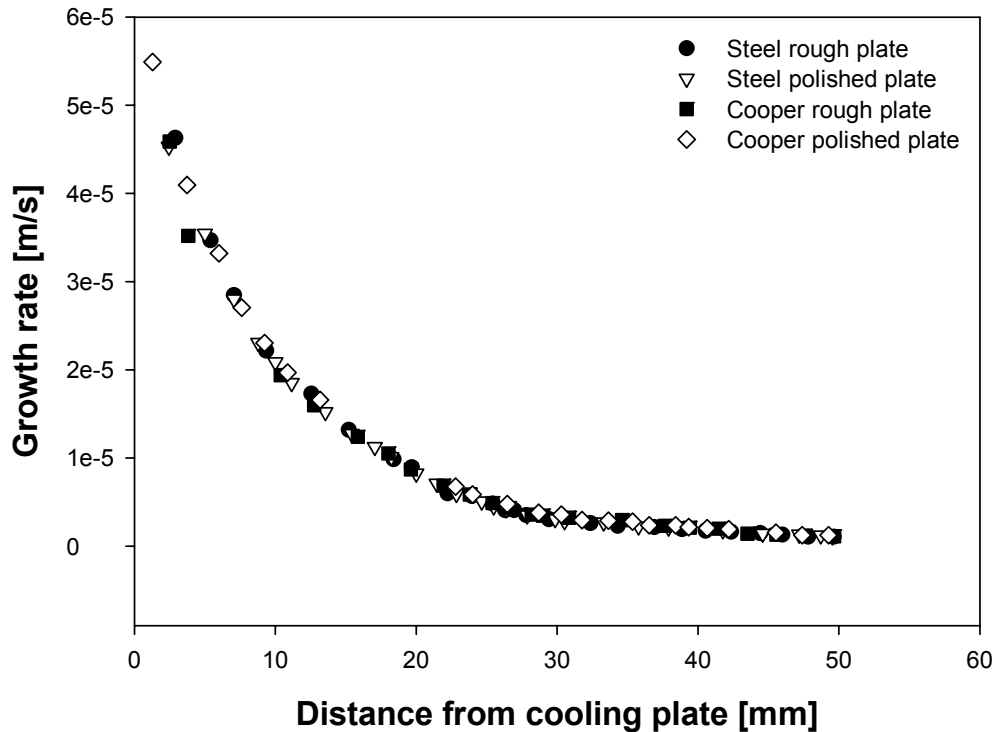


Fig. 5-35: Crystal growth rate for suspensions with 36 Vol.% solid loads frozen on different cooling plates

From the figure above it is easy to see that surface roughness has been found to have only insignificant influence on the growth behaviour. Interfacial tension received from different cooling plate materials also has been found to be of no importance and can be neglected, too.

5.2.2.3 Influence on crystal growth rate in dependence of moulding form materials and properties

Two different materials have been used to prepare the moulding form. For this purpose glass and plastic (Polyacrylic) material has been employ because both materials have different physical and chemical properties as well as roughness,

surface tension etc.. Both materials widely used in laboratory work and are easily to operate.

In Fig. 5-36 are the measurement results given for crystal growth rate in dependence of the molding form material. From the figure it is visible that for both materials the growth behaviour is identical, fast growing in the earlier stage (near the cooling plate) and a slow down with increasing the distance.

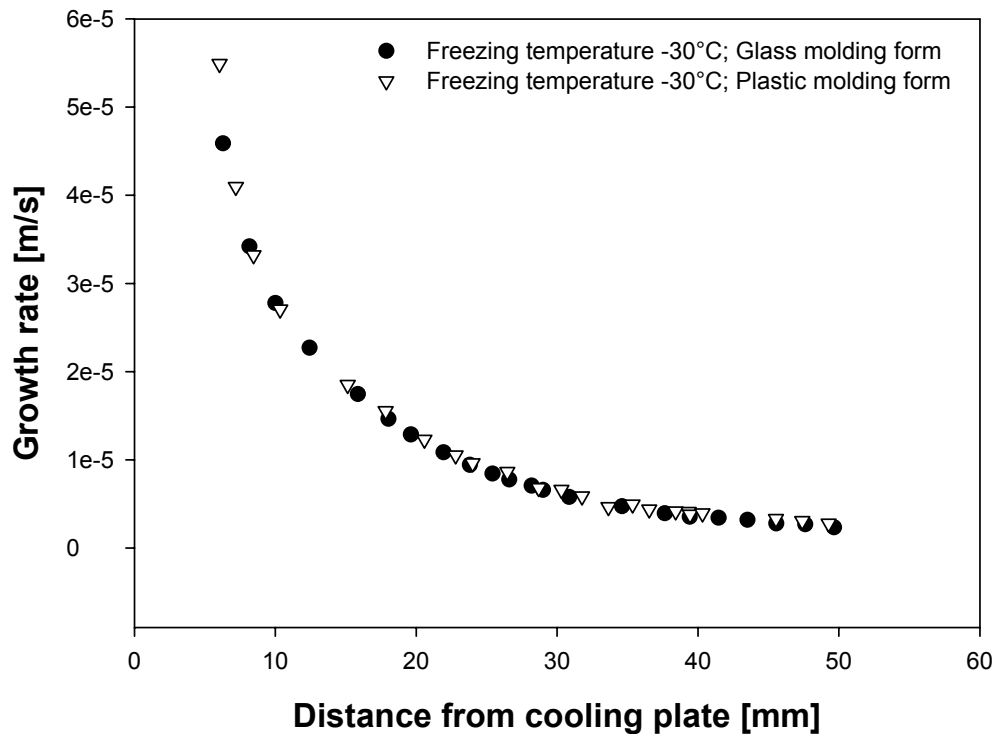


Fig. 5-36: Crystal growth rate for suspensions with 36 Vol.% solid load frozen at -30°C

From the figure above it appears that both curves lay at the same position. Therefore it has been concluded that the molding form material has only an insignificant influence and can be neglected.

5.3 Porosity and pore size distribution

In this Chapter the data and effects of suspension properties and freezing conditions on porosity and pore size distributions are given.

After the freezing process was completed the frozen samples were removed from the cooling cell followed by a removing from the molding form. The samples retain their shape gained from the molding form. The ice crystals have been melted and the remaining water evaporates after placing the specimens in a dryer at 70°C for 24h. Subsequent the samples were cut into peaces of 1cm in height. Porosity evolution was determined by mercury intrusion porosimetry together with a microscopically observation.

The mercury porosimetry measurements were made using a Porosimeter PASCAL Series containing two units 140 and 440. The first unit can increase the pressure of the mercury up to 400 kPa and the second unit increases the pressure on the mercury up to 400 MPa. Such pressure regions allow detecting pores with diameters from 100 μ m down to 0,001 μ m. A sample was placed in a dilatometer. Two parts form the dilatometer: the stem and the bulb. The stem is a calibrated glass tube joined at the bottom with a male cone fitting. Both the dilatometer stem and bulb are marked with the same number. The dilatometer has been characterized individually (blank measurement without sample) and this characterization has been used for measurement corrections.

A sample with mass approximately 0,1g was first evacuated, in the first measurement unit 140, to a pressure of 0,01 kPa to remove the rest of the water, which can remain in the inner part of the sample. In the second unit the measurements starts at atmospheric pressure. Identical pressure increasing speed has been used for all investigations. A computer has saved the data obtained from the measurements. The measurement device software has been employed to obtain measurement data for porosity and pore size distribution. The temperature in the laboratory room has been measured and the value set into the software for the calculation of the mercury density. The mercury density is used for the corrections in sample information and for the calculation of results of bulk and apparent density.

For all measurements the same mercury physical properties have been applied, contact angle sample- mercury 141° and 481 dyne/cm for mercury surface tension.

5.3.1 Porosity

5.3.1.1 Porosity dependence of solids load content

The influence of solids load content on porosity has been studied. In Fig. 5-37 are presented experimental results obtained for porosities of suspensions with various solid loads, frozen at -25°C . From the figure it can be seen that porosity decrease almost linearly as the distance from cooling plate decreases. Another point is that porosity increases with decreasing solid load contents. This is according to the water content, more water- more ice crystals respectively higher porosity.

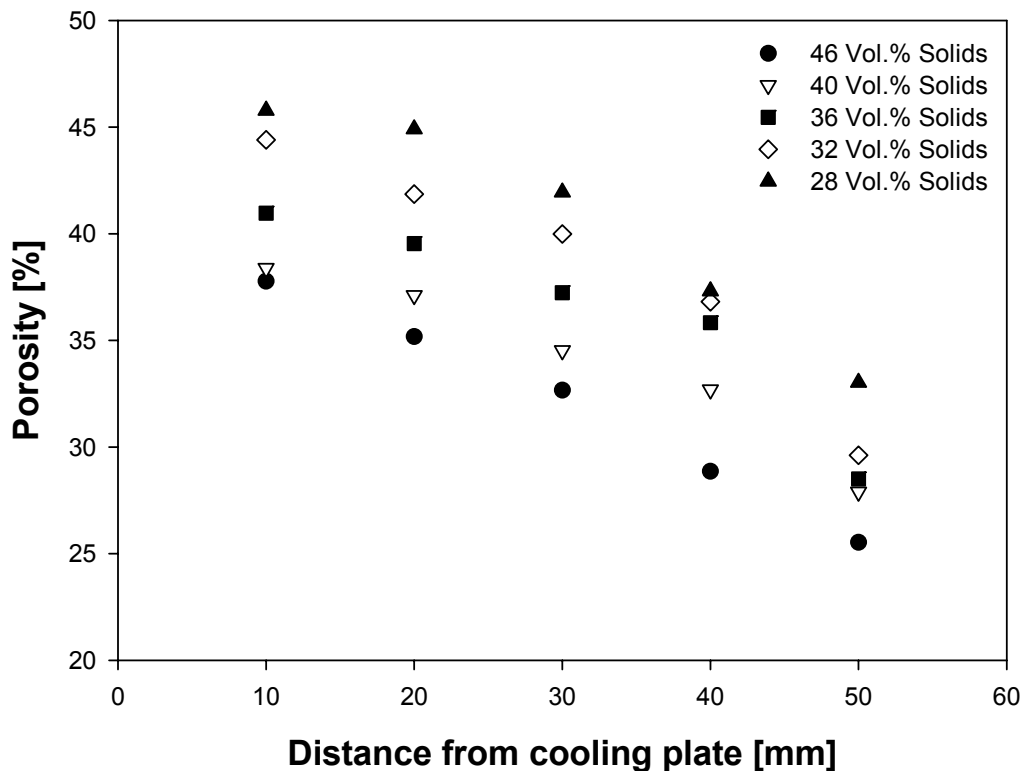


Fig. 5-37: Porosity evolution in dependence of solid load contents for samples frozen at -25°C on rough steel surfaces

To confirm the porosimetry measurements microstructural observations by an optical microscope have been done. In Fig. 5-38 are micrographs presented perpendicularly to the ice growth direction. The black spots on the micrographs correspond to the pores. The pores have their size, shape and morphology from the ice crystals. By comparing the both figures it can be seen that increasing of solid load content result

in less (in number) pores with smaller sizes which will result in a decreasing final porosity.

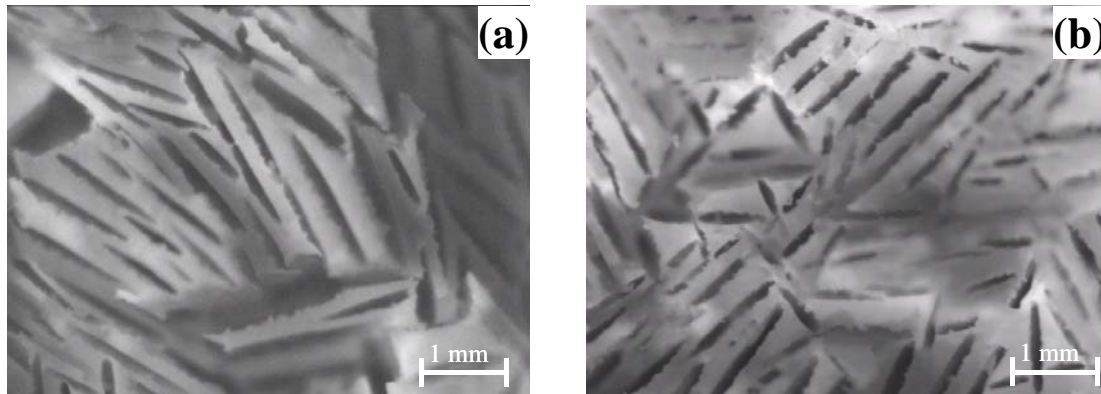


Fig. 5-38: Micrographs perpendicularly to the ice crystal growth direction, freezing temperature -25°C and distance from cooling plate 3cm. a) suspension with 36 Vol.% solids and b) 46 Vol.% solids

5.3.1.2 Porosity dependence of freezing temperature

The influence of freezing temperature on porosity has been investigated. Fig. 5-39 shows that the data obtained for suspensions with a 36 Vol.% solid load at different freezing temperatures. The figure shows that the porosity decrease with increasing distance from cooling plate. From the presented data it can be seen that the porosity remains the same behaviour for all investigated temperatures. Only the slope of the curves changes. It can also be noted that there is little difference between the values obtained for porosity at freezing temperatures -25 and -30°C comparison with the other freezing temperatures.

In Fig. 5-40 are the experimental results presented for suspensions with various solid load contents versus the freezing temperature. From the figure it is clearly to distinguish that the freezing temperatures result in different porosities. On the other hand this influence is slightly decreasing for freezing temperature values under -25°C . This suggests that the freezing temperature is one of the most effective parameters for the control of the porosity.

The rest of the data on porosity are presented in Appendix F.

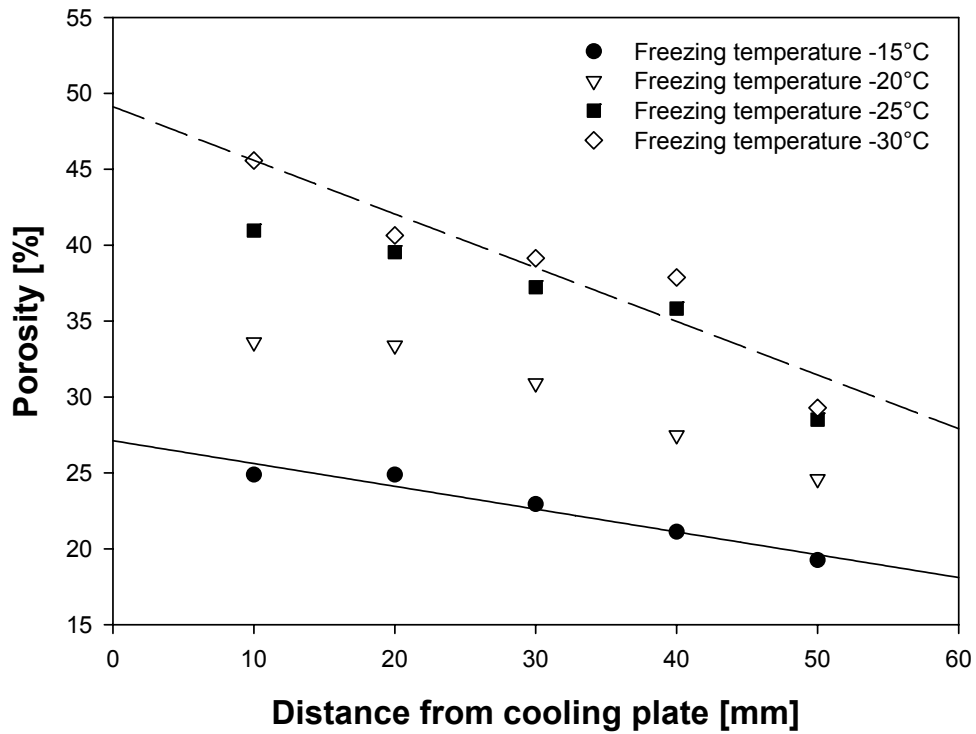


Fig. 5-39: Porosity progress dependence on freezing temperature for a suspension with 36 Vol.% solid load frozen on a rough steel plate

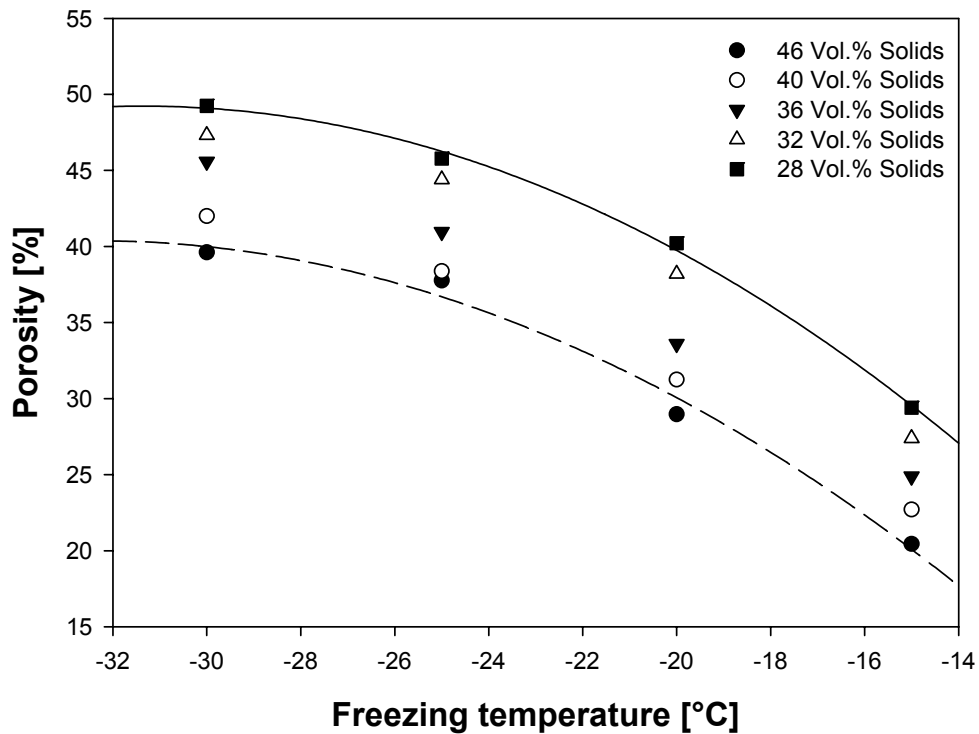


Fig. 5-40: Porosity in dependence on freezing temperature for various suspensions

5.3.1.3 Porosity in dependence of cooling plate materials

An example of a complete set of experimental mercury porosimetry data for a suspension with 36 Vol.% solids frozen at -30°C is shown in Fig. 5-41. The data represent porosity measurements obtained on different cooling surfaces. From the figure it can be seen that the curves follow the same behaviour.

The data have been linearly fitted and obviously show that the influence on porosity dependence on the cooling plate material is low. Therefore, it has been concluded that the cooling plate material has an insignificant importance in obtaining porosity.

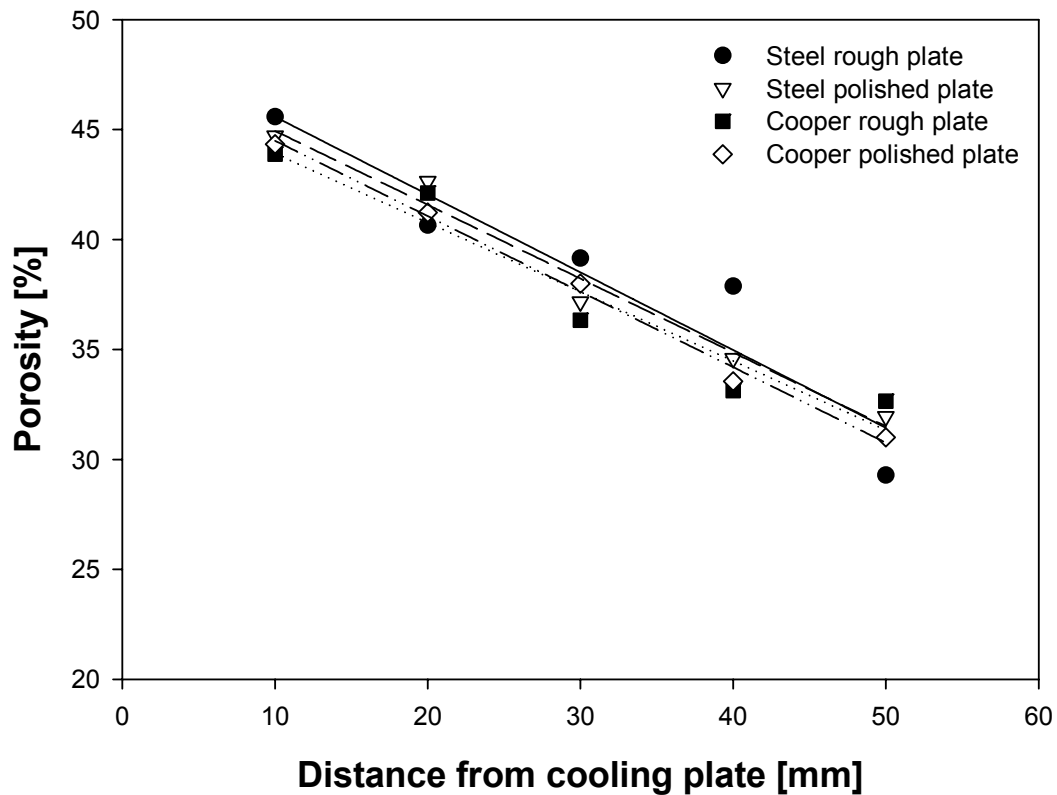


Fig. 5-41: Porosity dependence on cooling plate material for suspensions with 36 Vol.% solid loads frozen at -30°C

5.3.1.4 Porosity in dependence of moulding form materials

Porosity dependence of the molding form material and its properties has been investigated. Therefore plastic (Polyacrylic) and glass molding forms have been employed.

Fig. 5-42 shows experimental results obtained for porosity with glass and plastic molding forms. Here the plot represent the data for suspensions with 36 Vol.% frozen at -25°C .

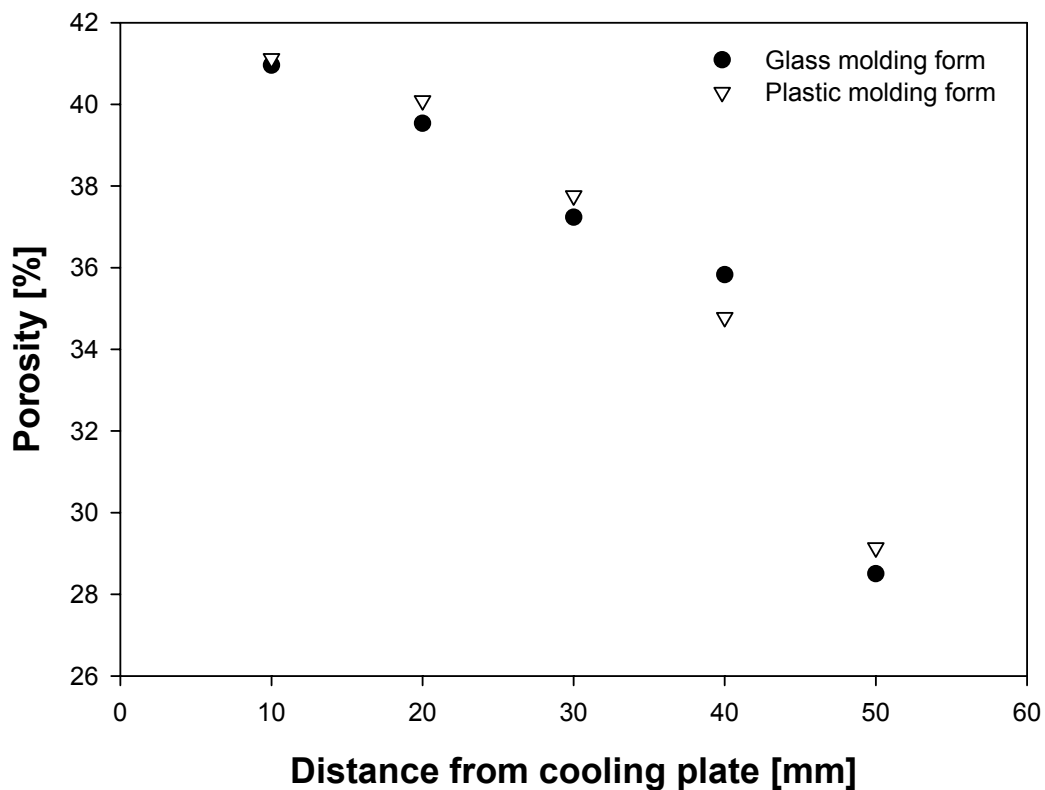


Fig. 5-42: Porosity dependence on molding form material for suspension with 36 Vol.% solid load, frozen at -25°C

From the figure above it appears that both curves follow the same behaviour. Significant difference in the porosity values cannot be found.

In contrast to the results obtained for the porosity in dependence of the freezing temperature and solid load content, the cooling plate and molding form materials have little influence. Therefore these parameters can be neglected.

5.3.2 Pore size distribution

The pore size distribution was calculated by mercury intrusion porosimetry. The same sample used for determining porosity has been used to determine the pore size distribution, too. The procedure has been the same as mentioned for porosity measurements.

The pore radius has been calculated by applying Washburn's equation (see Eq. 2.31) and conical and cylindrical model for pores. The macropores, with size over $1\mu\text{m}$ has been detected by using the first (Pascal 140) measurement device. Pores as small as ca. $1\mu\text{m}$ in diameter, or so-called mesopores, have been recognized under conditions of high pressure, which are measured by using the second unit (Pascal 440).

Figure 5-42 presents a typical result obtained when the mercury porosimetry technique is applied into the characterization of the samples. As can be seen, when the incremental volume is plotted versus pore diameter, two major peaks appear indicating the presence of pores in the sample.

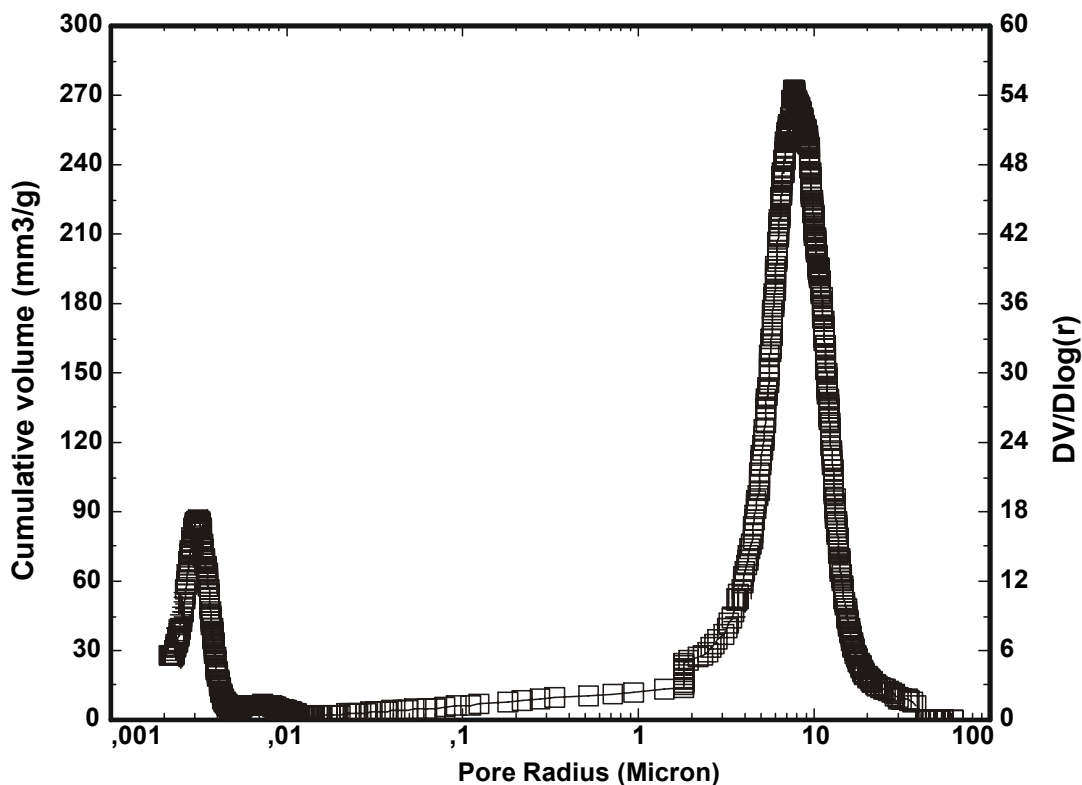


Fig. 5-43: Mercury intrusion porosimetry for suspension with 36 Vol.% solid load, frozen at -30°C and having a distance from cooling plate 2cm

The following can be seen from the Fig. 5-43: 1) the pore size distribution is bi-modal (bi-disperse) and 2) the macropores peak is higher and larger as the mesopores peak. Other authors have observed such bi-modal pore size distribution too [Fuk01, Net97, Rig01].

The pores formed by the ice crystals cause the large peak on the right hand side. The smaller peak (mesopores) on left hand side results from to the particle packing and arrangement and to the particles own porosity. Therefore, the particles have been observed by electron microscope. In Figs. 5-44 and 5-45 are the micrographs presented taken from the Al_2O_3 and SiO_2 particles surface. Here it can be clearly seen that the particle surface is very porous. On Al_2O_3 particles there have been pores detected with diameters 0,05 to 0,2 μm and on SiO_2 particle surfaces pores can be seen with diameters 0,1 to 0,3 μm .

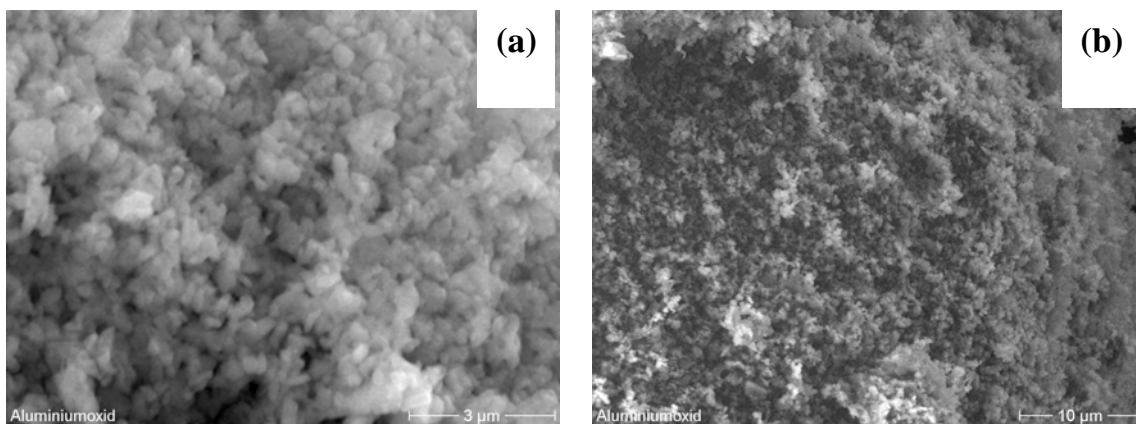


Fig. 5-44: SEM micrographs of Al_2O_3 particles surface

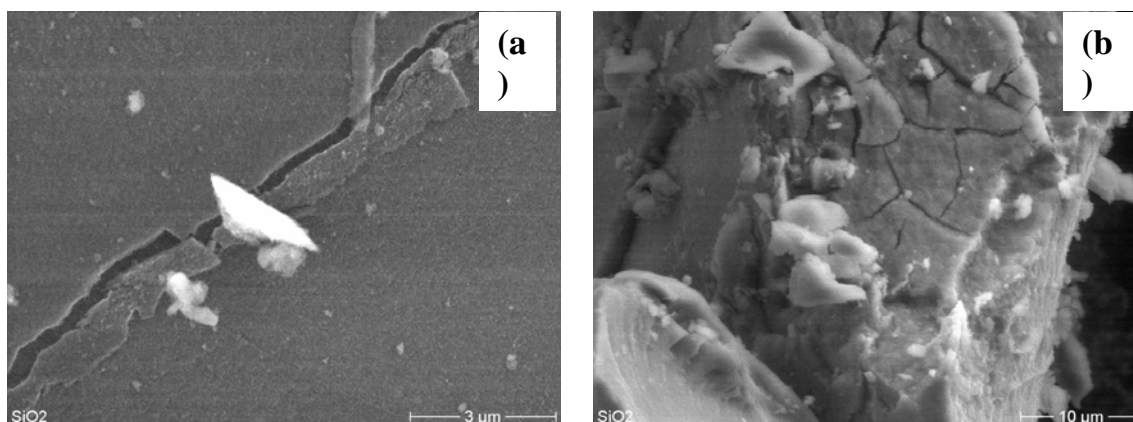


Fig. 5-45: SEM micrographs of SiO_2 particles surface

5.3.2.1 Pore size distribution in dependence of solid load content

The pore size distribution for macropores and their dependence on solid load content are shown in Fig. 5-46.

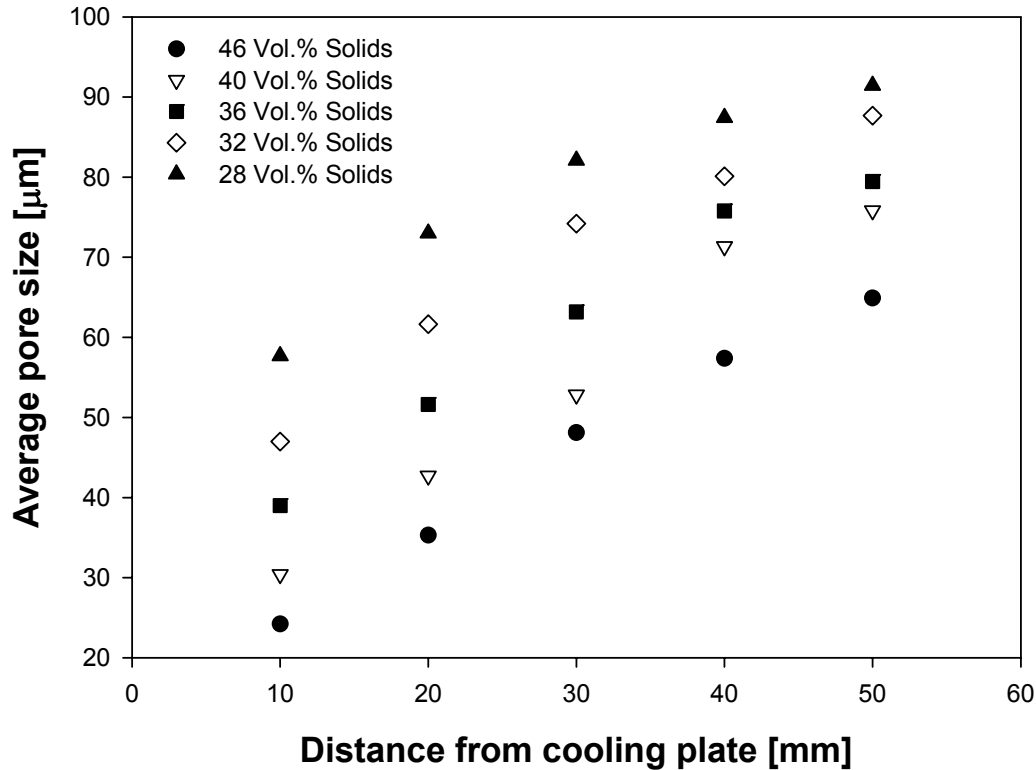


Fig. 5-46: Macropores size distribution for various suspensions frozen at -25°C

It can be seen from the figure that the pore size distribution is increasing with increasing distance from the cooling plate. By increasing the distance from the cooling plate the temperature gradient is decreasing therefore crystal growth is slowing down, which result in creation of bigger ice crystals respectively bigger pores. When the solid load in suspensions is decreasing, the average pore size is increasing, since the amount of water is increasing, which will result in a bigger and larger number ice crystals, therefore an increase in average pore size.

The presented results have been measured several times and averaged.

The same dependence has been observed also for mesopores. Fig. 5-47 shows the measurement results obtained for mesopores.

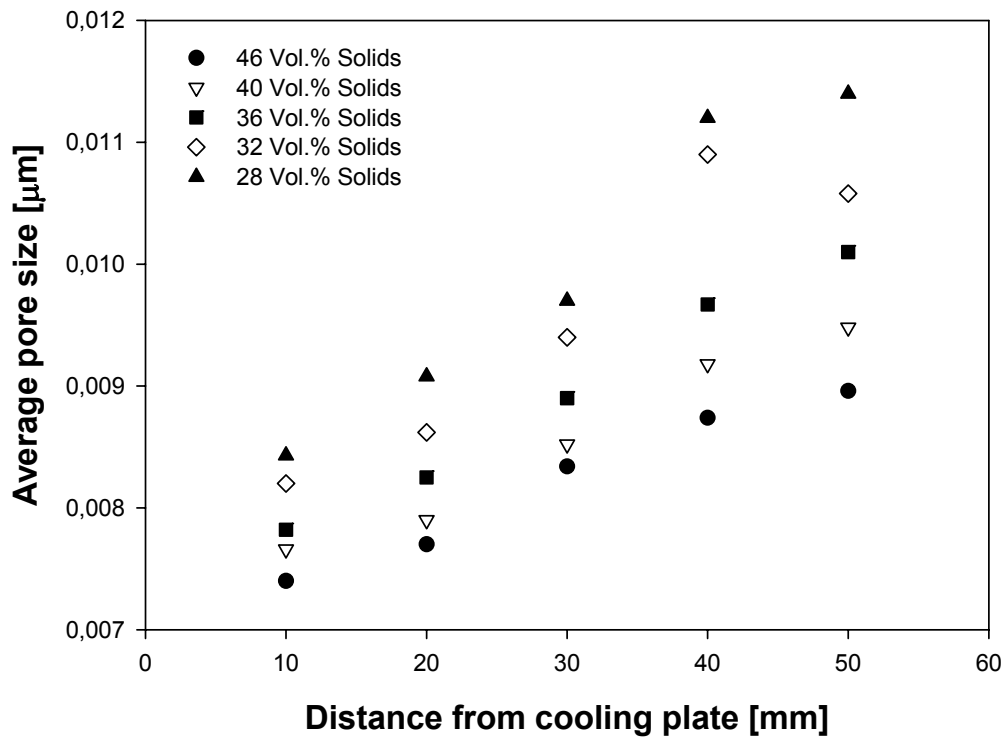


Fig. 5-47: Mesopores size distribution for various suspensions frozen at -25°C

Fig. 5-48 shows optical micrograph observations of pore size distribution for samples with different volume fraction of solids. Using this approach structures with pore size gradients, varying with distance from cooling plate, respectively can be created from one end to the other of the moulding form.

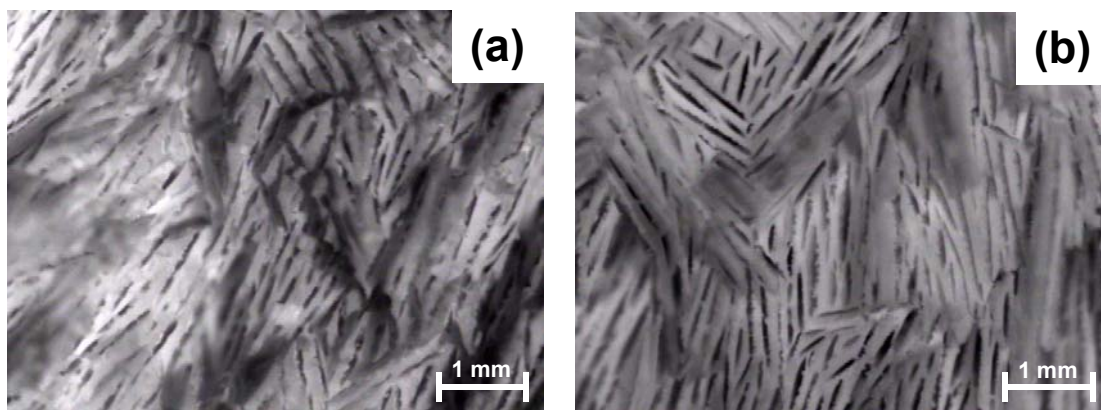


Fig. 5-48: Optical micrographs for samples frozen at -25°C (a) represent suspension with 40 Vol.% solid load and (b) suspension with 28 Vol.% solid load

5.3.2.2 Pore size distribution in dependence of freezing temperature

The freezing temperature can also manipulate the pore size distribution. Fig. 5-49 and Fig. 5-50 illustrate the ascendancy of freezing temperature over the pore size distribution for suspensions with 36 Vol.% solid loads. Even a small increase in temperature leads to a huge increase in average pore diameter. From both figures it can be seen that the pore size distribution has been shifted by 5 to 10% even with small increase/ decrease in freezing temperature. Also as presented in previous sections, the average pore diameter increases gradually as the distance from cooling plate increase.

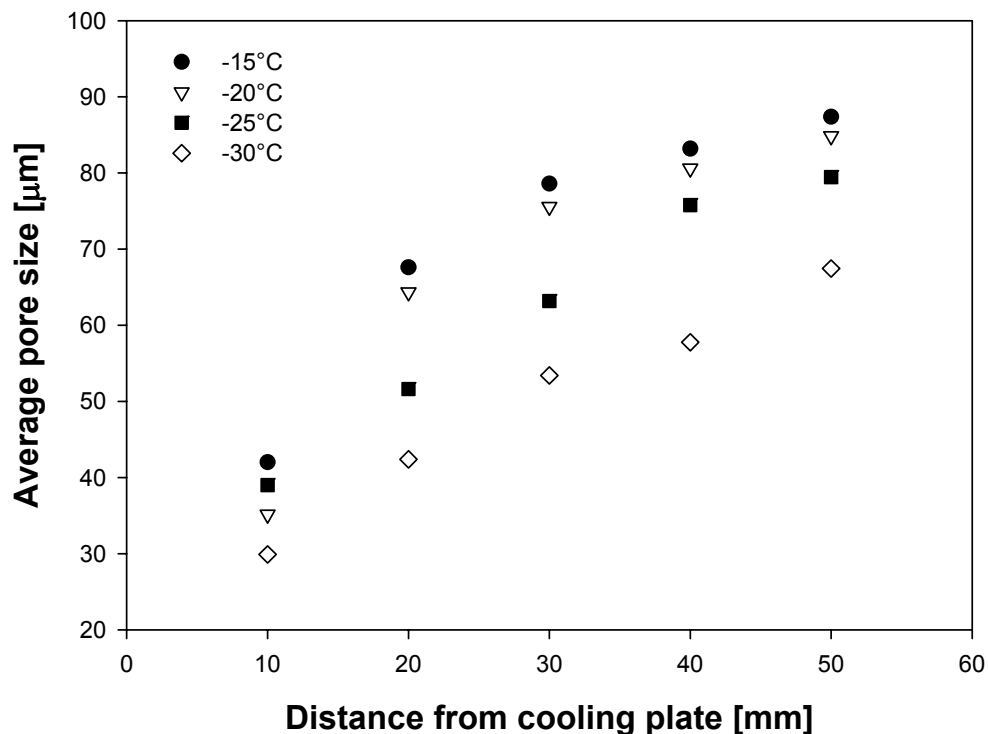


Fig. 5-49: Macropores size distribution for various freezing temperatures and suspension with 36 Vol.% solid load

The optical microscopy confirms the observations done by mercury porosimetry. Fig. 5-51 shows the occurrence of large pores in dependence of freezing temperature for slurry with 40 Vol.% solid loads. As can be seen from the micrograph a pore network arrangement and pore gradient has been created by changing the freezing temperature and distance from cooling plate.

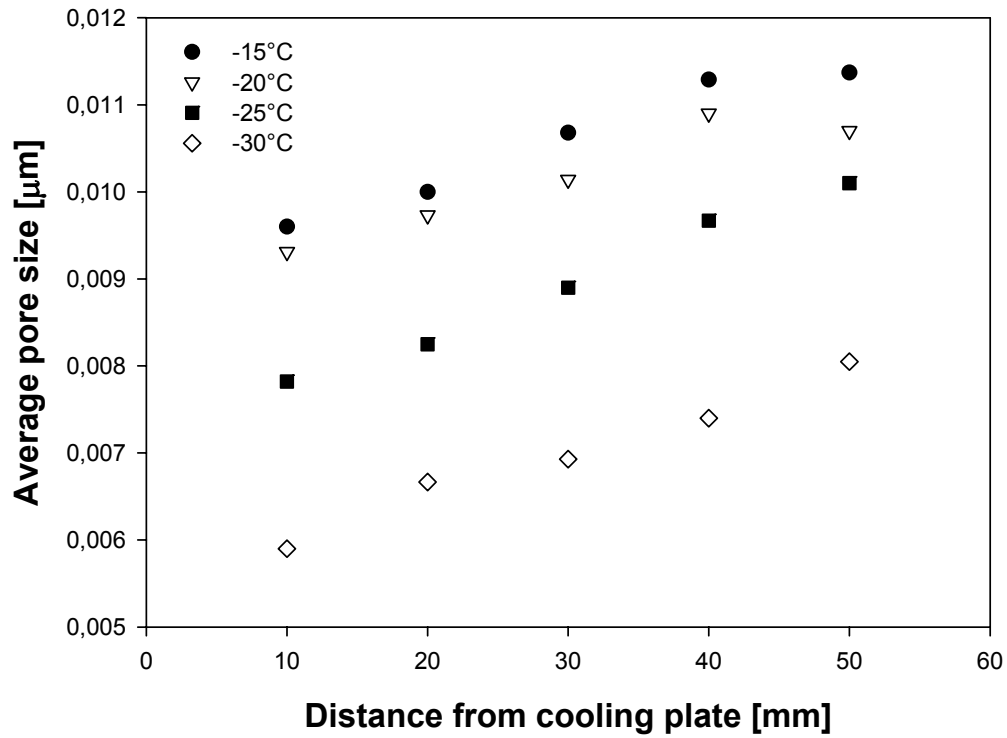


Fig. 5-50: Mesopores size distribution for various freezing temperatures and suspension with 36 Vol.% solid load

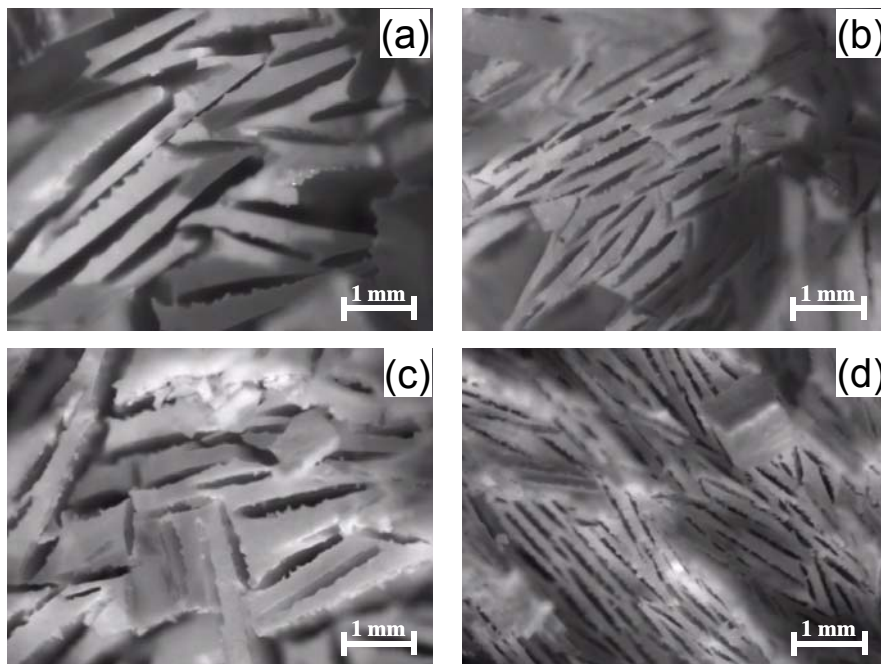


Fig. 5-51: Micrographs of the samples taken perpendicularly to the crystals growth direction. (a) and (b) freezing temperature -15°C , (c) and (d) -25°C . (a) and (c) 5cm distance from cooling plate, (b) and (d) 2cm.

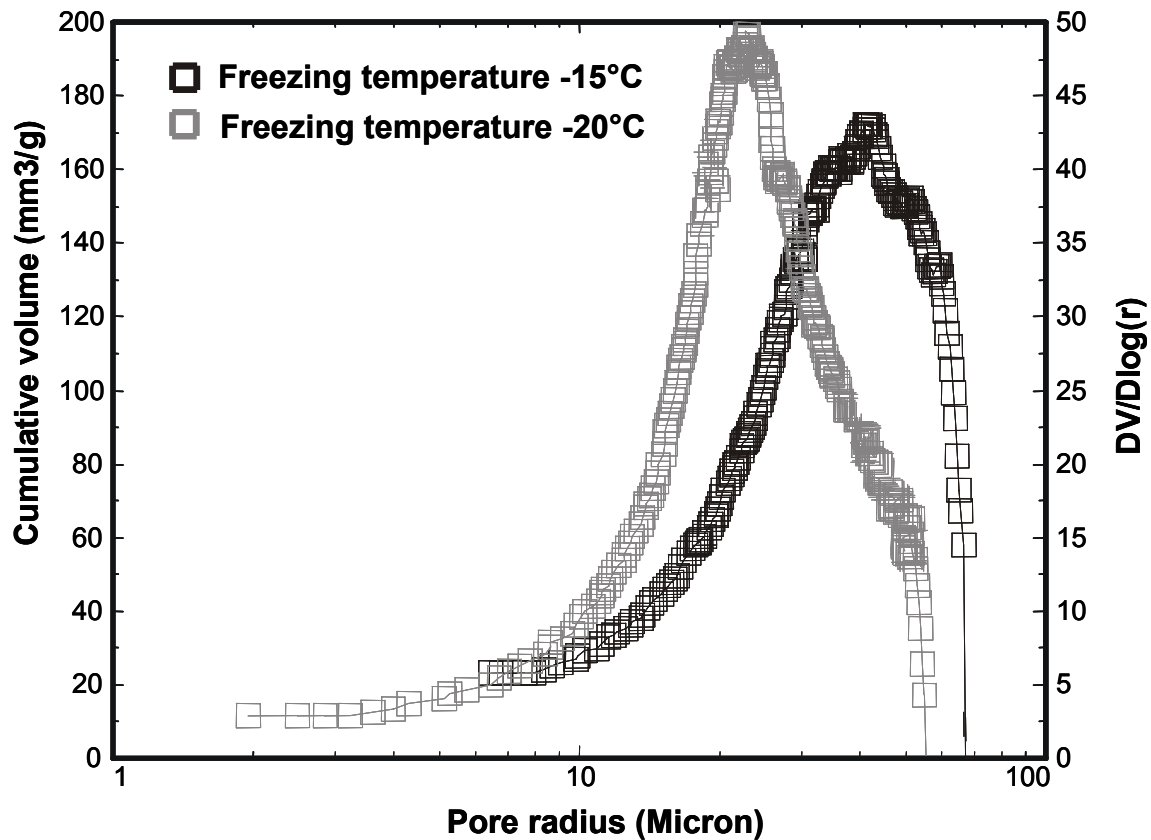


Fig. 5-52: Mercury intrusion porosimetry measurements for macropores in dependence of freezing temperature. Suspension with 36Vol.% solid load

Fig. 5-52 shows two mercury porosimetry measurements for samples with 36 Vol.% solid load and a distance from cooling plate of 2cm. From the figure it appears that the pore size distribution remained uniform and relatively narrow after increasing the freezing temperature.

The rest of results for pore size distribution are presented in Appendix F.

5.3.2.3 Pore size distribution in dependence of cooling plate materials

Fig. 5-53 represent the experimental results obtained by mercury intrusion porosimetry for pore size distribution in dependence of cooling plate materials. The same cooling plates have been used as in the previous chapters. The results obtained for macropores size distribution are in a good agreement with the results obtained for porosity and its dependence from cooling plate material. Also here has

been observed only a small influence on pore diameter gained from the cooling plate material. Such a divergences in experimental results can be accumulated from measurements errors.

Significant influence on pores diameter achieved by different cooling plate materials have not been observed, therefore the properties of the cooling plate material can be neglected.

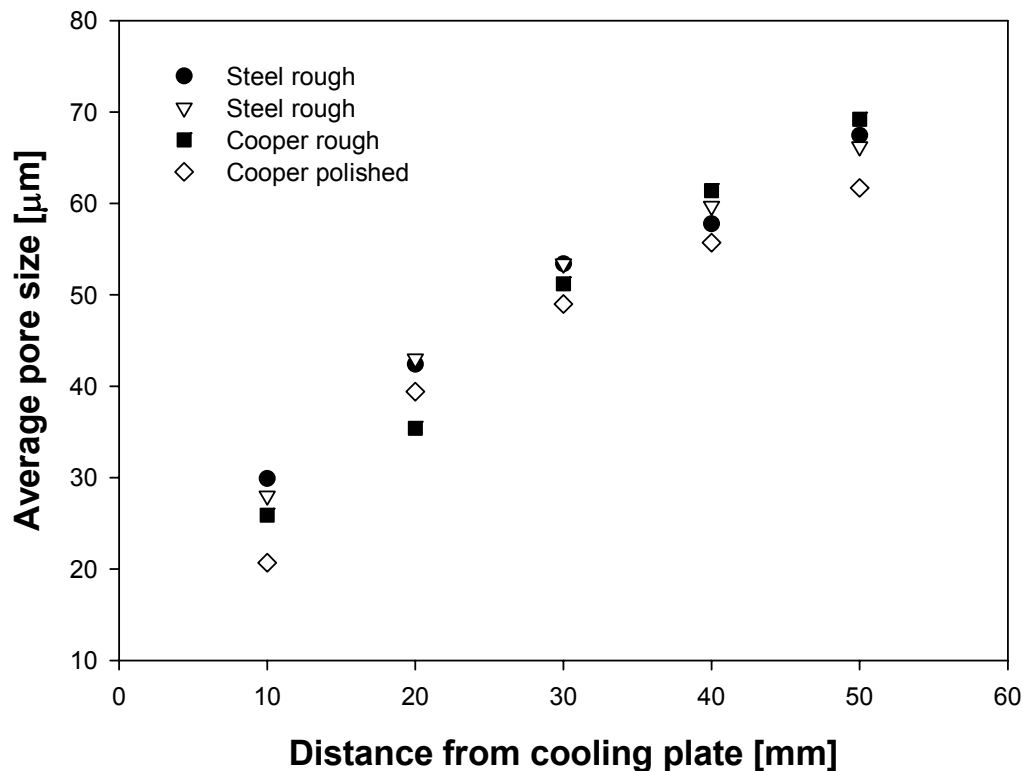


Fig. 5-53: Pore size distribution for sample frozen at -25°C on different cooling plates materials and 36 Vol.% solid load

5.3.2.4 Pore size distribution in dependence of moulding form materials

The dependence of pore size distribution on moulding form material is shown in Fig. 5-54. The results for macropores again have been found, as behaviour, in a very good agreement with the results obtained for porosity. The same molding form has been used as in the section for porosity. From the figure obviously can be seen that the influence of the moulding form material on pore size is negligible.

Both curves follow the same manner and have only a small difference, which can be attributed to measurement errors. Therefore the influence of the moulding form on the pore size distribution can be neglected.

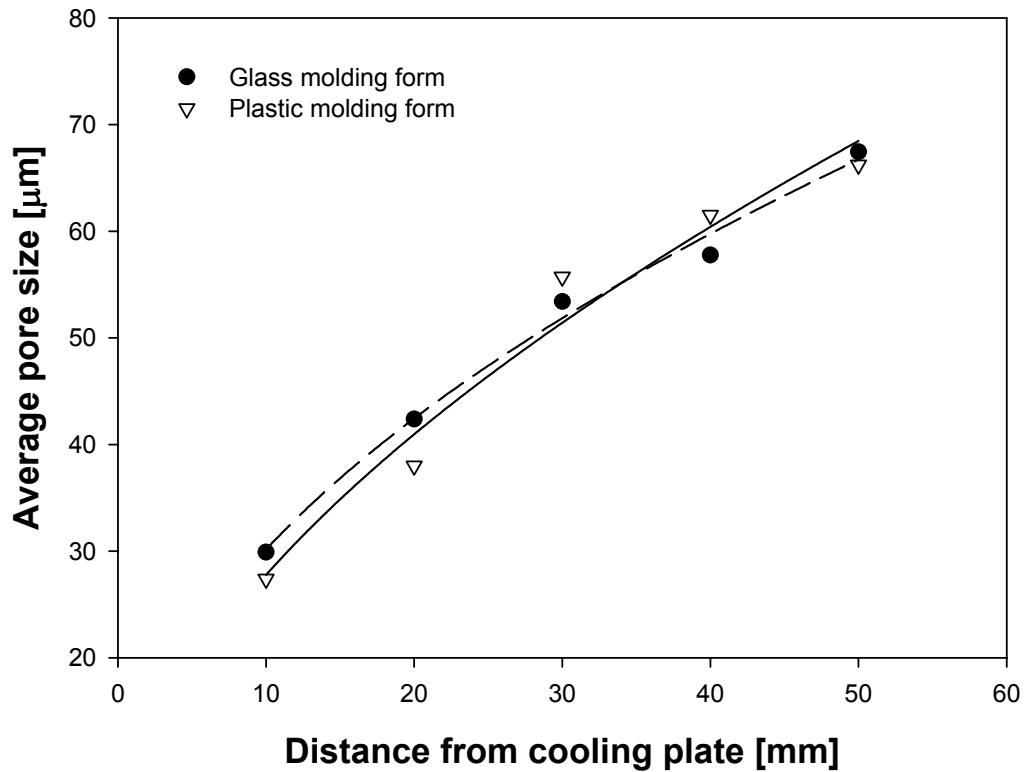


Fig. 5-54: Pore size distribution for sample frozen at -25°C in different moulding forms and 36 Vol.% solid loads

6. Discussions

6.1 Discussions of rheological properties on the starting slurries and the dependence on porosity as well as the pore size distribution

The analysis performed in the previous section (especially porosity and pore size distribution) shows how the particular microstructures of the porous materials may be affected by the solid load content. Therefore, it is advisable to study and discuss the role of solid load content on starting slurry characteristics and especially porosity, pore morphology and pore size distribution. Good knowledge and understanding of these parameters will enable to design an optimal control of pore characteristics. The rheological measurements showed pseudoplastic behaviour of the slurries, indicating a well-dispersed solid phase in the suspension (see Chapter 4.1.2). The rheology of the starting slurries varies significantly depending on solids contents. Density measured at 25°C and porosities, for samples frozen at -25°C and a distance from cooling plate of 1 cm, versus slurry solid load content are presented in Fig. 6-1.

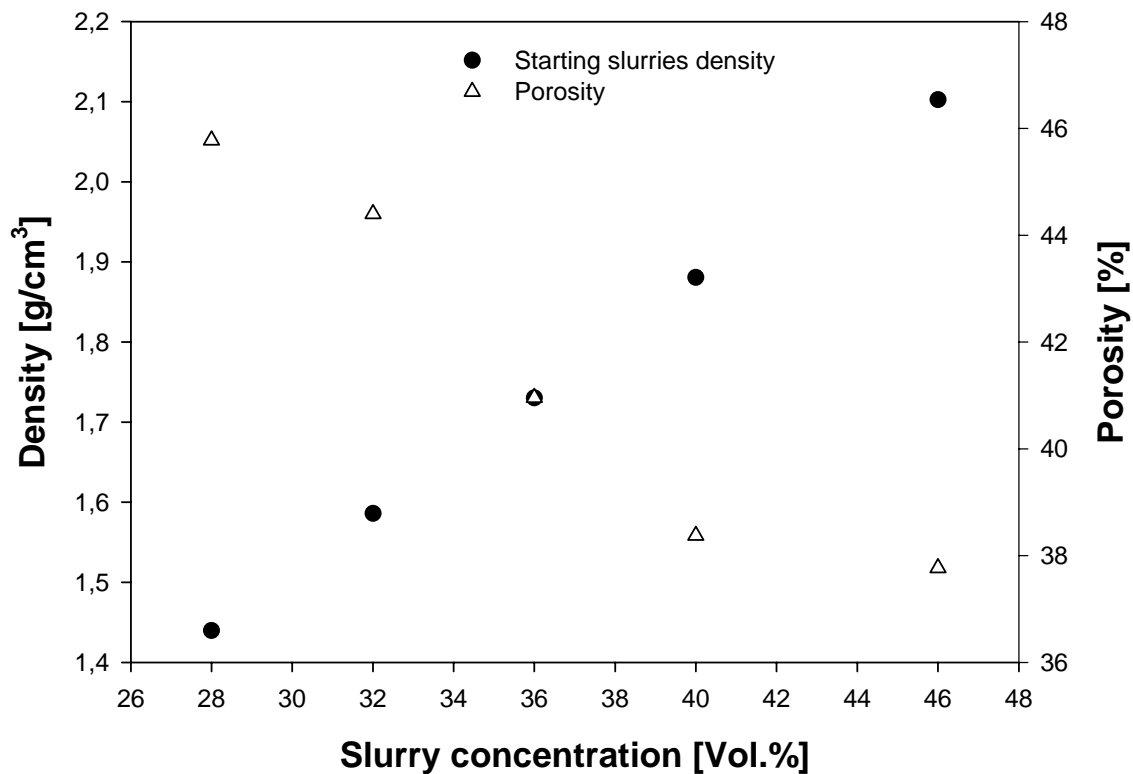


Fig. 6-1: Density and porosity in dependence of slurry concentration

From this figure it can clearly be seen that the starting slurry density increases with increasing slurry concentration. This is in accordance with less liquid phase in the suspensions. In case of decreasing slurry concentrations large pores can be obtained and because of the lower viscosity the slurries can be easily handled. On the other hand it will decrease the mechanical properties of the obtained materials. The increase of volume fraction of solids, hence less water, determines the created materials after freezing, hence the degree of porosity as shown in Fig. 6-1. The obtained pores result from the ice crystals and the porosity of the particles themselves, which is of less significance. Furthermore, a good control of the starting slurries physical properties such as density can promote a route to control porosity as well as the pore size. In Fig. 6-2 are micrographs presented, of cross sections perpendicularly to the ice growth direction, showing the microstructural evolution of samples frozen at -25°C . No cracks or defects have been observed. The change in the pore size results only from different solid load contents, because all other parameters have been kept constant. These pores shown in Fig. 6-2 are generated after sublimation of the ice crystals.

By increasing slurry concentration many water molecules are bond to the particle surface [Sof01].

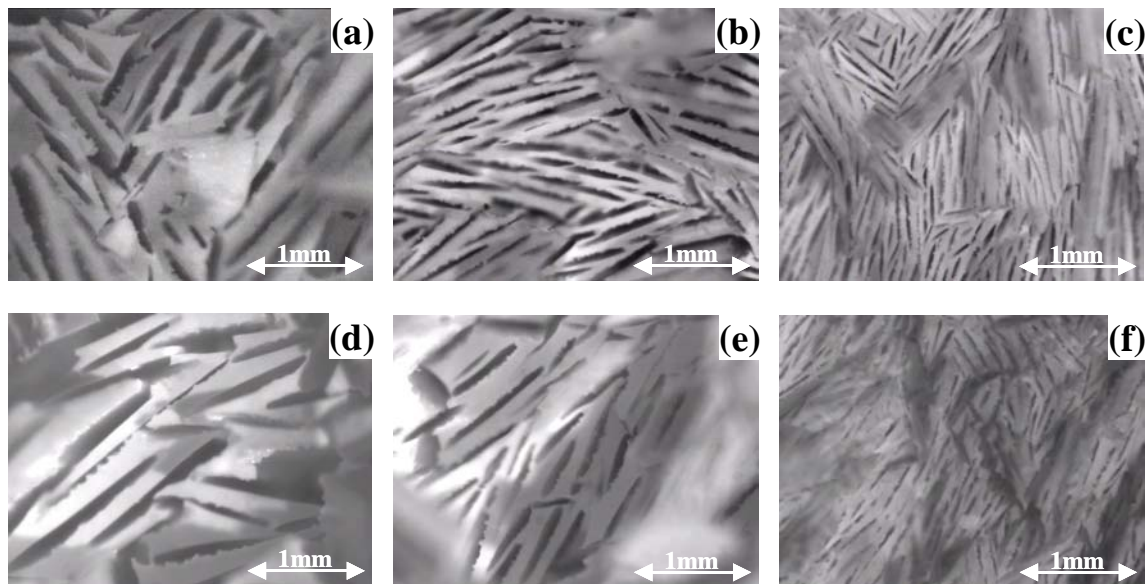


Fig. 6-2: Cross sections (a, b, c 40 Vol. % solid load; d,e,f 36 Vol. % solid load), a-d 5 cm distance from cooling plate: b-e 3 cm and: c-f 1 cm

Increase of density and viscosity by increasing slurry concentration leads to formation of aggregates for a ceramic skeleton formation, which is formed due to the freezing. The bigger the aggregates are the greater are the possibilities to settle due to gravitational forces. The same behaviour has been observed by Terpstra et al. [Ter95]. Therefore, the suspensions have been electrostatic stabilized by using Polyacrylic acid. By this way the pH of the suspensions has been shifted between the Isoelectric Point (IEP) of Al_2O_3 , which is between 8-9 and SiO_2 between 2 and 3 [Ree88]. Lange et al. [Cha91, San00] reported on an aqueous alumina– zirconia suspensions in which the pH was shifted between IEP of the both materials. The aggregation did lead to a mixture of the both materials that was not disrupted during consolidation.

Since ceramic particles with different sizes have been used (see chapter 3.1) a better degree of packing between the ceramic particles can be expected. Increasing the size of the used particles leads to an increasing permeability. Therefore, large amounts of water stays closed in such a spaces and voids of the aggregates. Due to the incorporation of water the mass transport in the suspension volume becomes more difficult. The “locked” amount of water cannot easily be taken out due to the physical resistances and does not take place in the continuous macropores formation process (see Fig. 6-3).

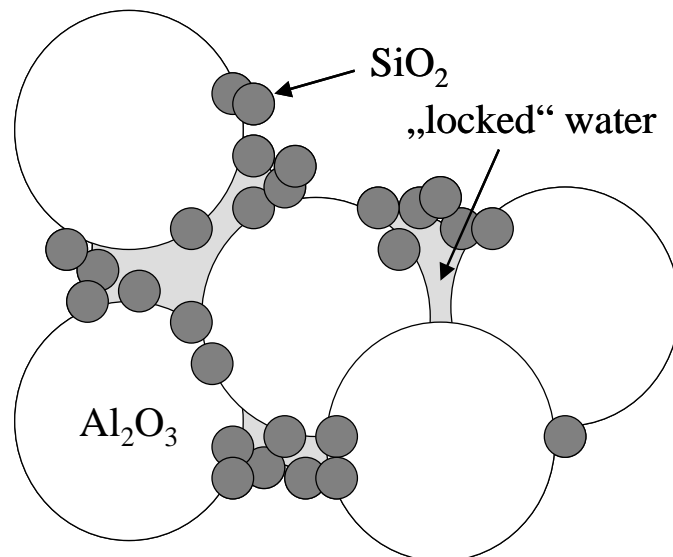


Fig. 6-3: Schematic view of aggregates for ceramic skeleton formation

Fig. 6-4 shows the density difference according to the distance from the cooling plate. The data on the samples after the freezing have been obtained by mercury intrusion porosimetry.

Densities of the samples have been found to increase linearly with decreasing distance from the cooling plate. This can be attributed to a settling of the particles to the bottom. In a freeze-casting process two processes are competing with each other. First the ice crystals are stimulated to grow from bottom to the upper face in vertical direction because of the temperature gradient. On the other hand the ceramic particles settle because of their weight. In case of low freezing, respectively slow crystal growth rates large crystals will be formed. There might exist a place at which the freezing front will meet a particle front. Such an effect has been observed when the slurries were frozen at -5°C . The bottom and the upper phase of the samples were very hard. Between them only a crumble phase has been observed. The samples have been very brittle and not suitable to a processing even at the highest solid load contents.

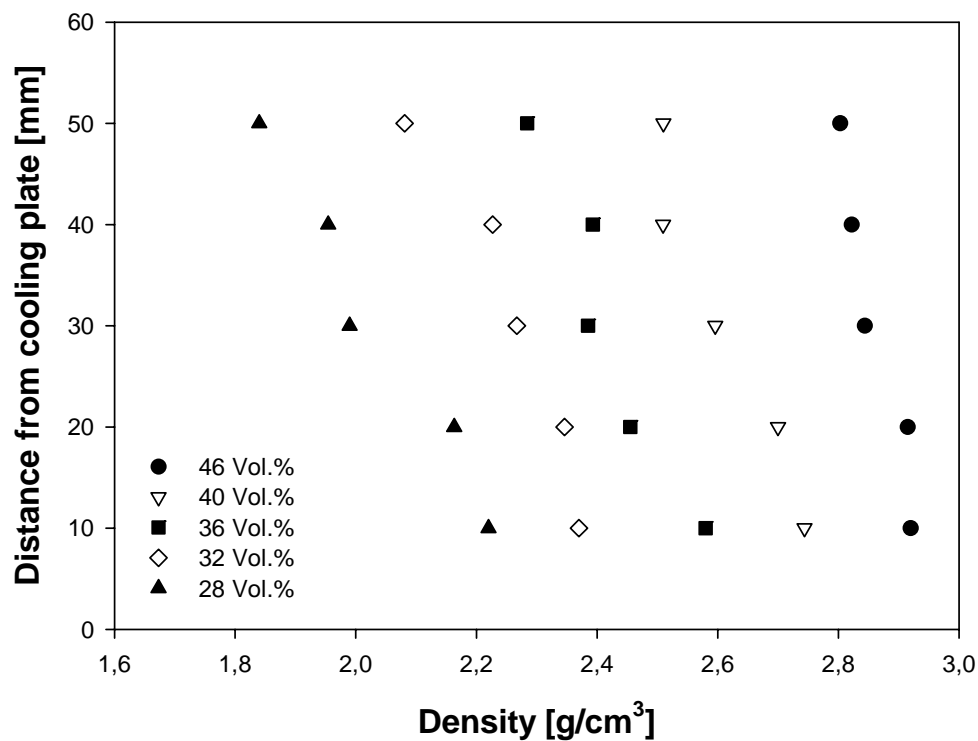


Fig. 6-4: Samples density in dependence of distance from cooling plate.
Freezing temperature -25°C

Fig.6-5 shows the results obtained for starting slurry densities in dependence of solid load contents. The plot shows the density values obtained from mercury intrusion porosimetry. From the figure it can be seen that all curves follows the same manner when increasing suspension concentration. Also the differences between starting slurry density and after the freezing have found decreasing with lower solid contents. At the upper face the density was found with only a little margin to the starting slurry density. This result is another evidence for the fact that particles settling. Low slurry concentrations correspond to more water, respectively, more free space for particle movements. Also the possibility for particle interactions is less therefore less agglomeration happens. With increasing solid load the difference between the densities of the frozen samples decreases.

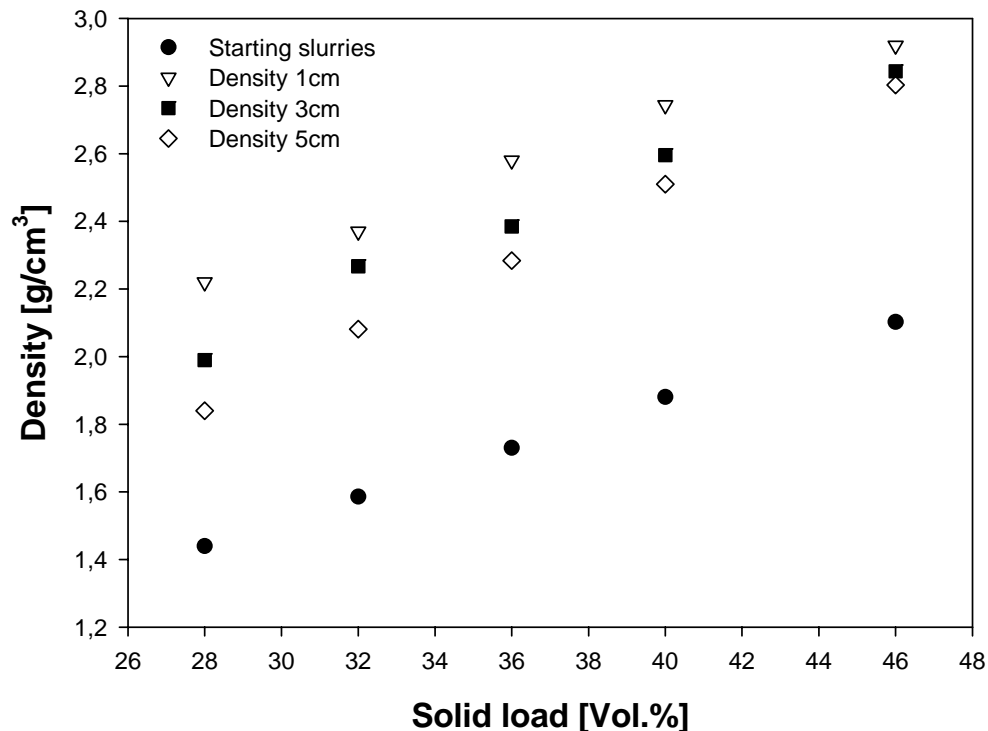


Fig. 6-5: Starting slurry density and density after freezing in dependence of solid load content. Freezing temperature -25°C

At the highest solid load content the samples exhibit almost no density gradient. This result can be attributed to a better dispersion of particles in the suspension volume. The density of the samples has been measured by the Archimedes method. The

samples were positioned in a measurement cylinder with known amounts of water and the cylinders were covered to prevent water evaporation. After 24h the water level was measured and from the level margin of the samples the density was calculated. A good agreement in the values between Archimedes method and the results obtained by mercury intrusion porosimetry has been found. Therefore, it has been concluded that most of the pores are open pores or interconnected ones.

6.2 Discussions on contact angle, interfacial tension and nucleation kinetics

According to the classical theory the nucleation process requires that the nucleus overcomes a certain Gibbs energy barrier [Mul01]. These nucleuses are aggregates formed of water molecules, which are transformed to solid state, ice. Eq. 2.2 gives the Gibbs energy change. In this equation the interfacial energy is a very important factor. The interfacial energy is a function of temperature, because the interfacial energy is related to the surface energy of the substance [Bal98], and the surface energy is dependent on temperature. Therefore, it needs to be taken into consideration. According to Haasner [Haa02] and Na [Na03] a change of materials roughness will result in change of the contact angle respectively in interfacial energy. Such a change can be attributed to an increase of the contact area between substrate and new-formed phase Fig. 6-6.

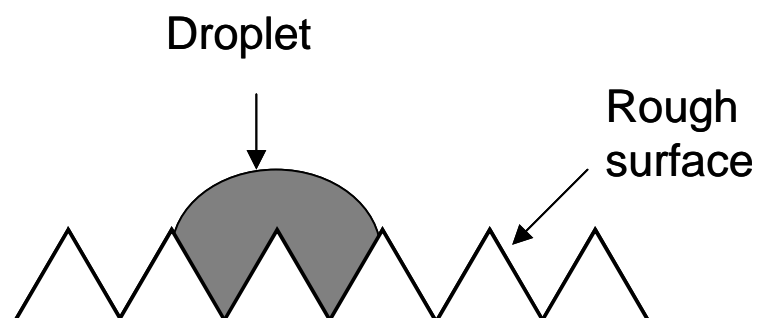


Fig. 6-6: Effect of roughness on the nucleus contact area

Roughness can be taken into account by using Wenzel's equation.

$$\cos \theta = r_w \frac{\sigma_{sl} - \sigma_{cs}}{\sigma_{cl}} \quad (6.1)$$

Wenzel uses Young's equation and applies a correction factor r_w where r_w is divided as actual surface area to the planar surface area. The Wenzel equation means that a surface with a higher roughness will lead to an increase of the wetting angle. In the previous chapter the results of contact angle measurements in dependence of the cooling surface have been presented (see Chapter 5.2.1.2). Four surfaces with wide ranges of roughness have been investigated (see Fig. 6-7). An effect on contact angle in dependence of cooling surface roughness has not been observed in the presented results (see Fig. 6-12). According to Mullin [Mul01] in case of increasing the contact angle an increase of the energy required for nucleation can be expected and will shift the system energy toward homogeneous nucleation (see Fig. 5-25), which requires higher energies and is not favourable. Fig. 6-7 shows the energetic margin between homogeneous and heterogeneous nucleation for rough steel surfaces. From this figure it can be seen that the energy requires for heterogeneous nucleation is obviously lower.

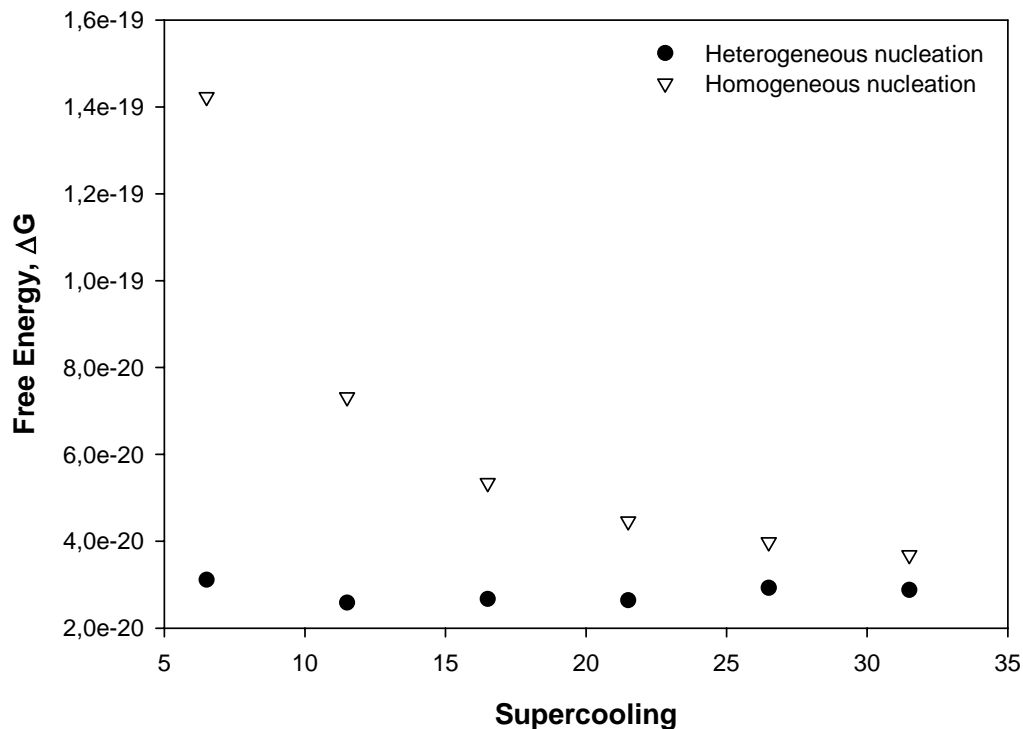


Fig. 6-7: Free energy versus supercooling for rough steel surface and slurry with 36 Vol.% solid load

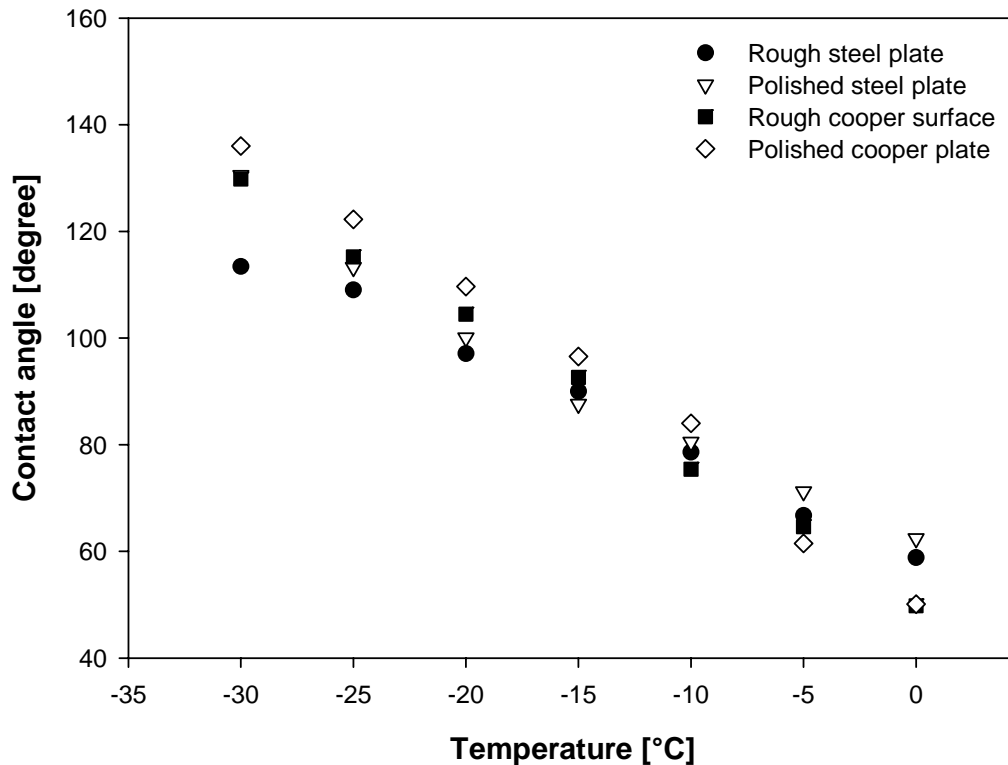


Fig. 6-8: Contact angle measurements for suspension with 36 Vol.% solid loads on different cooling plate surfaces

As previously noted, in Chapter 5.2.1.2, each reported contact angle was measured several times at different points on the same surface and averaged. The differences in contact angles obtained from different cooling surfaces are shown in Fig. 6-8. In each case the data exhibit the same general temperature dependence behaviour of increasing contact angle by decreasing the operating temperature. The standard deviation for contact angle measurements was less than 5% of the averaged values at each cooling surface. The measured contact angle shows little variations with changing the cooling surface material and temperature as the main parameter affecting contact angle. From the figure it can be seen that only a small difference of the contact angle has been obtained in dependence of the plate material or roughness. The same results also have been achieved for the interfacial tension. Fig. 5-17 clearly shows that the interfacial tension is influenced by material and only a little deviation have been observed by roughness changes.

The averaged values have been used to calculate the f -function needed to obtain the free energy values for heterogeneous nucleation (Eq. 2.9 and 2.8). Fig. 5-25 shows the calculations obtained of the f -function, Eq. 2.9. As can be seen all curves have the same behaviour and lie on almost the same place. According to classical nucleation theory by changing surface or surface properties each curve should have an own character. Therefore 4 different surfaces, materials and roughness, have been investigated and used as cooling plates. As can be seen from the Fig. 5-25 the effect of the f -function obtained from different cooling plate materials have not been observed. In case such effects exist they are too small to be detected. From here it can be concluded that the cooling surface material and properties play an almost insignificant role in state of design and control of nucleation.

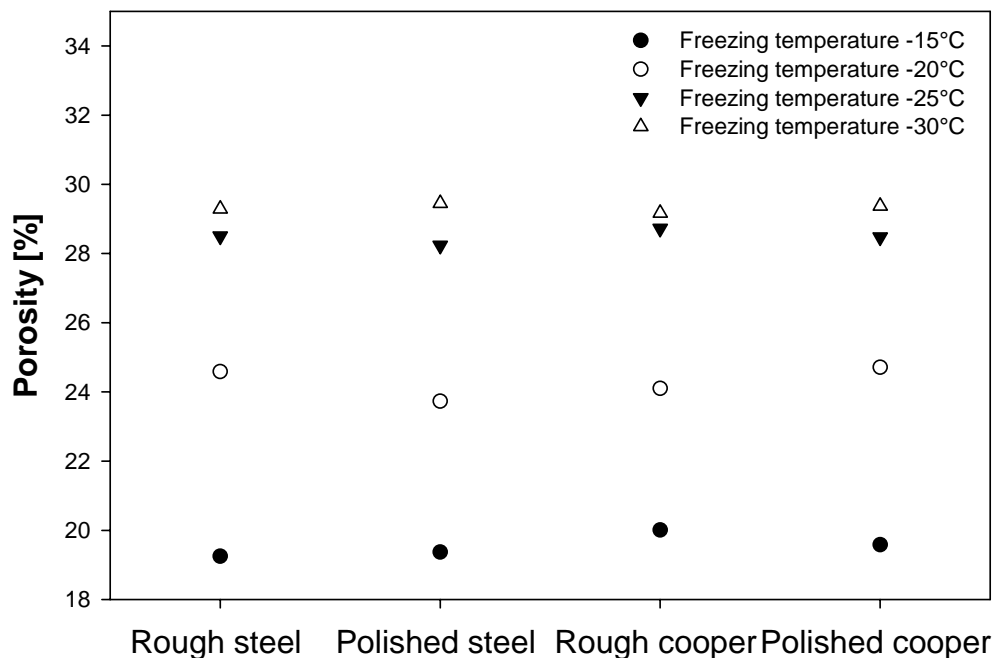


Fig. 6-9: Porosity for suspension with 36 Vol.% solid load and 1cm distance from cooling surface in dependence of cooling plate material

Fig 6-9 shows the changes of porosity in dependence of cooling plate material. In case the cooling surface influences the nucleation process it will affect the critical nuclei size. As presented above the porosity is strongly dependent on the ice crystals size. Therefore, difference in the porosity values near the cooling surface should be

achieved. As can clearly be seen significant changes in porosity values have not been observed even by changing the freezing temperature. The deviations in the values correspond to the measurement errors. The same results have been obtained for the pore radii presented in Fig. 6-10.

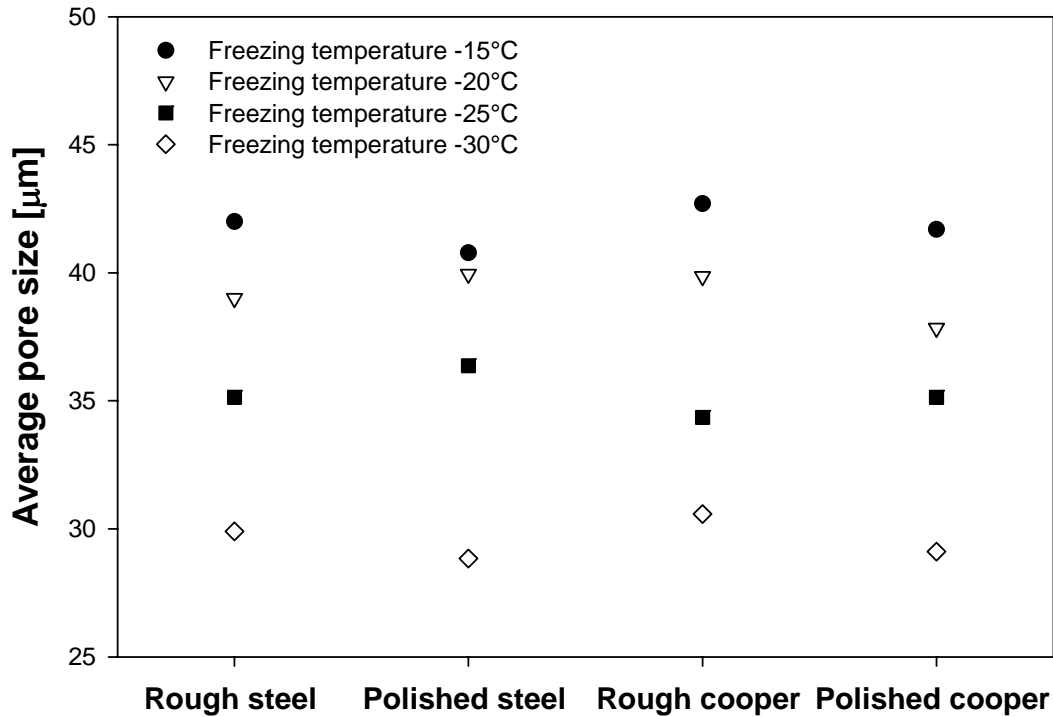


Fig. 6-10: Average pore radius for suspension with 36 Vol.% solid load and 1cm distance from cooling surface in dependence of cooling plate material

In Fig. 5-42 results for porosity values are presented in dependence of moulding form materials. From the figure it can be seen that both curves follows the same manner and the deviation in results is about 3-5% which can be accorded to the measurement errors.

Fig. 5-54 shows the experimental results for pore size distributions obtained for suspensions with the same solid load content and frozen at the same temperatures where only the moulding form material varies. Small differences in pore radius values have been detected but are in a good agreement according to the measurement mistakes. Evidently it is shown that the moulding form material does not significantly affect the pore size distribution even near the cooling plate surface.

If the nucleation process starts on the moulding form surface change in porosity and pore size distribution should be detected in the state of obtaining the critical nuclei with different sizes. From the presented results such a difference has not been observed. From all above presented results it can be concluded that the nucleation process is almost independent of the cooling plate and the moulding form material and properties. Therefore, it has been supposed that nucleation occurs on ceramic particles surface. Padilla and Talanquer [Pad01] reported that in case of heterogeneous nucleation of supersaturated vapours on spherical aerosol-like substrates the work of formation for the critical nucleus increases when the radius of the aerosol particles decrease in a given supersaturated vapour. According to this statement it can be supposed that in case of the presence of two materials with different particle size, for Al_2O_3 700nm and for SiO_2 14nm in diameter, the nucleation process will occur on the alumina particles surface because it is energetically preferable. From the literature it is known that the alumina particles are very hydrophilic. Therefore a building of a surrounding layer of the water molecules can be expected. The information obtained from the company shows that the alumina particles have a total porosity of 59,4%, surface area 60- 80 m^2/g and an average pore diameter 3,5nm. Such conditions of high surface area, porous structure, therefore high roughness can be considered as optimal conditions for heterogeneous nucleation. The particle surface has been studied by SEM. Figs. 5-44 and 5-45 show alumina and silica particle surfaces, respectively. From the micrographs it can be seen a very rough and porous surface of the alumina particles while the silica particle surfaces is smoother and only some cracks have been observed. By using Fletcher's and Gorbunov's theory it can be predicted that nucleation occurs inside the particle pores. Fig. 6-11 shows the results obtained for crystal growth in dependence of the volume fraction of solids. As can be seen the volume fraction of solids strongly influences the crystal growth where by increasing the solid volume fraction crystal growth exponentially increases. Such results have been observed at all freezing temperatures and distances from the cooling plate. This result can be attributed to less water, which needs to be crystallized, due to increasing solid loads. The time needed for nucleation and complete sample freezing (crystallization) is reduced because the ceramic particles are "inert" for the crystallization process. Fig. 6-12 shows the time needed for nucleation obtained from the cooling curves (see Fig. 5-28).

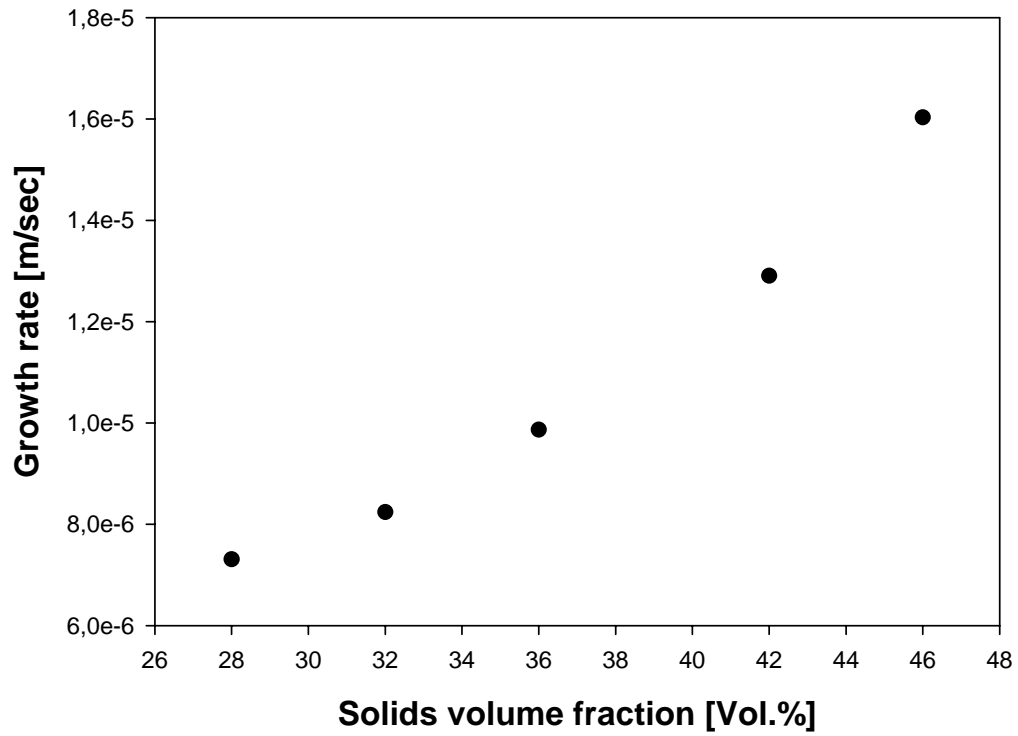


Fig. 6-11: Crystal growth rate for suspensions frozen at -25°C and distance from cooling plate 1cm

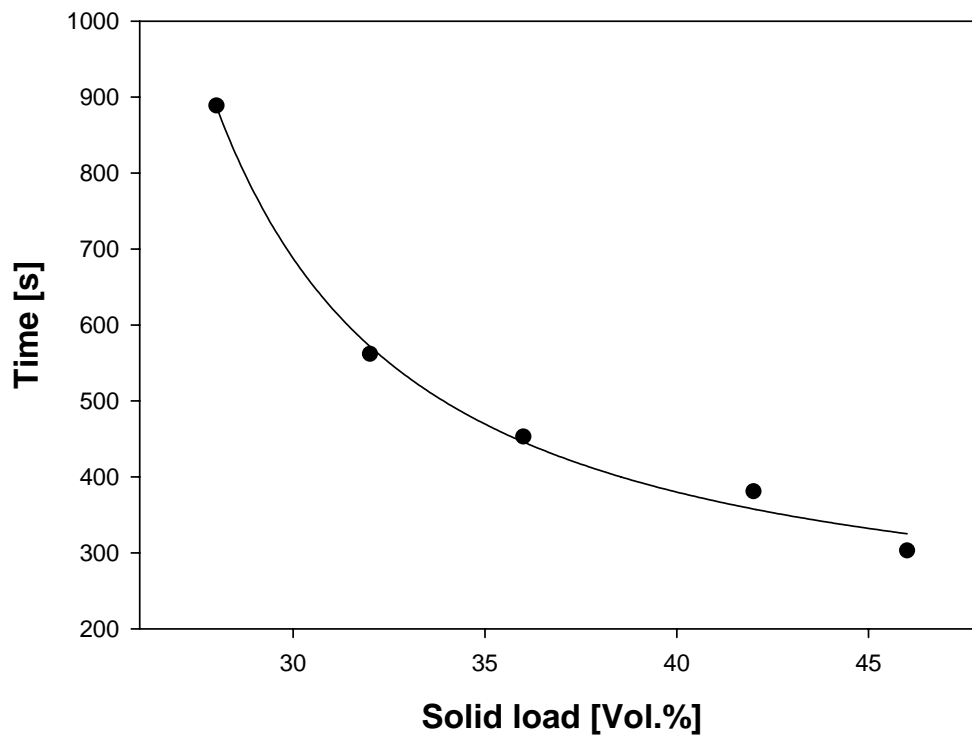


Fig. 6-12: Time needed for nucleation obtained for slurries cooled with $0,08\text{K/min}$

The time has been determined from time and temperature at which nucleation occurred until the system reach a stable cooling regime again. This result can be accorded to a better thermal conductivity inside the suspensions by increasing the solid load content. Thermal conductivity is the property that determines the working temperature levels of a material, and it is an important parameter in problems involving steady state heat transfer [Sant00]. Fig. 6-13 presents the thermal conductivity for all components in the slurries. From the figure is clear to be seen that alumina is the component, which continuously increase its thermal conductivity at decreasing temperature. Silica slightly decreases his thermal conductivity at temperature decrease. It is also apparent that two different regions can be identified for water. In the first region the thermal conductivity is decreasing by decreasing temperature down to 0°C. Region two starts at 0°C where a step appears at the water freezing temperature (crystallization starts) and ice thermal conductivity increase by decreasing temperature. In the second case a better and faster thermal distribution inside the slurries can be achieved.

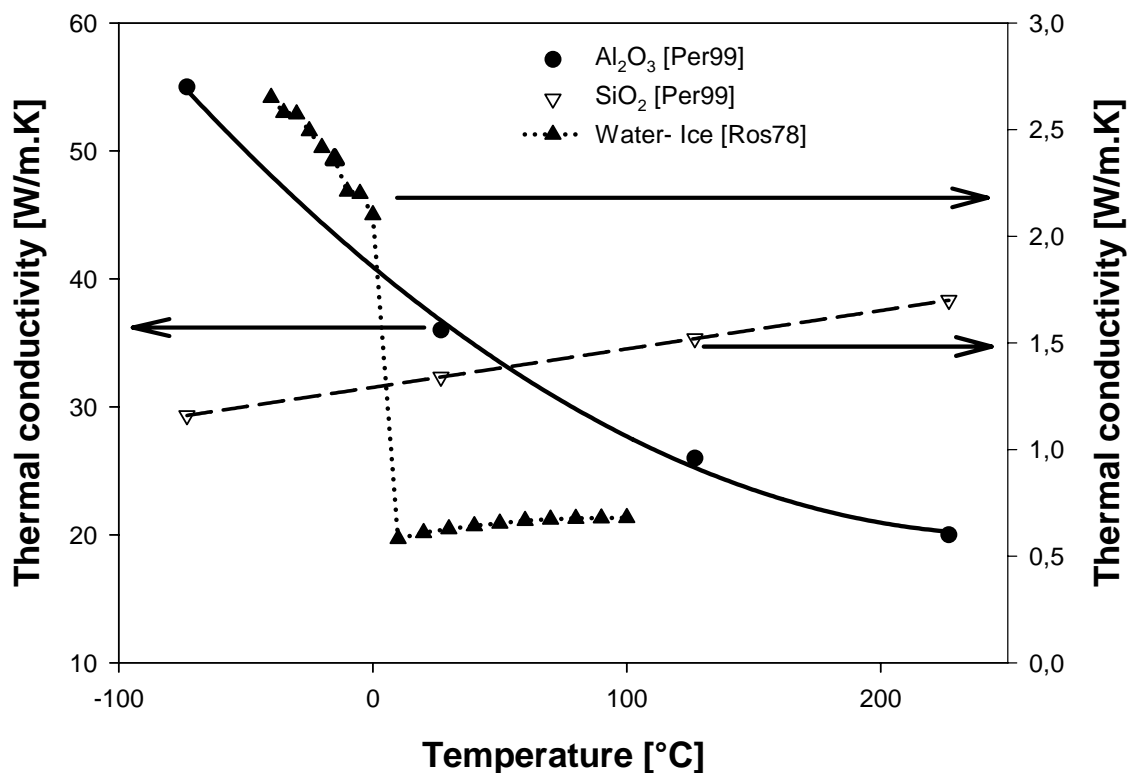


Fig. 6-13: Thermal conductivity for the slurries components

Crystal growth rate is temperature dependent as it was shown in Fig. 5-33. Driving force for the growth of ice crystals was found to be the temperature difference between the cold side (moulding form bottom) and the warm side (moulding form upper side), therefore an increase in the slurries thermal conductivity will result in faster growth.

In Fig. 6-14 are the calculated values for thermal conductivity plotted at various temperatures and solid load contents in the slurries. Apparent is that the thermal conductivity is strongly influenced by solid loads and slightly increase by decreasing temperature.

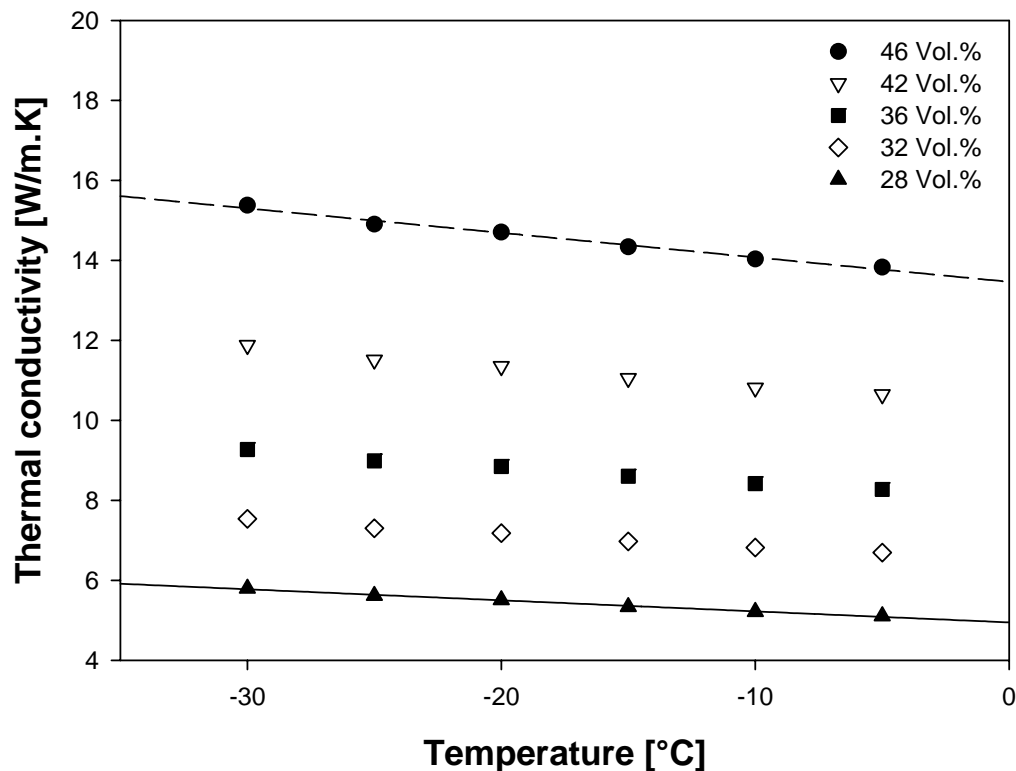


Fig. 6-14: Thermal conductivity for different slurries at various temperatures

From the economical point of view higher crystal growth is preferable [Kim01]. An increase of solid load content and decrease of freezing temperature will cover such a request. Also by increasing of solid load content and increase of mechanical stability of the products can be expected. For all industrial needs an optimum between solid loads and obtained porosity, as well as pore size distribution needs to be found according to the desired properties.

6.3 Porosity and pore size distribution

Fig. 6-15 (a) shows optical micrograph of porous samples taken at different distances from cooling plate prepared from slurry with 36 Vol.% solid loads and frozen at -15°C . The pores are distributed uniformly throughout the whole sample. That three-dimensional structures have been obtained can be seen by the micrographs of the next layer. The micrographs shows that the pores have a well-defined shape even by changing the distance from cooling plate or, as mentioned in the previous chapters, pore size gradient have been obtain in dependence of distance from cooling plate. The pores obtain their morphology from ice crystals. Therefore it was reasonable to suppose that there exists a dependence between pore size and crystal growth.

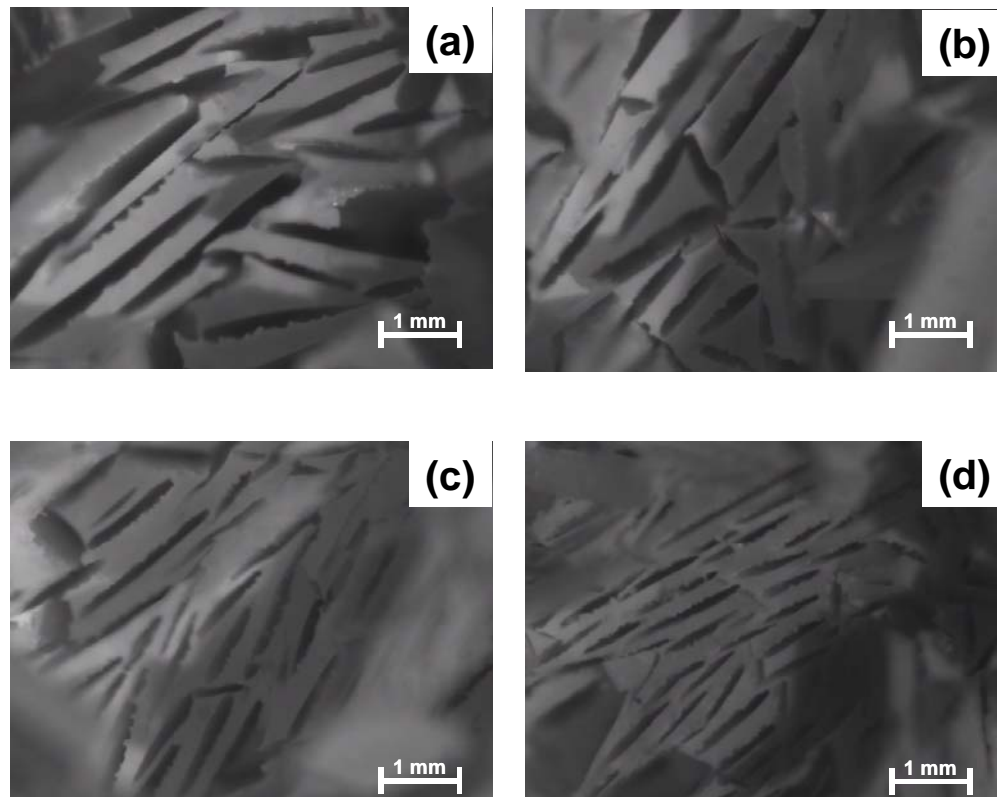


Fig. 6-15: Micrographs taken from samples cross sections perpendicularly but different distances from the cooling plate to the ice crystals growth direction for slurry with 36 Vol.% solid load frozen at -15°C . Micrograph (a) correspond to 5cm distance from cooling plate, (b) 4cm, (c) 3cm and (d) 2cm

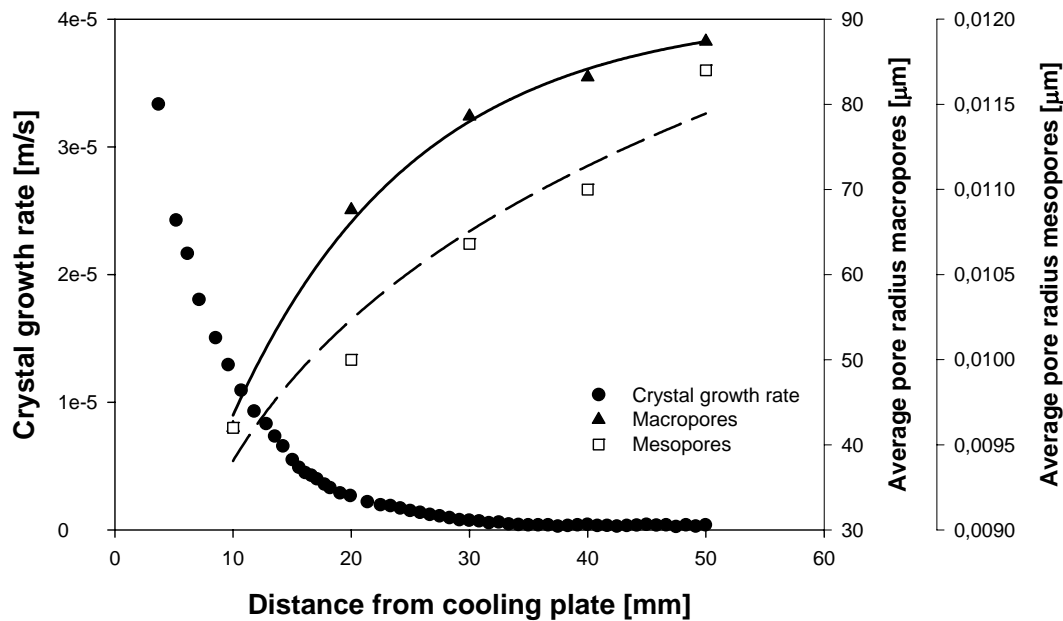


Fig. 6-16: Crystal growth rate, macro and mesopores in dependence of distance from cooling plate for slurry with 36 Vol.% solid load frozen at -15°C

Fig. 6-16 shows the dependency between crystal growth rate, macro and mesopores average radius and distance from cooling plate. It is apparent that the average pore radius is strongly dependent on the crystal growth rate. By decreasing the growth rate the pore radius increases. In Fig. 6-17 the pores radius is presented versus the crystal growth rate for slurry with 36 Vol.% solid loads frozen at different temperatures. An exponential decrease has been recognized for all curves. Generally it is known that at low crystal growth rates, respectively low temperature gradients, crystals with bigger sizes are build. This result indicates that the pore radius can widely be controlled by managing crystal growth. Therefore a good control of the temperature gradient between bottom and upper face of the moulding form needs to be achieved. The same behaviour has been observed for the investigated slurries at all freezing temperatures at all used cooling surfaces. From Fig. 6–17 also it can be seen that the increase of pore radius is greater at lower freezing temperature, therefore an increase of the pore size gradient has been observed. On the other hand processing at such a “high” temperature is not recommended from the industrial point of view because it takes too much time, (as has been shown in the previous chapter) for a complete freezing of the samples. In case such a pore size or pore

gradient needed a decrease of the products thickness or an increase of the solid load content is recommended. Also an overloading with solids is not recommended because in this a case lot of water molecules will be bond on the ceramic particle surfaces or will be incorporated inside the aggregates, which can cost elimination of the freezing process.

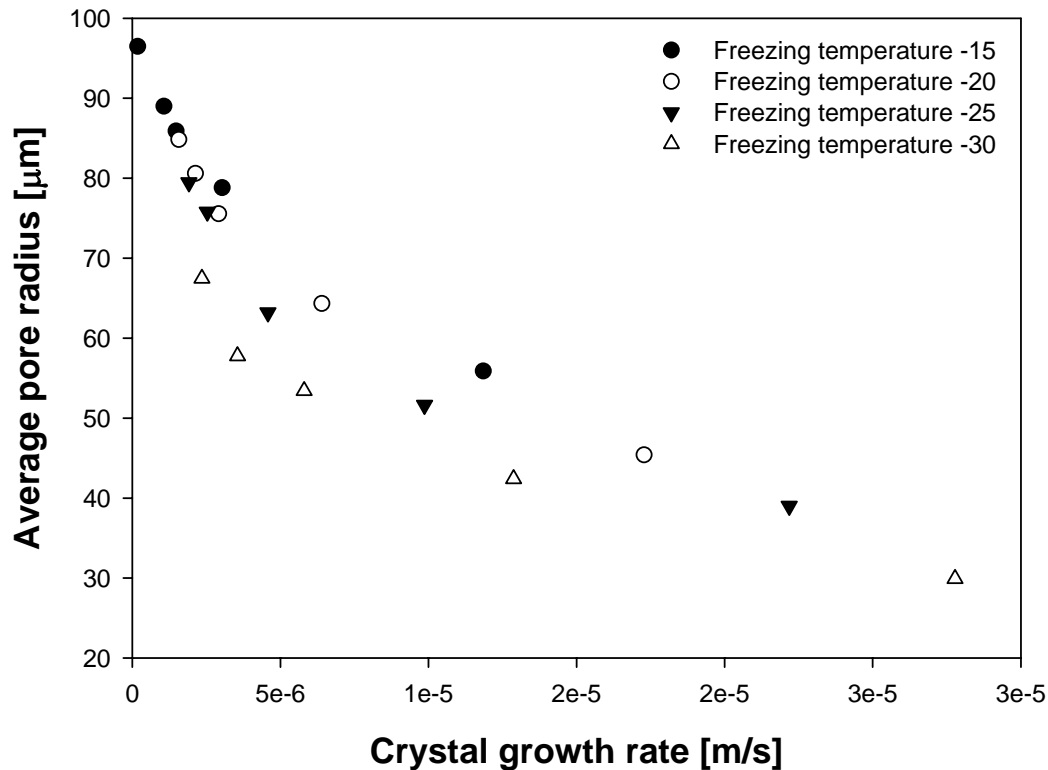


Fig. 6-17: Macropores average radius in dependence of crystal growth rate for a slurry with 36 Vol.% solids frozen at different temperatures

The dependence between an average pore radius and the obtained porosity has also been investigated. Fig. 6–18 illustrates the effect of the pore radius and the porosity in dependence of distance from cooling plate. From the figure it can be seen that with increasing the average pore radius the porosity decrease. This is in accordance with the volume of the created pores. Small pores have a higher surface therefore higher cumulative volume, which results in an increase of the degree of porosity. The results are presented in Fig. 6-19. The data presented above show that controlling the temperature gradient could control the average pores radius. Therefore the composition of the slurries and the freezing parameters are the key parameters, which determine the resulting pore size and morphology as well as the final porosity.

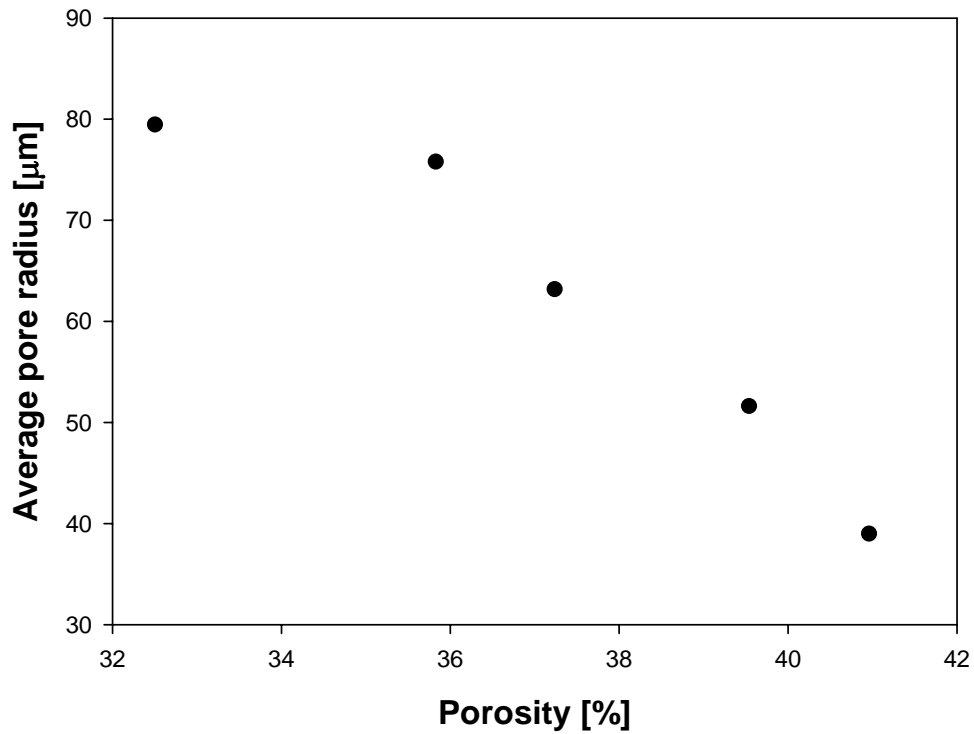


Fig. 6-18: Macropores average radius in dependence of porosity for a slurry with 36 Vol.% solids frozen at -25°C

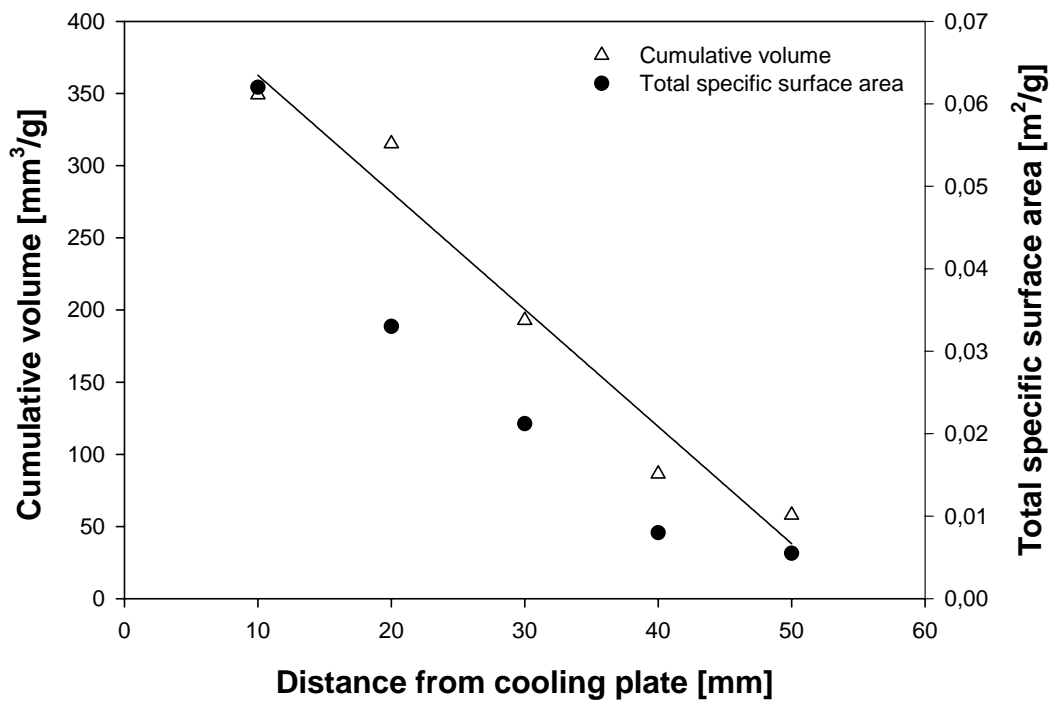


Fig. 6-19: Macropores cumulative volume and total specific surface area for a suspension with 36 Vol. % frozen at -25°C

All results presented here are for macropores. Also for mesopores the same parameters dependences have been observed. Fukasawa et al. [Fuk01, Fuk01a] reported that the mesopores disappeared when sintering was applied. Therefore all investigations here have been focused on the macropores development.

7. Conclusions

Macroporous ceramic materials with tailor-made pore size and porosity have been developed from aqueous slurries via the freeze casting route.

By following the evolution of porosity and pore size distribution it has been found that the main factors affecting those parameters are: bulk freezing temperature, ice crystal growth, temperature gradient between bottom and upper face and starting slurry composition.

The experimental results obtained for the rheological properties of the starting slurries have been found in conformity with experimental data and theoretical prediction methods reported by other authors. On the basis of rheological measurements, the influence of ceramic particles content on the slurries properties was discussed. It has been found that the starting slurry conditions influenced the pore size distribution as well as the density of the samples after freezing.

A pore size and porosity gradient in dependence of product thickness has been obtained by varying the temperature gradient, respectively ice crystals growth rate.

The conditions for the occurring of nucleation, and furthermore crystal growth have been investigated. The nucleation kinetic data have been carried out. Attempts to fit the results to the classical nucleation theory have been done. It has been found that the critical nucleus size in dependence from the cooling plate and the moulding form material are restricting and are not in agreement with the classical theories.

The same behaviour as in dependence from cooling plate and moulding form material has been found for the obtained pores with respect to size and morphology. Therefore it has been concluded that nucleation occurs on the surface of the ceramic particles. This suggestion was confirmed by the study of nucleation kinetics. This conclusion is interesting from the industrial point of view because cheaper materials can be used for preparation of cooling surface and moulds.

The result has been found in good agreement with the theories for active site nucleation.

The variations of solid load content and freezing temperature lead to an optimal to be achieved properties.

The results confirm that the processing behaviour of suspensions from bimodal ceramic particles is rather complicated and cannot be understood exclusively on the basis of existing packing theories. Therefore a modelling of the process can only be

done on the bases of physical properties such as ice crystal growth rate and suspension density. This is especially true, if the particles are not ideally dispersed, which is the case for many suspensions. More knowledge is needed concerning the structure of such suspensions.

The production of ceramic microstructures requires development efforts in the field of microstructural shaping. It seems that freeze casting is one of the most promising methods for developing of multicomponent ceramics for microstructural applications, because of its well controllable pore size, as well as porosity, its simplicity and environmental friendliness.

8. Zusammenfassung

Makroporöse keramische Materialien mit entsprechender poröser Struktur und Porösität wurden aus wasserhaltigen Schlickern über das freeze casting erzeugt. Bei der Untersuchung zur Entwicklung der Porösität und der Porengrößenverteilung wurde festgestellt, dass die Grundfaktoren, die wirken folgende Parameter sind: Gefriertemperatur, Eiskristallwachstum, Temperaturgradient zwischen Boden und oberer Seite des keramischen Basisschlickers.

Die experimentellen Ergebnisse, die sich ergeben bei der Untersuchung der rheologischen Eigenschaften der Basisschlicker, wurden mit experimentellen Daten und theoretischen Ansätzen, die von anderen Autoren, veröffentlicht wurden, komplettiert und verglichen. Auf Grund der rheologischen Messungen wurde der Einfluss des Gehaltes der keramischen Partikeln auf die Eigenschaften der Schlicker festgestellt. Die Eigenschaften des Basisschlicker haben Einfluss auf die Porengrößenverteilung, frieren der Proben.

Die Porengröße und Porosität ergeben sich, in Abhängigkeit von der Dicke der Probe. Bei einer Änderung des Temperaturgradienten, verändern sich entsprechend die Eiskristallwachstumsgeschwindigkeiten. Die Bedingungen für das Eintreten einer Keimbildung, und danach einem Wachsen von Kristallen, wurden untersucht. Die Kinetik der Keimbildung wurde herausgearbeitet.

Es wurden Versuche durchgeführt, um die Ergebnisse mit der klassischen Keimbildungstheorie zu qualifizieren.

Es wurde auch festgestellt, dass der kritische Keimradius in Abhängigkeit von der gefrorenen Oberfläche und der Gussform als Material begrenzt wird. Das gleiche Phänomen der Abhängigkeit vom Material der frierenden Oberfläche wurde für die gebildeten Poren, d.h. Größe und Morphologie festgestellt. Aus diesem Grunde- ist festzuhalten, dass die Keimbildung auf der Oberfläche der keramischen Partikeln stattfindet.

Es folgt als Schlussfolgerung aus den o.g. Ergebnissen für den Blickwinkel der Industrie einen interessanten Aspekt.

Es können billigere Materialien für die Herstellung der Gussform benutzt werden da die Oberflächen für die Keimbildung nicht relevant sind.

Dieses Ergebnis ist in sehr guter Übereinstimmung mit den Theorien für „active site nucleation“. Aus den verschiedenen Variationen von Feststoffgehalt und Gefriertemperatur werden über eine Optimierung die gewünschten Eigenschaften erlangt.

Die gefundenen Ergebnisse bestätigen, dass das Verhalten der Suspensionen mit bimodalen keramischen Partikeln sehr kompliziert ist. Die Ergebnisse bleiben nicht ganz verständlich und sind nicht zur Gänze der existierenden „Packing theorie“ zu beschreiben.

Aufgrund der genannten Effekte kann das Modellieren des Prozesses nicht nur auf Grund der physikalischen Eigenschaften, wie

Kristallwachstumsgeschwindigkeit und Feststoffgehalt entwickelt werden.

Das ist besonderes in den Fällen gültig, bei denen die keramischen Partikeln nicht ideal im Volumen verteilt sind, wie es bei fast allen Suspensionen der Fall ist.

Mehr Wissen über die Struktur von Suspensionen ist nötig um alle Effekte zu erfassen.

Es sieht so aus, dass das freeze casting eine viel versprechende Methode für das Herstellen von keramischen Materialien aus vielen Komponenten mit Mikrostruktur ist . Das gutea Kontrollieren der Porengrößen und der Porosität ist dafür der Hauptgrund neben der hohen Umweltfreundlichkeit des Verfahrens.

9. List of Symbols

A	constant
A_c	crystal surface area
A_{hkl}	areas growth rates of all the faces on a crystal
A_{hs}	area of the heat transfer surface
b	constant (Eq. 4.1)
B	plate surface
ΔC	supersaturation (=C _c -C*) (kmol/m ³)
C	volumetric specific heat
C_c	concentration of solution
C*	saturation concentration
c	concentration of clusters
c*	concentration of clusters at equilibrium
D_{AB}	Diffusion coefficient (m ² /s)
d	distance between two parallel plates with surface A
d_m	Molecular diameter (m)
E_G	activation energy
F	share force
F_{elect}	electrostatic potential energy between charged particles
F_{steric}	steric potential energy between particles resulting from adsorbed species
F_{structural}	structural potential energy between particles resulting from nonadsorbed species
F_{total}	total interparticle potential energy
F_{vdW}	van der Waals potential energy between particles
f(m,x)	volume factor on a convex spherical surface
G	overall linear growth rate
G₁	first stage free energy
G₂	second stage free energy
G₃	third stage free energy
G_{cryt}	critical free energy
ΔG	free energy
ΔG_s	free energy between the surface of the particle and the bulk

ΔG_v	is the volume free energy change of the transformation per unit volume
ΔG_v	free energy between a very large particle and the solute in solution
h	thickness
ΔH_f	Enthalpy of fusion
ΔH_w	latent heat of water (335kJ/kg)
J	nucleation rate
J_0	nucleation rate prefactor
K	Equilibrium (distribution) coefficient, factor
K_g	constant
k	Boltzmann's constant
k_g	constant
k_t	thermal conductivity
L	characteristic dimension (length)
M_c	crystal mass
m	surface parameter (= $\cos\theta$)
n	fitting parameter (Eq. 4.3)
p	constant (Eq.4.1 recommended value 2/3)
P_e	external pressure
r	nuclei's radius
r^*	nuclei's critical radius
r_p	pores radius
r_w	Wenzel's correction factor (r_w =actual surface area/planar surface area)
R	radius of a spherical particle
R_G	overall mass growth rate
S	Supersaturation ratio ($S= c/c^* = \sigma+1$)
S_a	area of an active site
S_{sl}	solid-liquid interfacial area (a.k.a. contact area)
T	temperature
T_m	melting temperature
T^*	is the solid-liquid equilibrium temperature in Kelvin
t	time
V	volume of the sample
V_B	bulk volume
V_c	cumulative mercury volume

V_{cl}	closed pores volume
V_{hkl}	face growth rate
V_{op}	open void volume
V_{max}	total mercury volume penetrated into the sample at the end of measurement
V_{tot}	total volume
V_v	void volume
W	water content
W_{in}	non-equilibrium water at the beginning of nucleation process
$W^*(T)$	equilibrium unfrozen water content
X	ratio of R to r^*
α	factor proportional to fraction of particle surface area taken up by a cavity
v	molecular volume
σ	is the liquid-vapour interfacial tension
σ_c	is the critical interfacial tension in Zisman's plot
σ_{cl}	is the crystal-liquid interfacial tension
σ_{cs}	is the crystal-solid interfacial tension
σ_m	is mercury surface tension
σ_{sl}	is the solid-liquid interfacial tension
θ	contact angle
θ_a	active site cluster contact angle
θ_m	mercury contact angle
θ_o	background surface cluster contact angle
ψ	angle used to describe a cluster on a spherically convex surface
ϕ	angle used to describe a cluster on a spherically convex surface
ϕ_{sl}	volume fraction of solids
ϕ^*_{sl}	fitting parameter (Eq. 4.3)
ε	porosity
$\dot{\varepsilon}$	is the strain rate
ε_{app}	apparent porosity
ε_{cl}	closed porosity

ε_e	effective porosity
ε_{tot}	total porosity
ε_{app}	apparent porosity
ρ	crystal density
ρ_{AD}	apparent density
ρ_{BD}	bulk density
ρ_s	slurry density
β	area shape factor
λ	volume shape factor
λ	viscosity
η_0	low share viscosity
η_l	viscosity of the liquid phase
η_r	relative viscosity
η_s	suspension viscosity at specific share rate
η_{sr}	relative high shear rate viscosity
η_0	low share viscosity
η_∞	high share viscosity
τ	characteristic time of crystallization
τ_s	the applied share stress

Appendix A

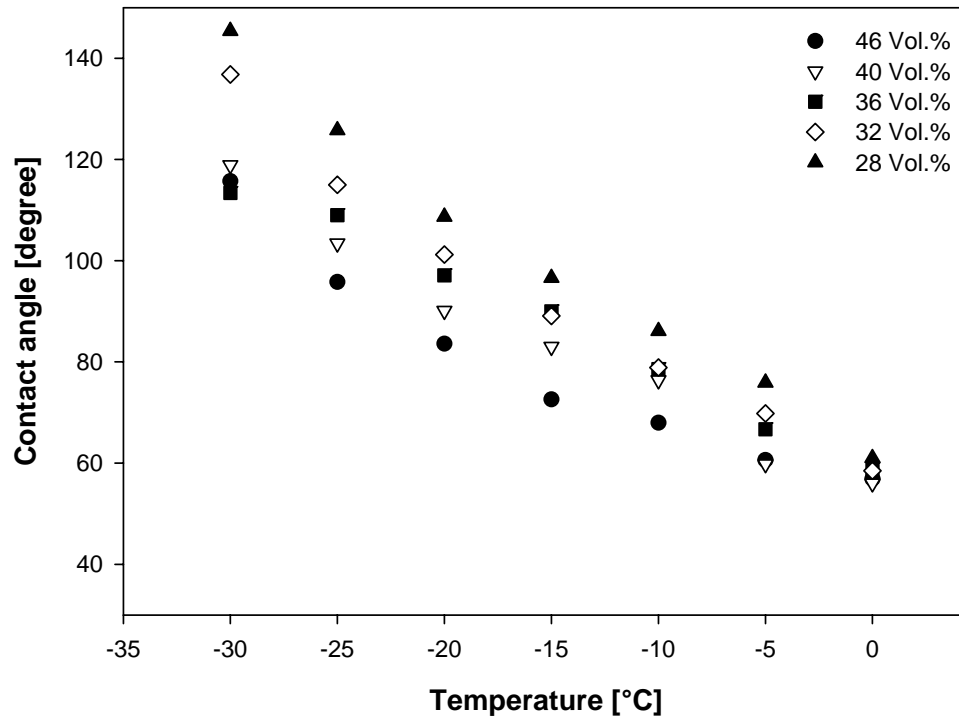


Fig. A.1: Contact angle versus temperature for rough steel surface

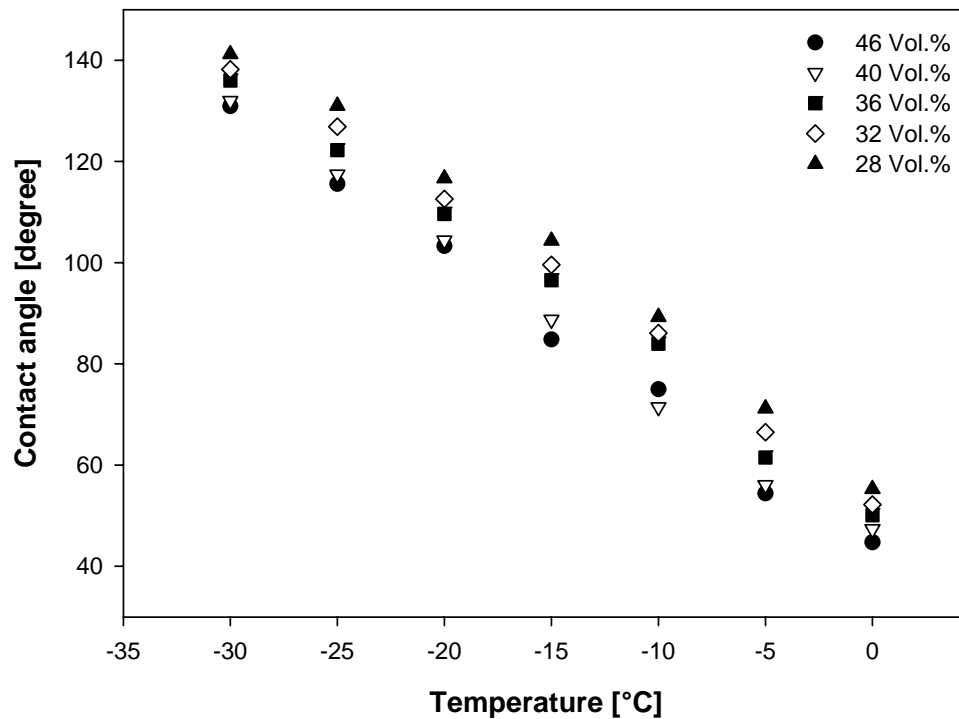


Fig. A.2: Contact angle versus temperature for polished cooper surface

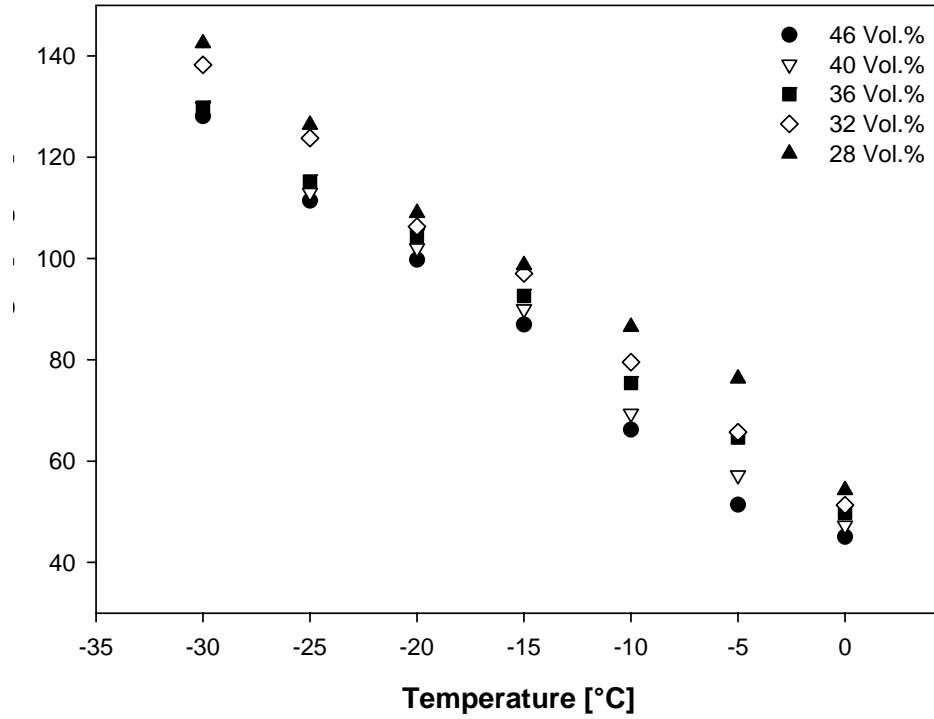


Fig. A.3: Contact angle versus temperature for rough copper surface

Appendix B

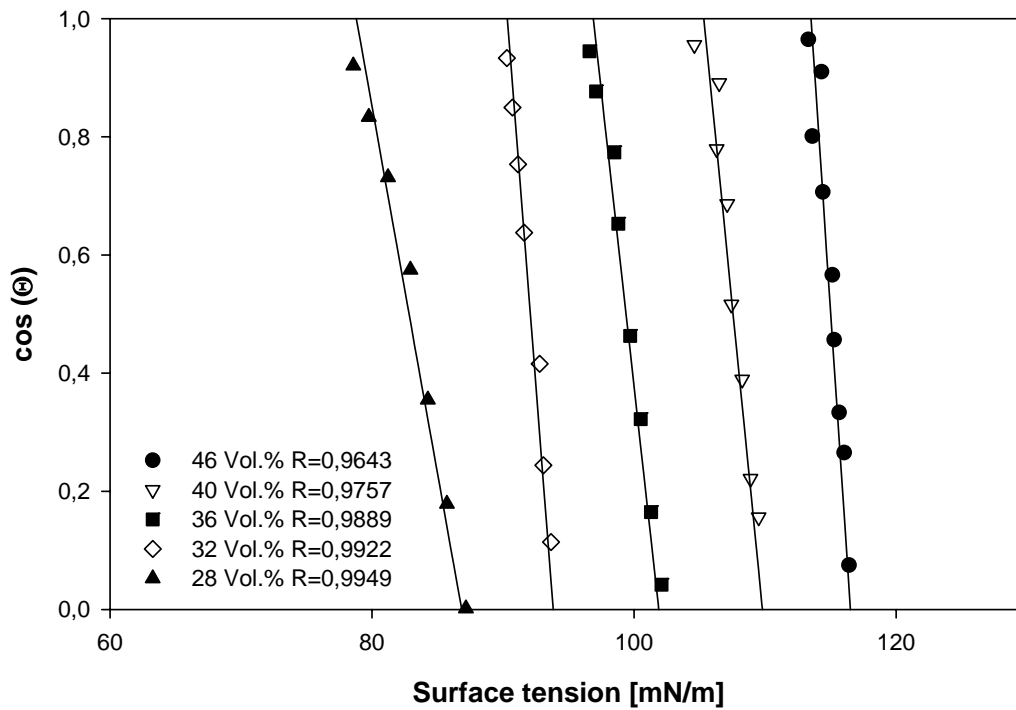


Fig. B.1: Zisman's plot for polished steel surface

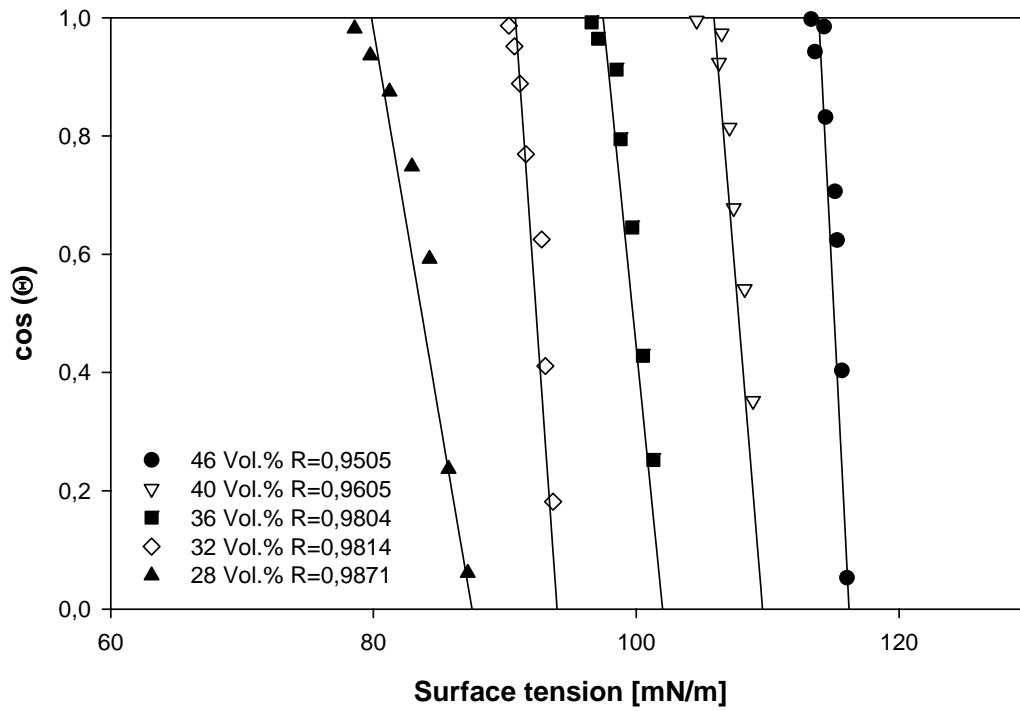


Fig. B.2: Zisman's plot for rough cooper surface

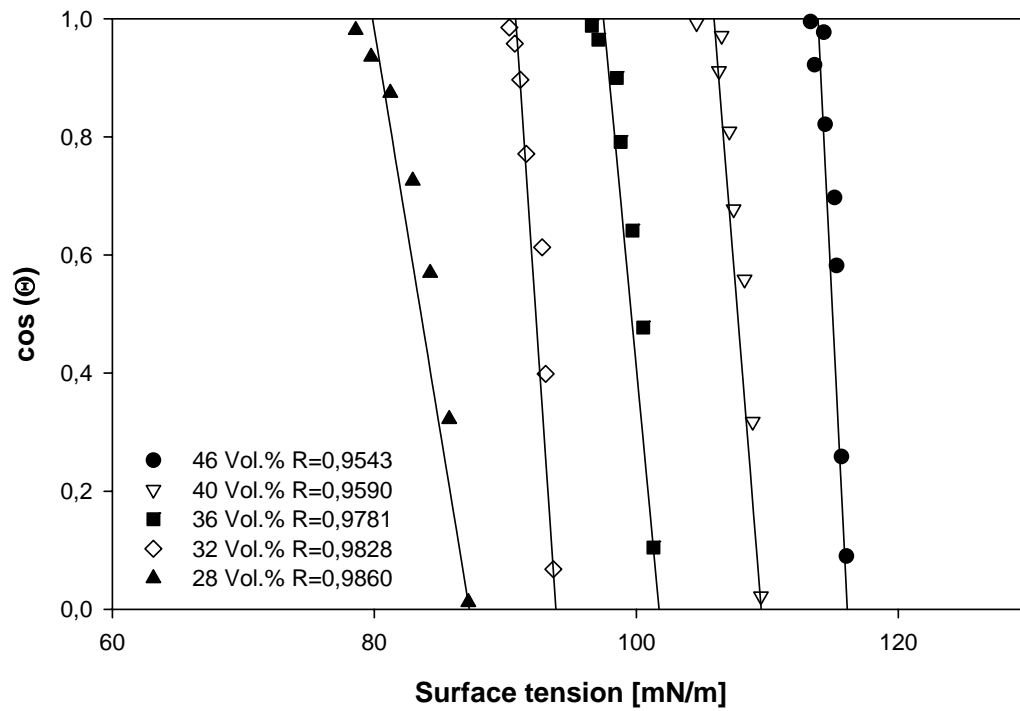


Fig. B.3: Zisman's plot for polished cooper surface

Appendix C

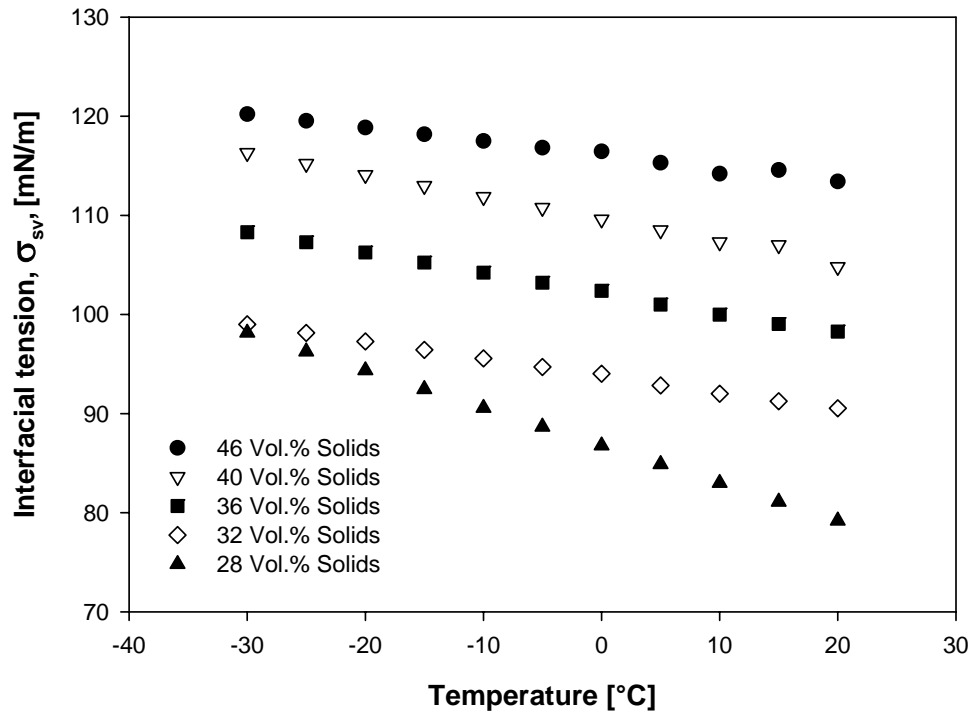


Fig. C.1: Calculated solid vapour interfacial tension for polished steel surface

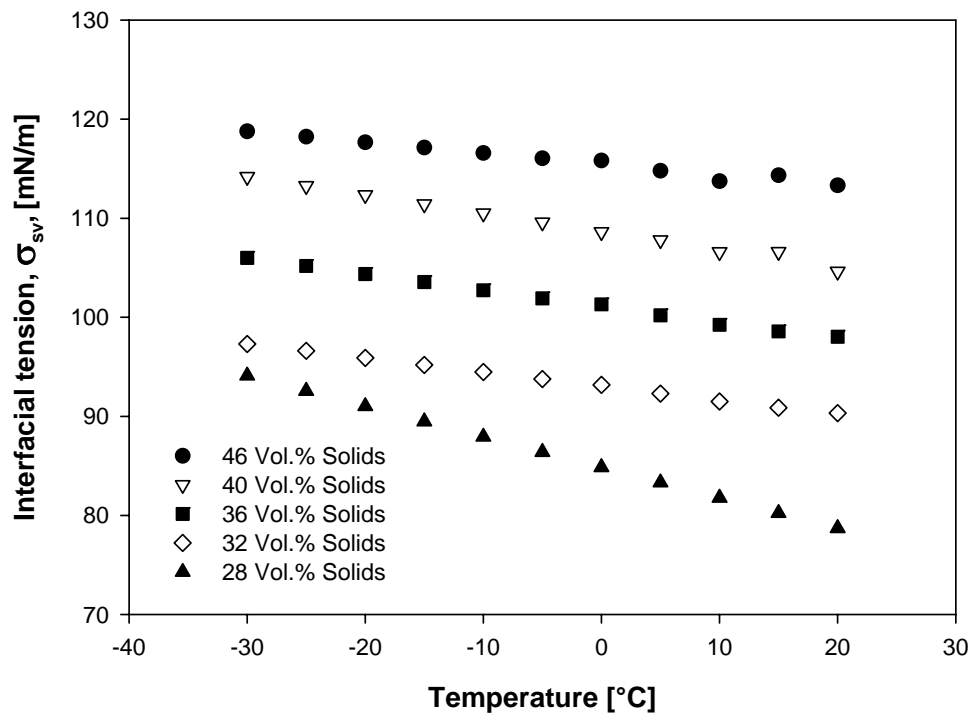


Fig. C.2: Calculated solid vapour interfacial tension for rough cooper surface

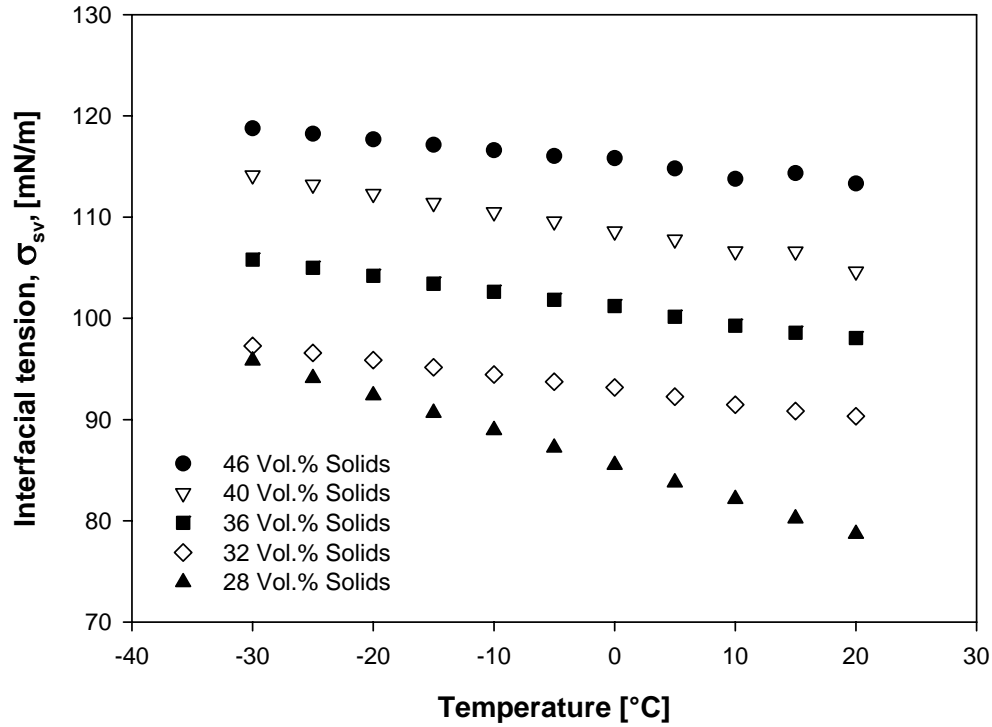


Fig. C.3: Calculated solid vapour interfacial tension for polished copper surface

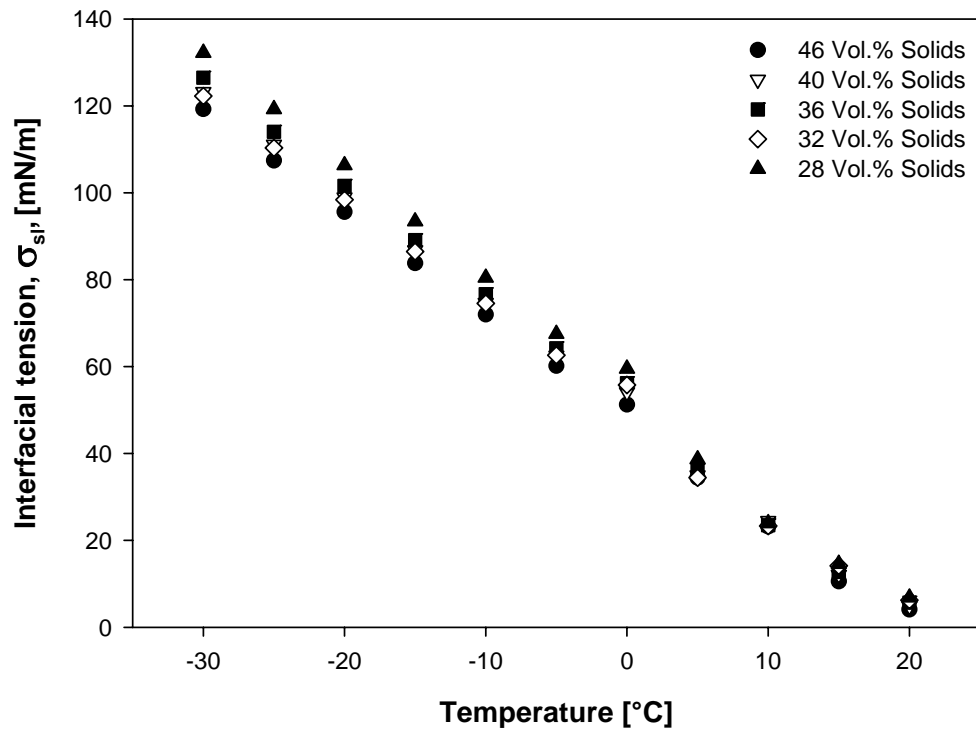


Fig. C.4: Calculated solid liquid interfacial tension for polished steel surface

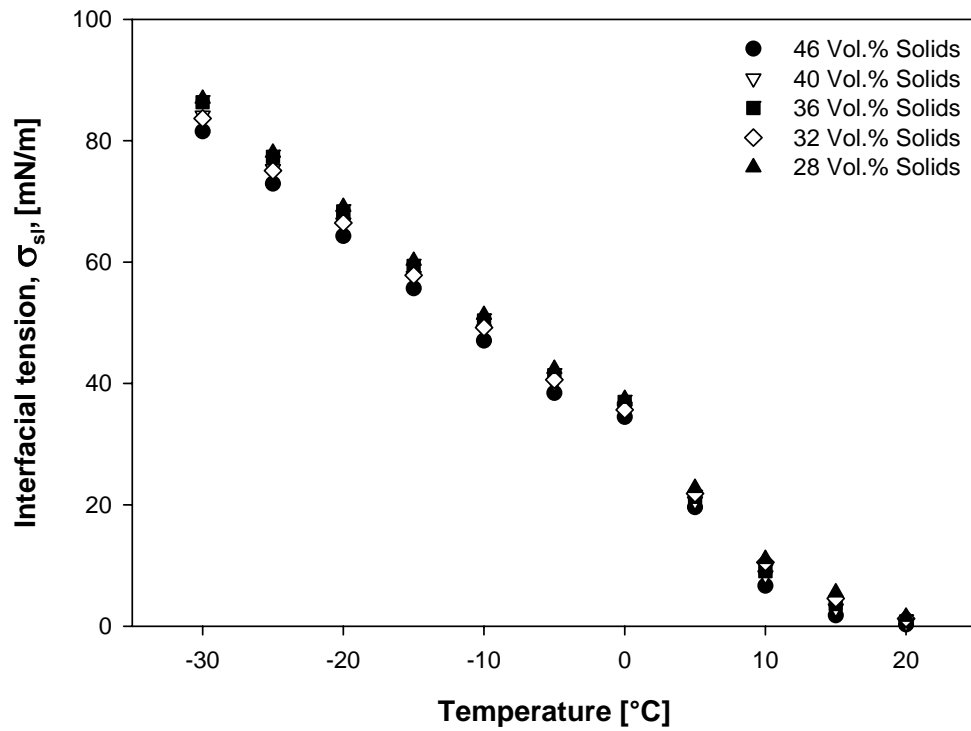


Fig. C.5: Calculated solid liquid interfacial tension for rough cooper surface

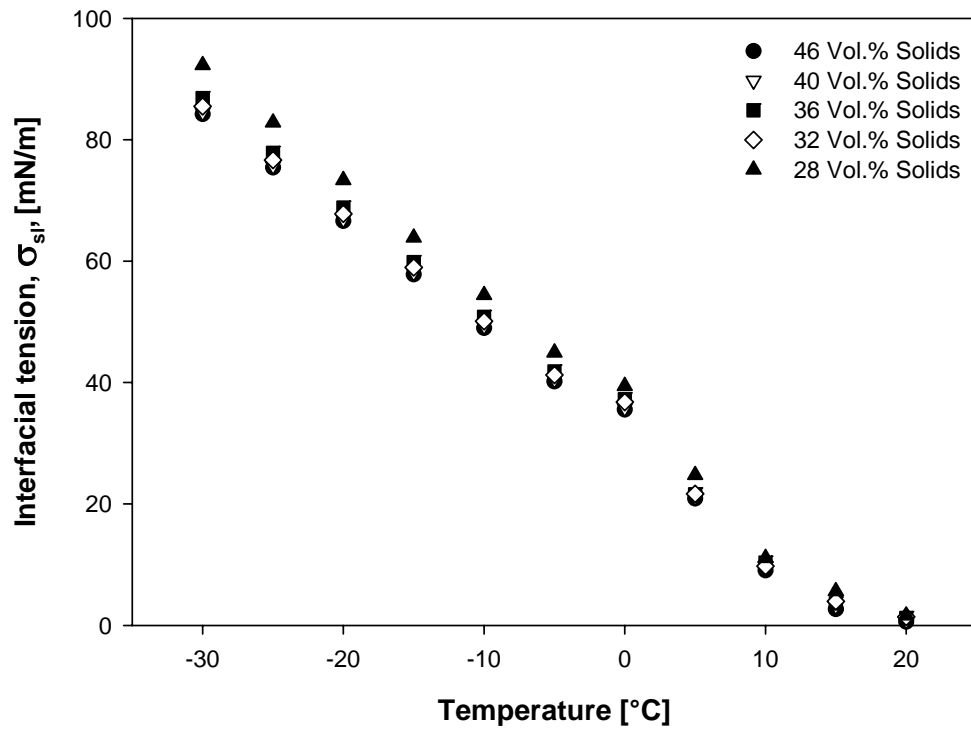
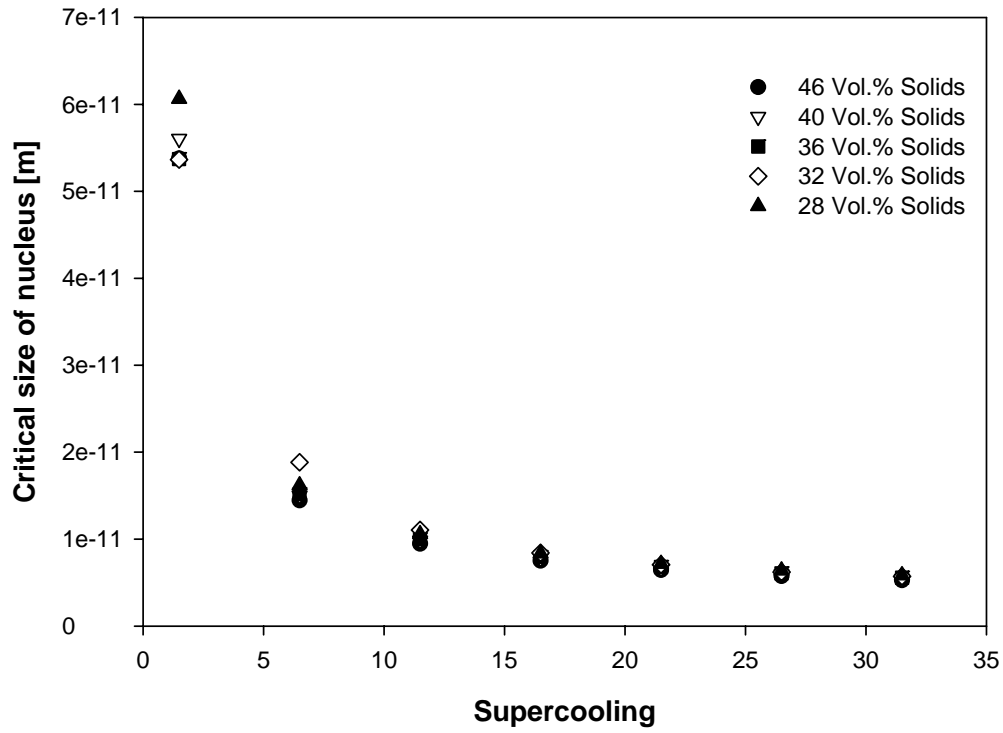
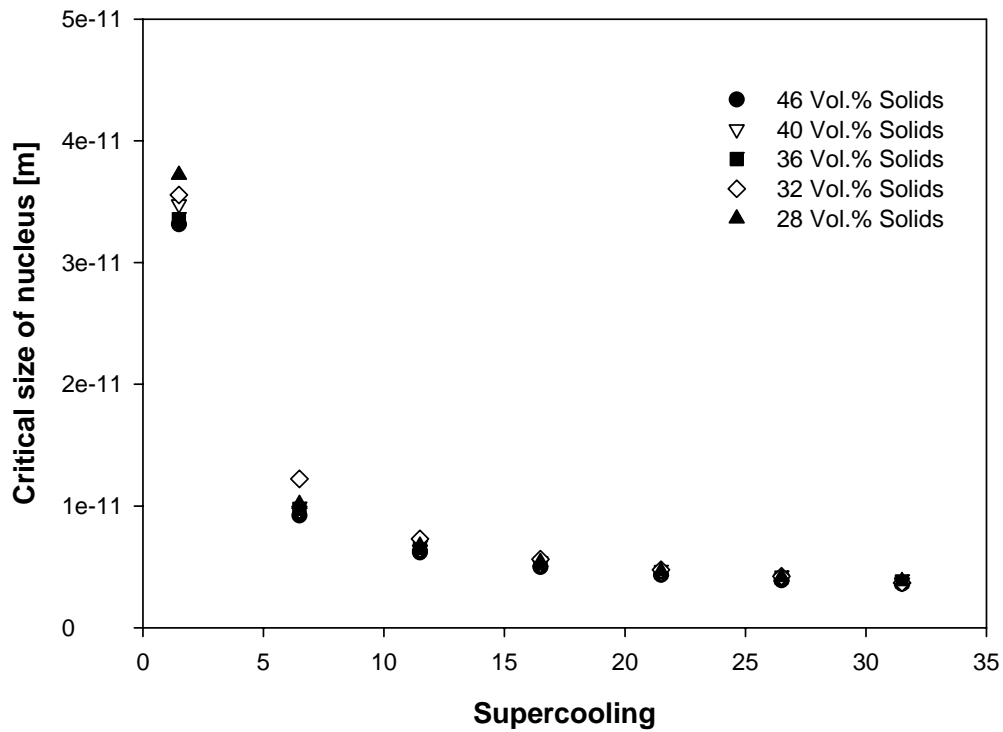


Fig. C.6: Calculated solid liquid interfacial tension for polished cooper surface

Appendix D

*Fig. D.1: Critical nucleus size for polished steel surface**Fig. D.2: Critical nucleus size for rough cooper surface*

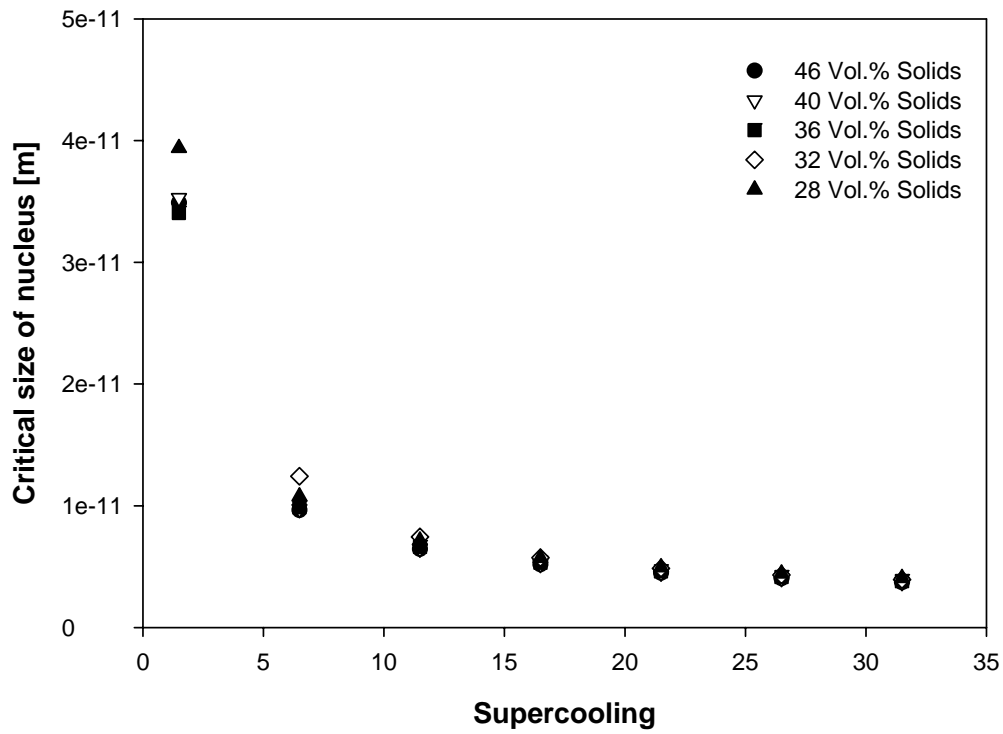


Fig. D.3: Critical nucleus size for polished copper surface

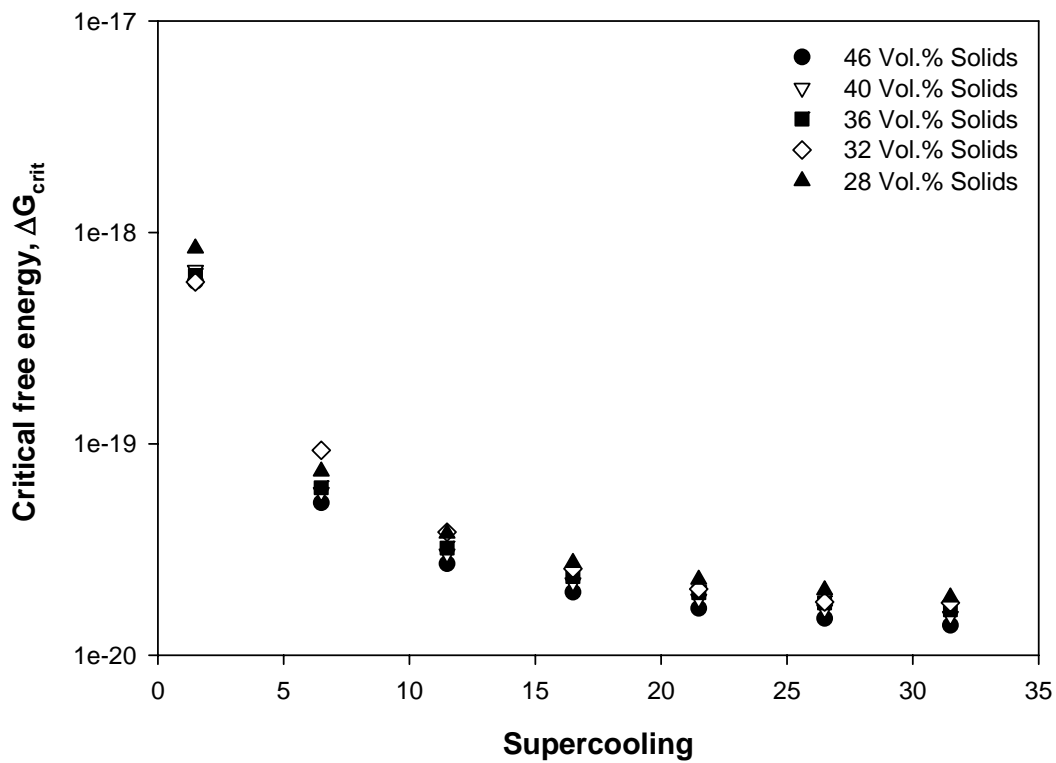


Fig. D.4: Critical free energy for polished steel surface

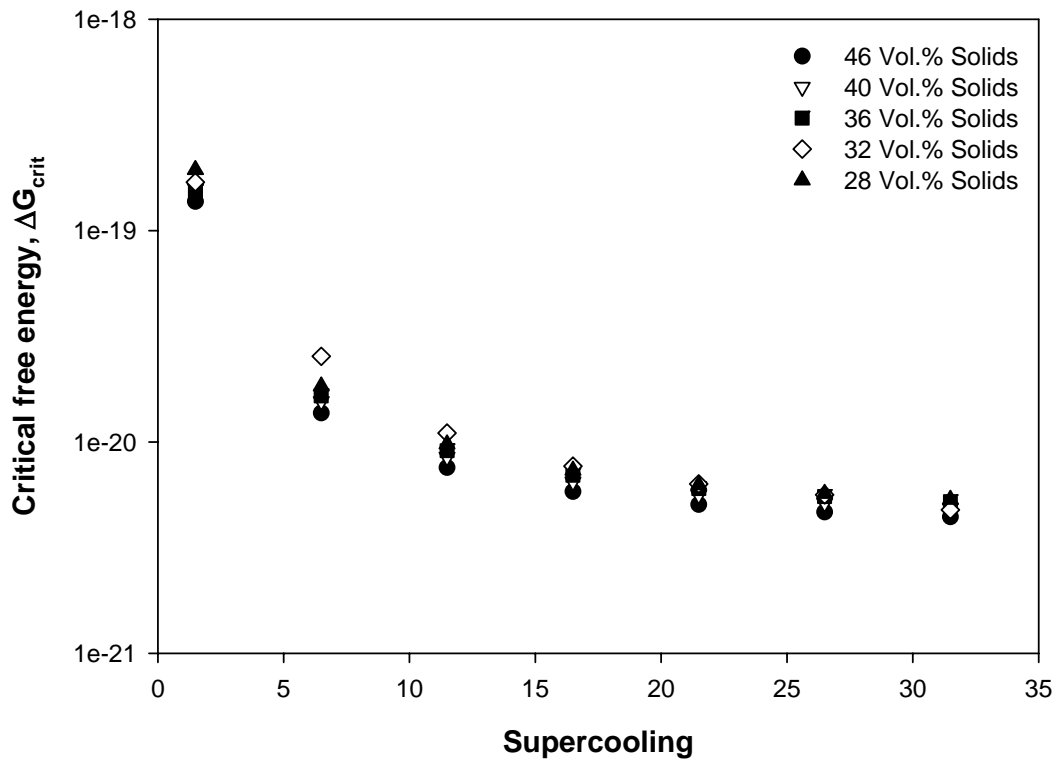


Fig. D.5: Critical free energy for rough copper surface

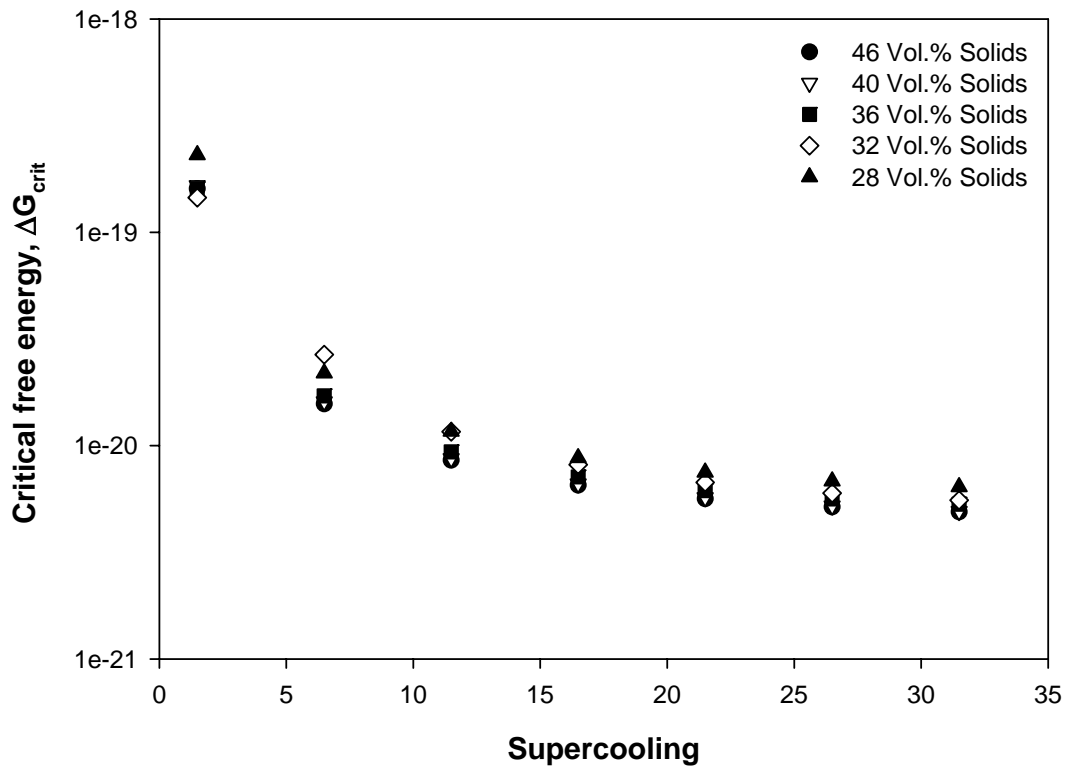


Fig. D.6: Critical free energy for polished copper surface

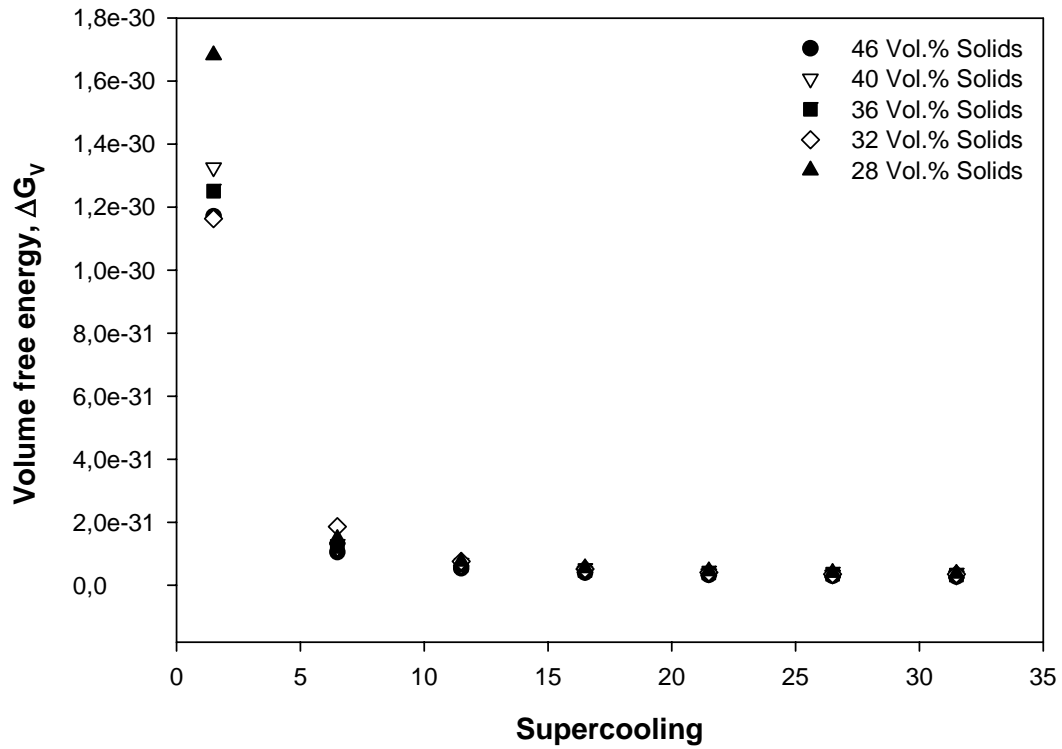


Fig. D.7: Volume free energy for polished steel surface

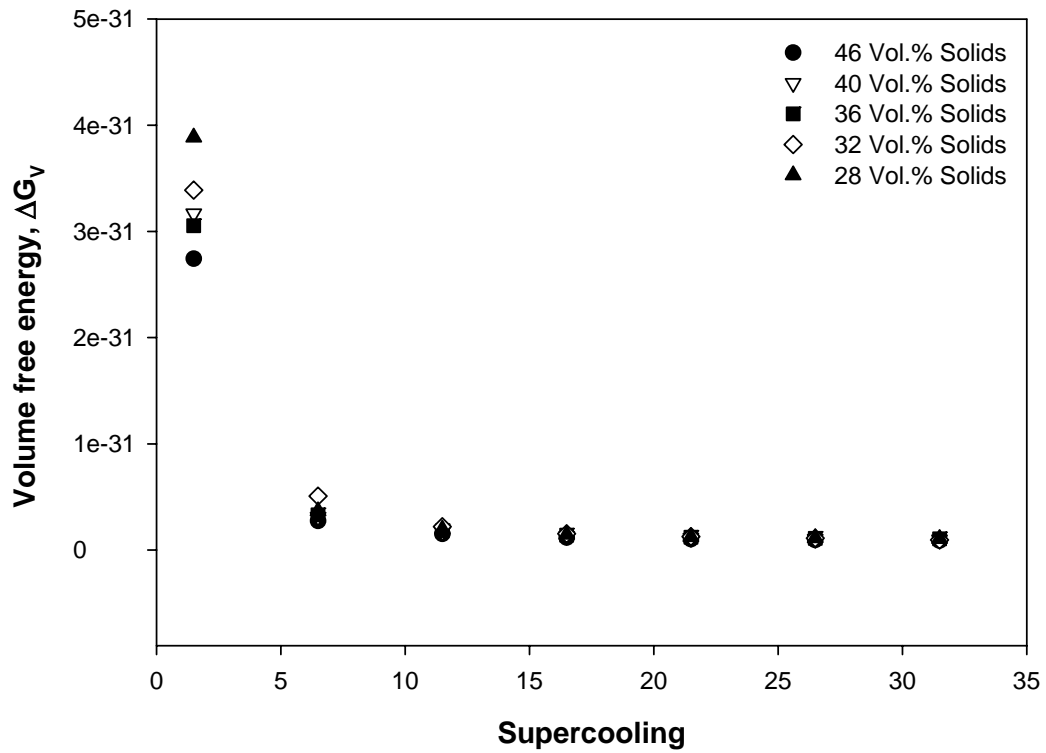


Fig. D.8: Volume free energy for rough cooper surface

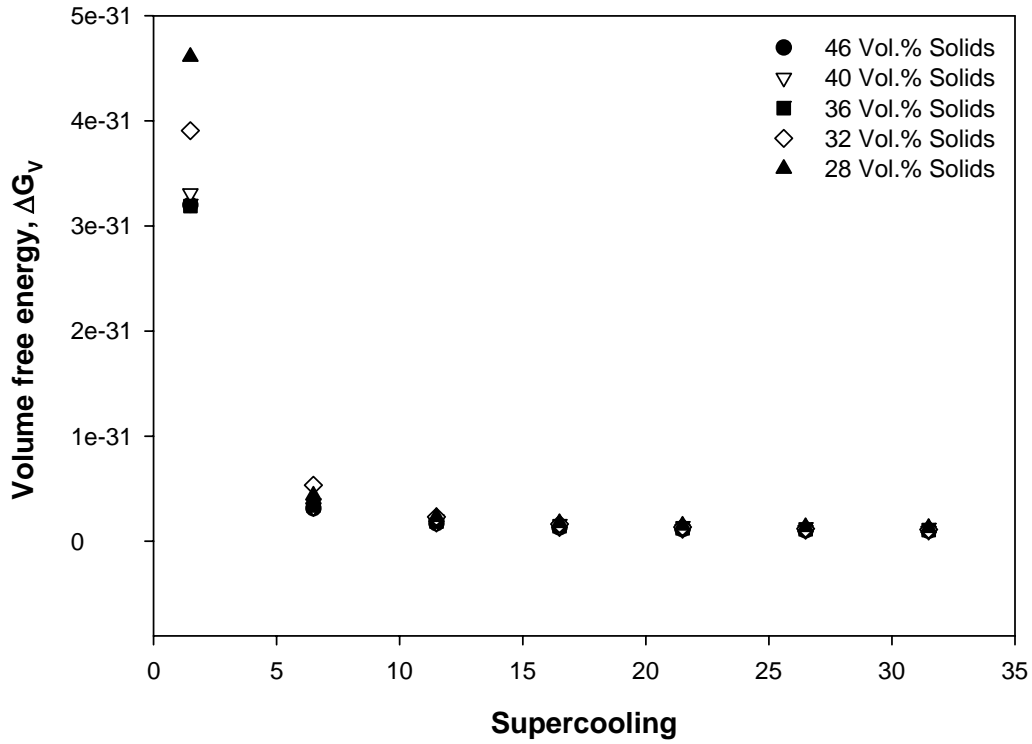


Fig. D.9: Volume free energy for polished copper surface

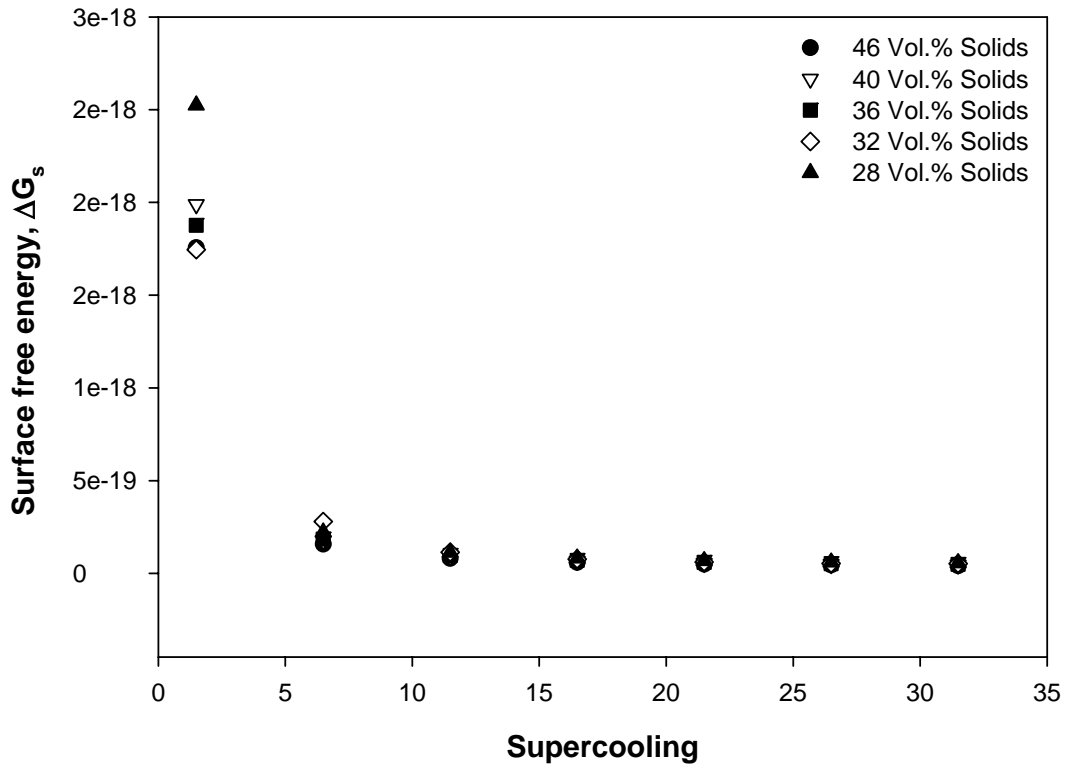


Fig. D.10: Surface free energy for polished steel surface

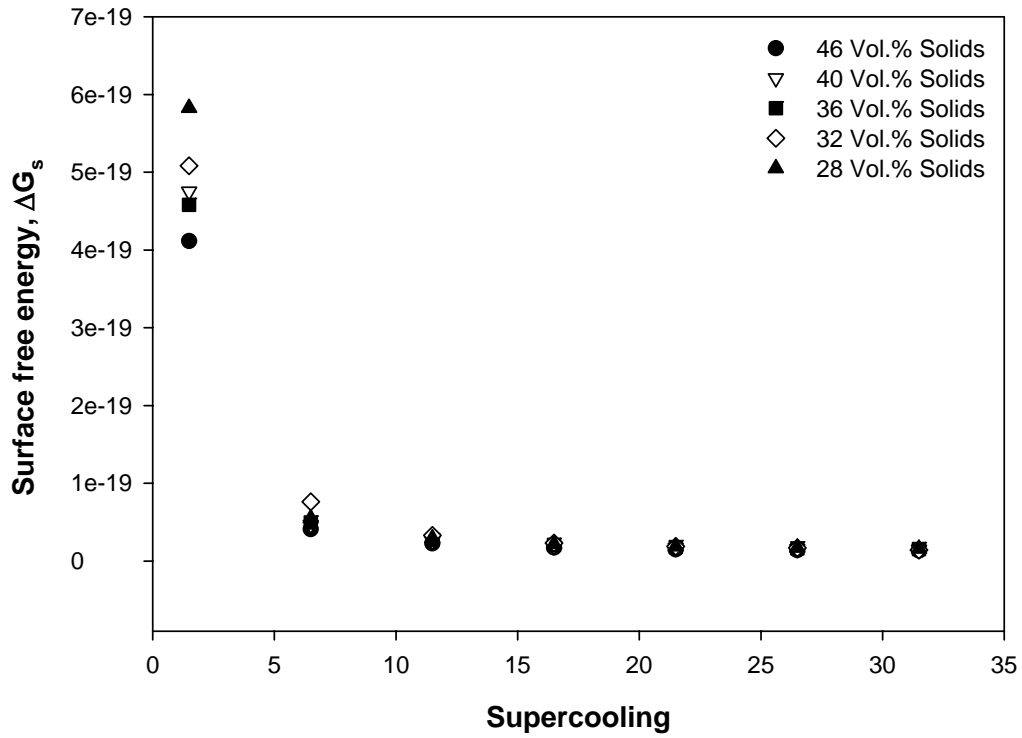


Fig. D.11: Surface free energy for rough copper surface

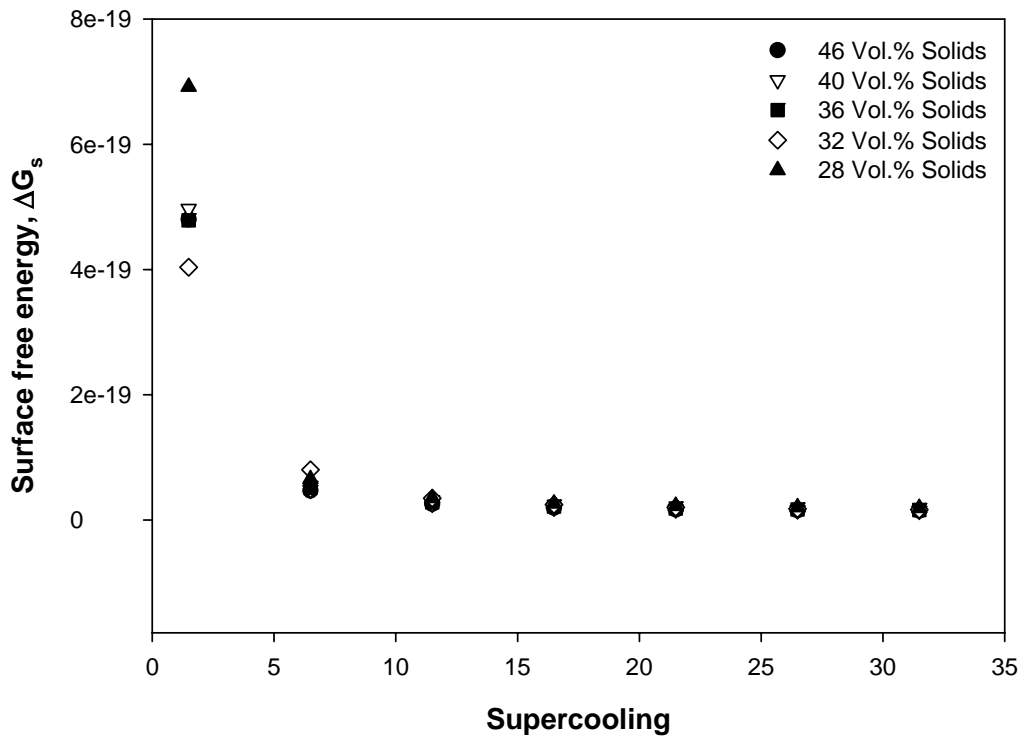


Fig. D.12: Surface free energy for polished copper surface

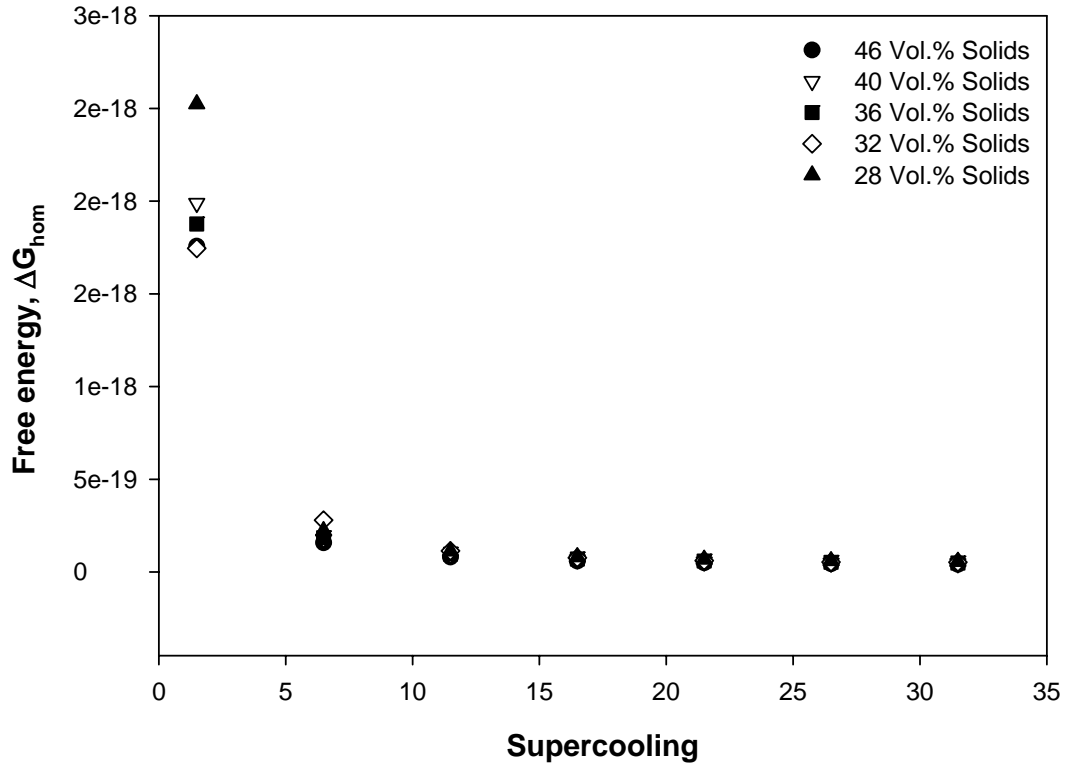


Fig. D.13: Gibbs free energy for homogeneous nucleation on polished steel surface

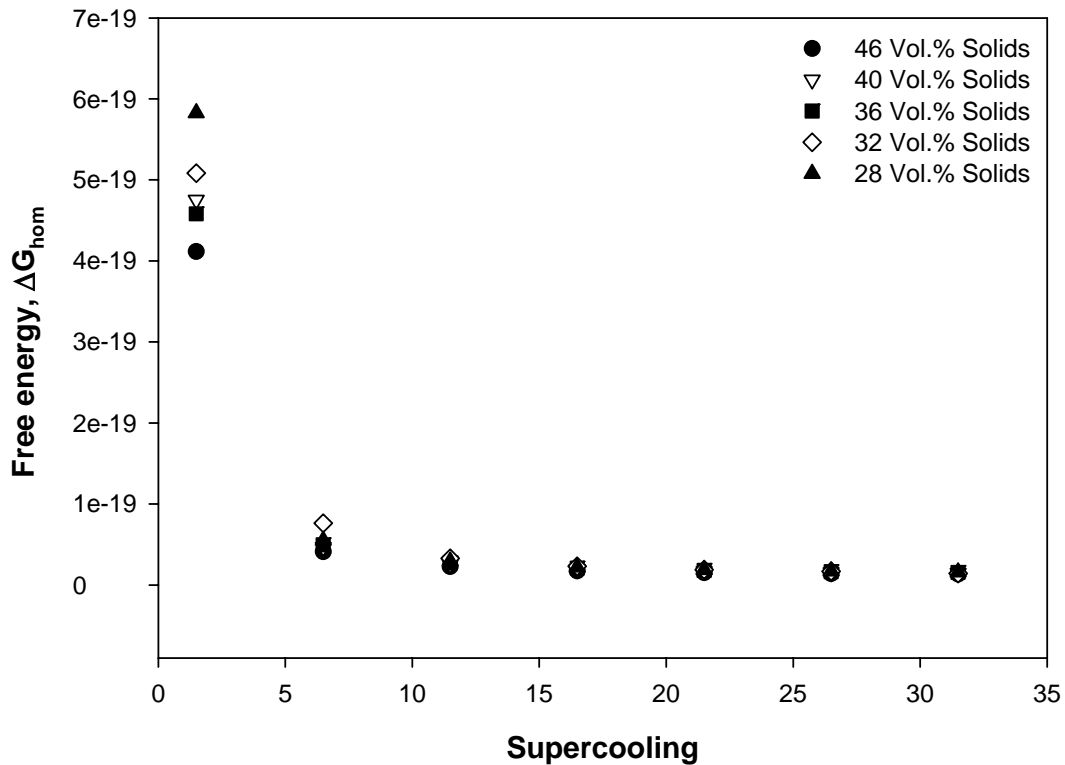


Fig. D.14: Gibbs free energy for homogeneous nucleation on rough copper surface

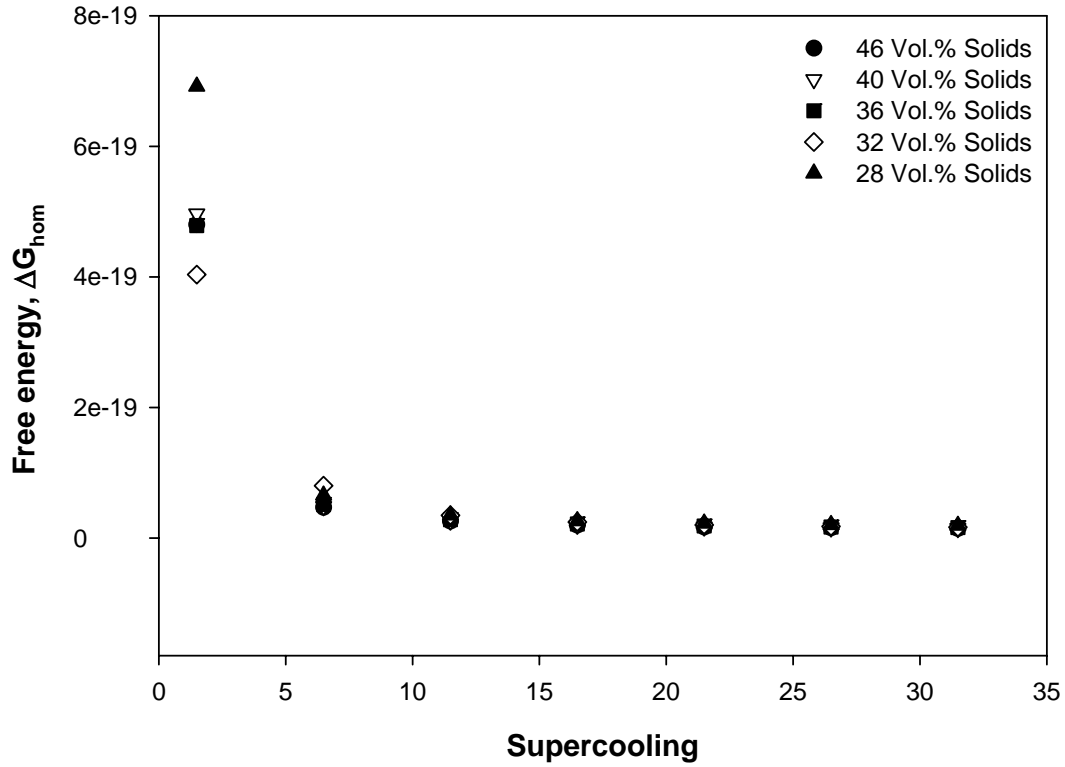


Fig. D.15: Gibbs free energy for homogeneous nucleation on polished copper surface

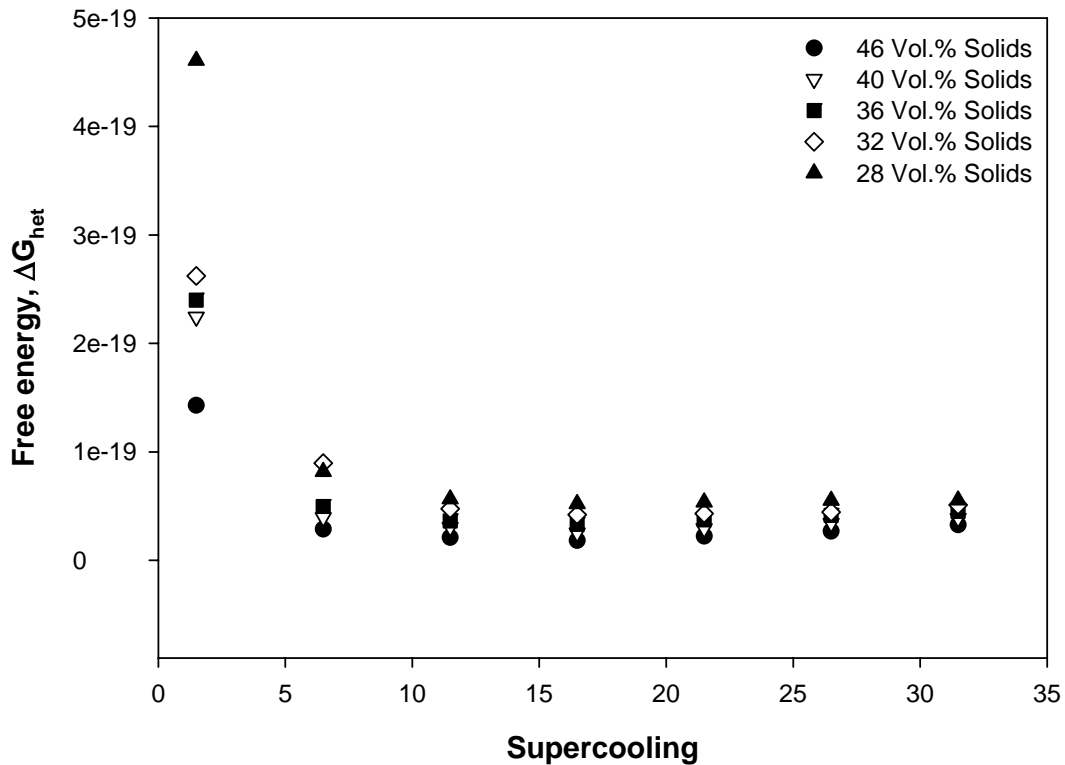


Fig. D.16: Gibbs free energy for heterogeneous nucleation on polished steel surface

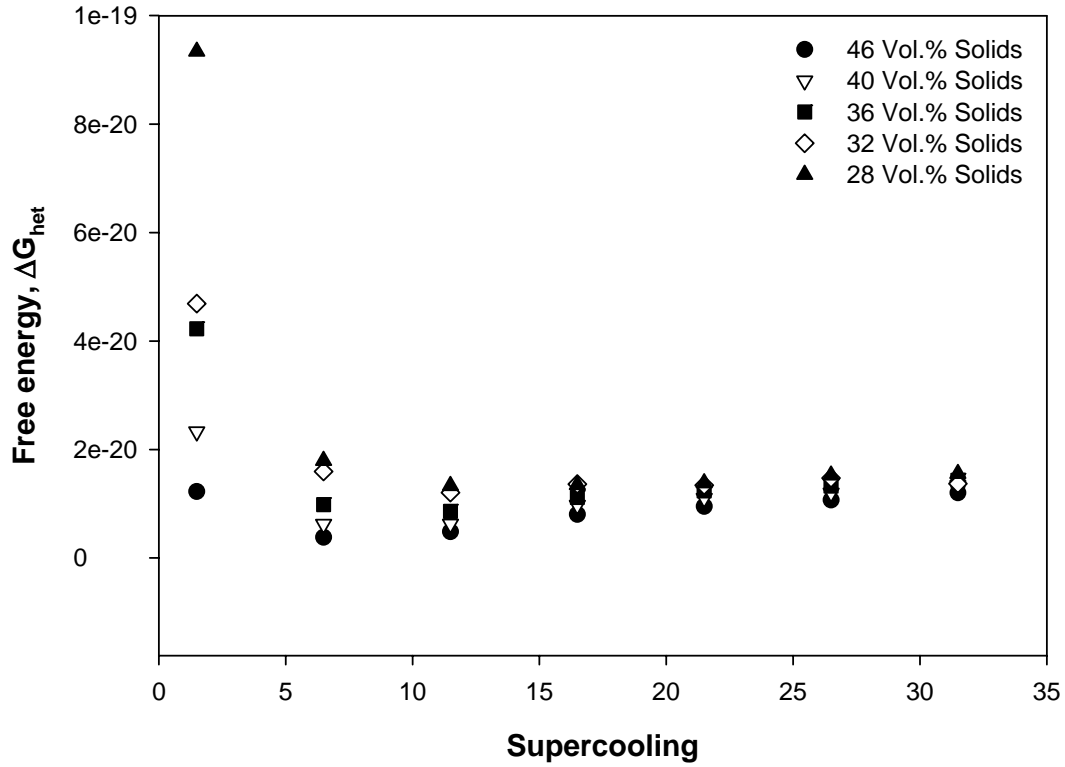


Fig. D.17: Gibbs free energy for heterogeneous nucleation on rough copper surface

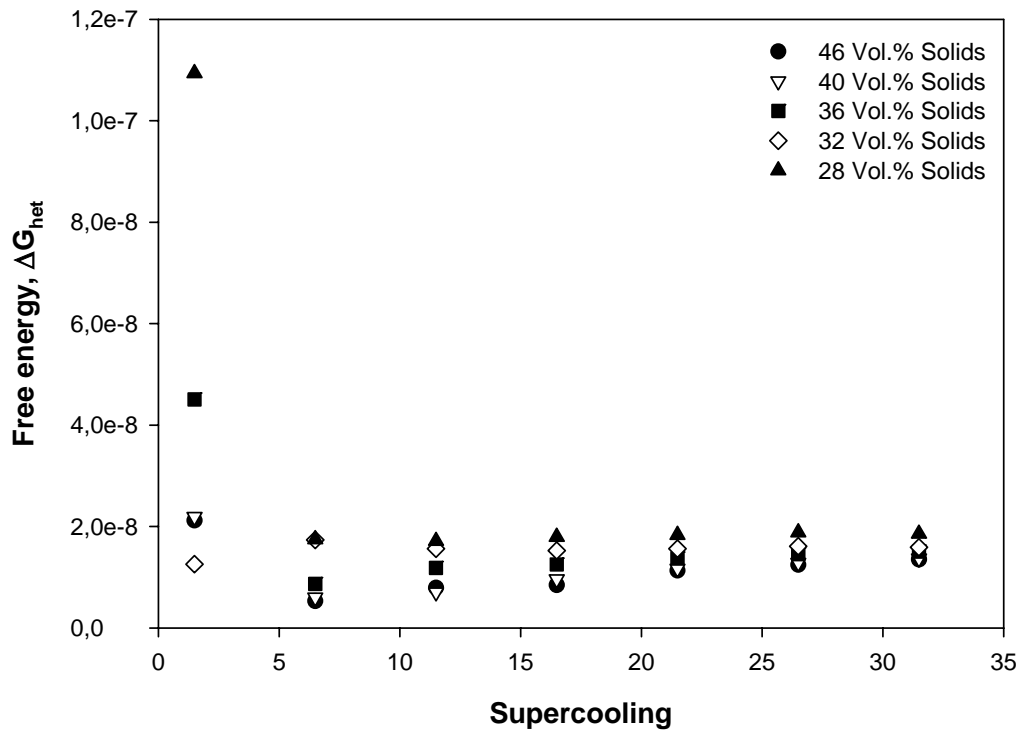


Fig. D.18: Gibbs free energy for heterogeneous nucleation on polished copper surface

Appendix E

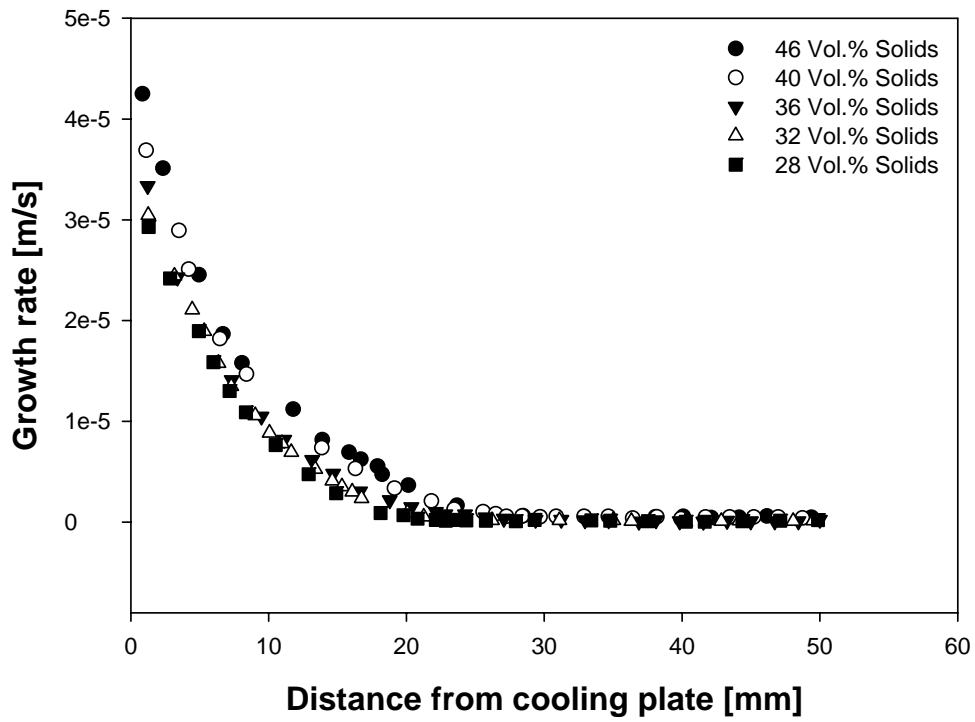


Fig. E.1: Crystal growth rate for suspensions with different solid loads content frozen at -10°C

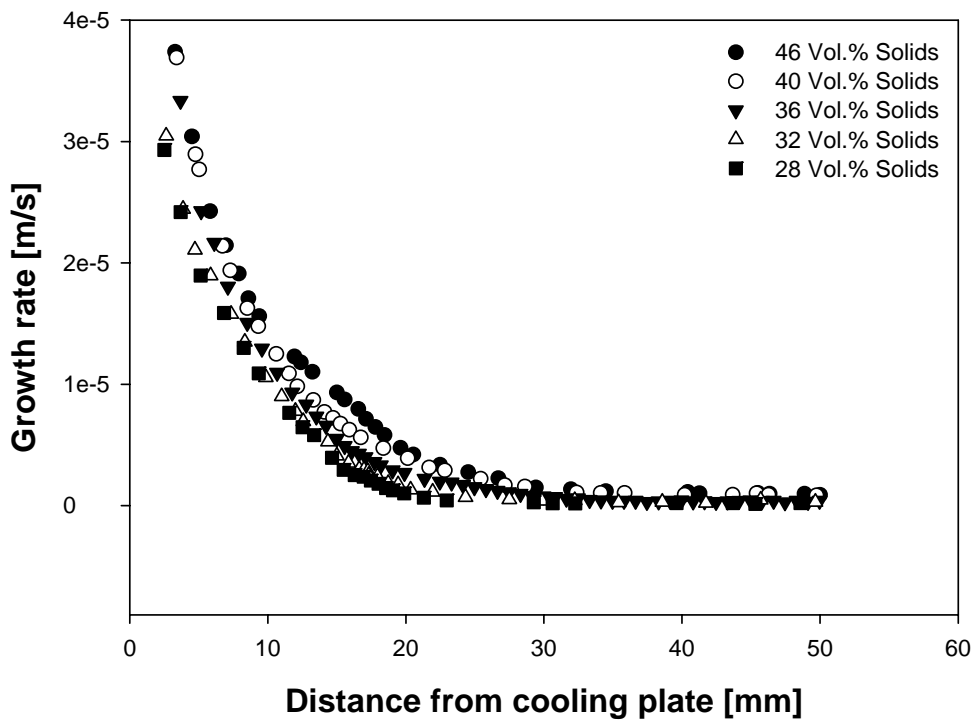


Fig. E.2: Crystal growth rate for suspensions with different solid loads content frozen at -15°C

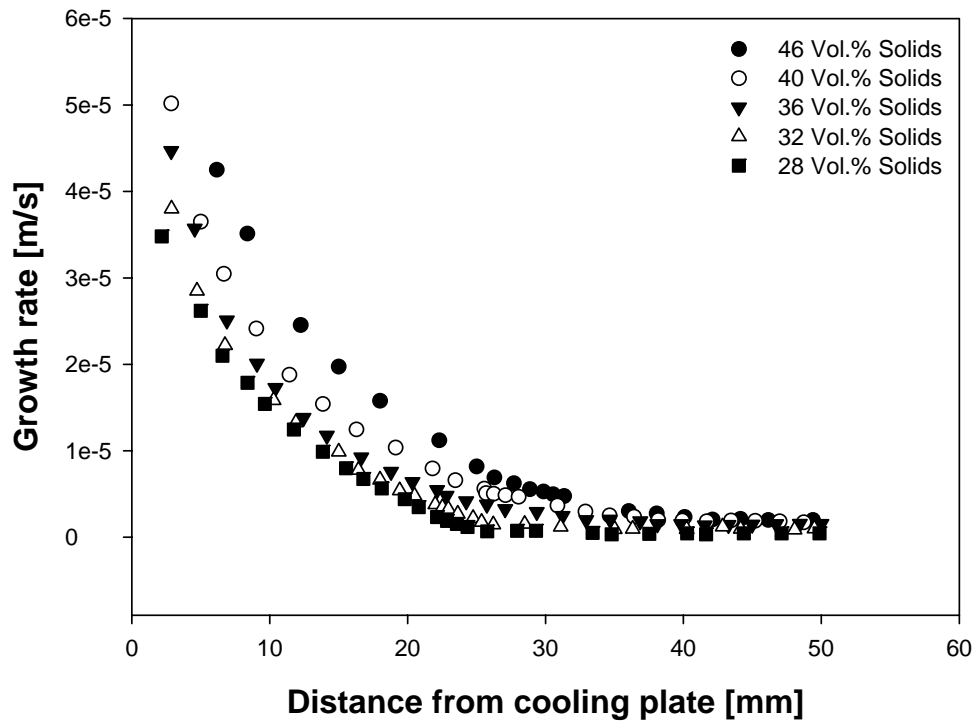


Fig. E.3: Crystal growth rate for suspensions with different solid loads content frozen at -20°C

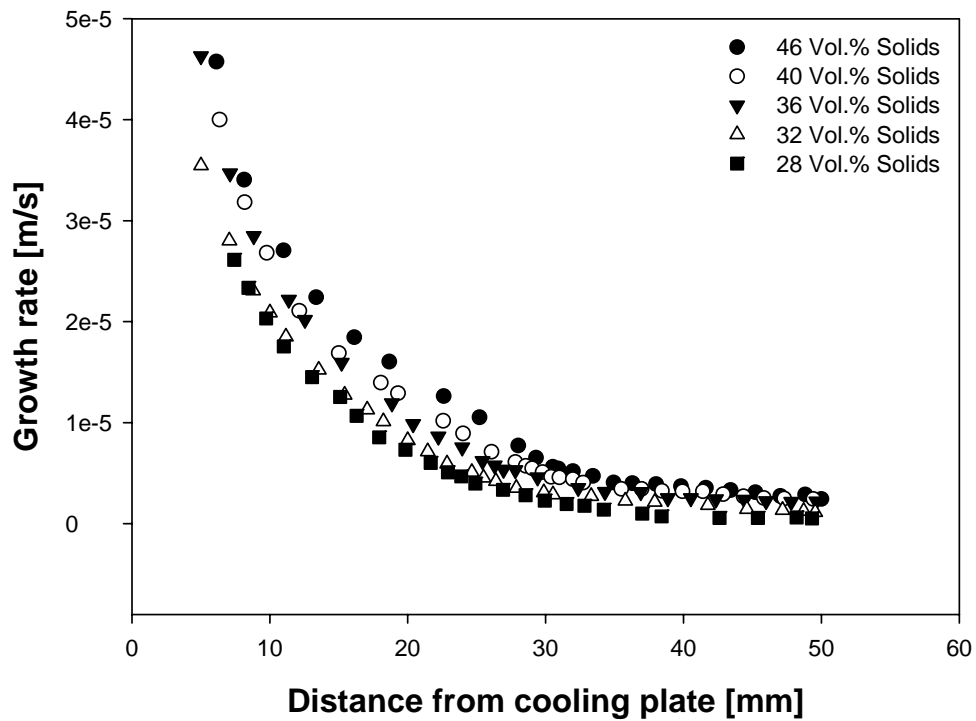


Fig. E.4: Crystal growth rate for suspensions with different solid loads content frozen at -25°C

Appendix F

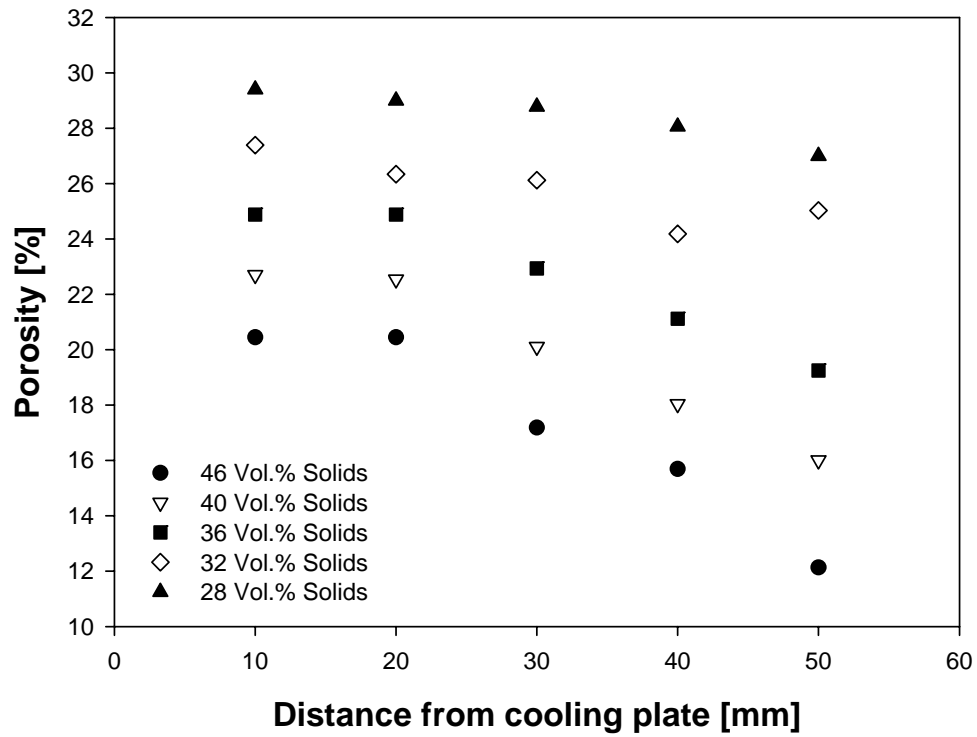


Fig. F.1: Porosity for suspensions with different solid loads frozen at -15°C

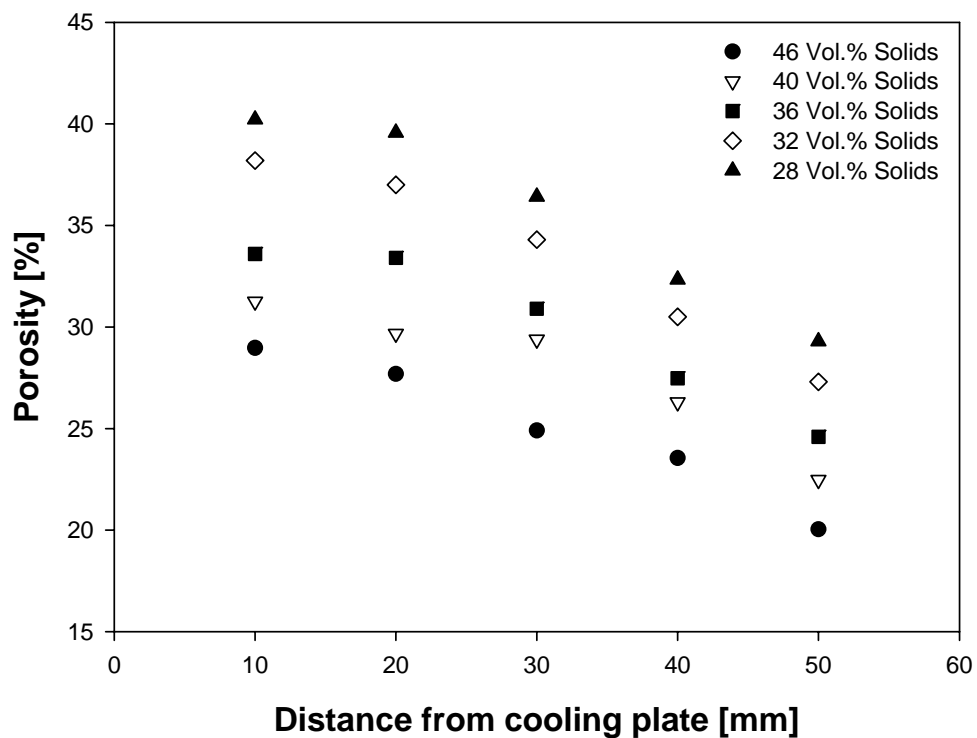


Fig. F.2: Porosity for suspensions with different solid loads frozen at -20°C

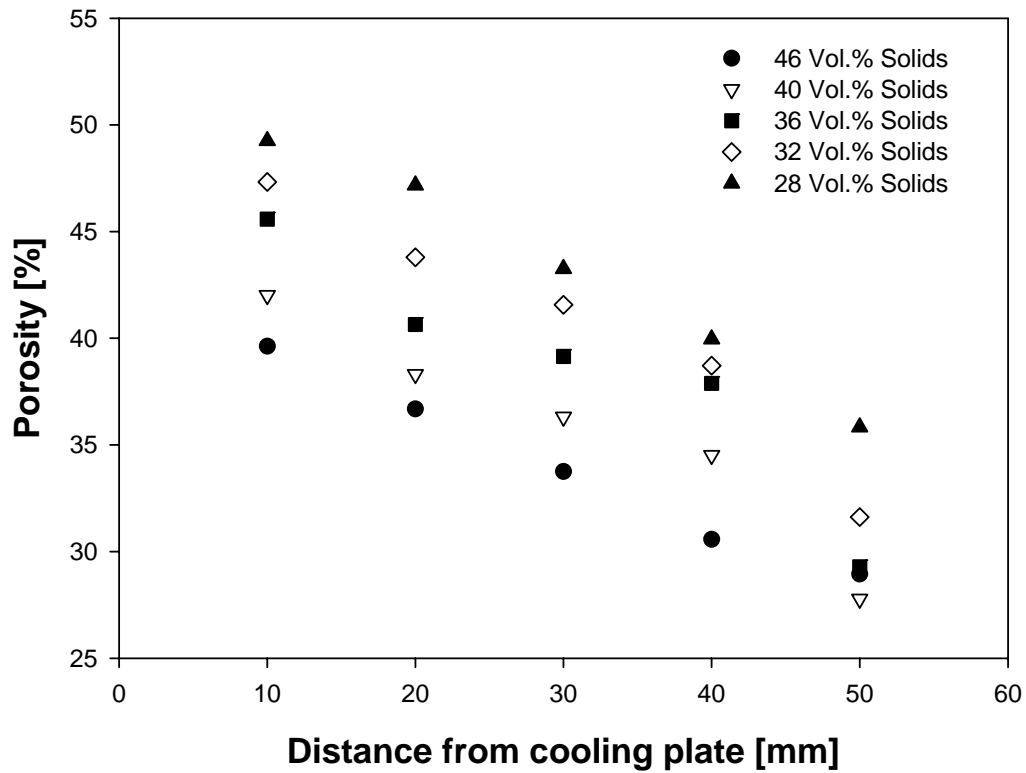


Fig. F.3: Porosity for suspensions with different solid loads frozen at -30°C

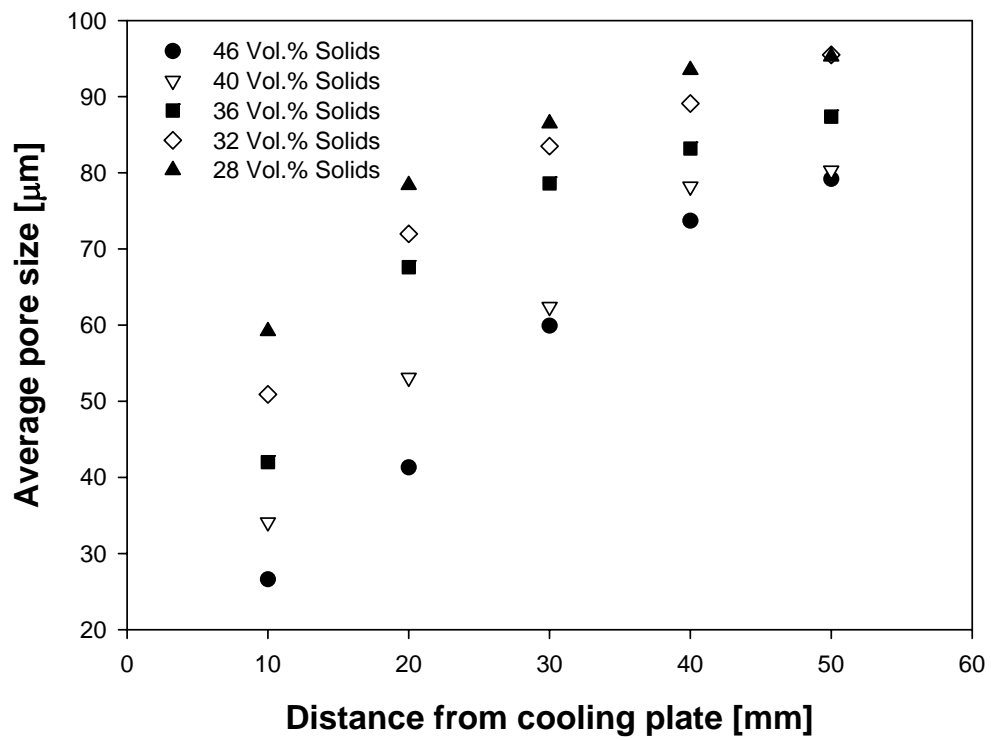


Fig. F.4: Macropores size distribution for various suspensions frozen at -15°C

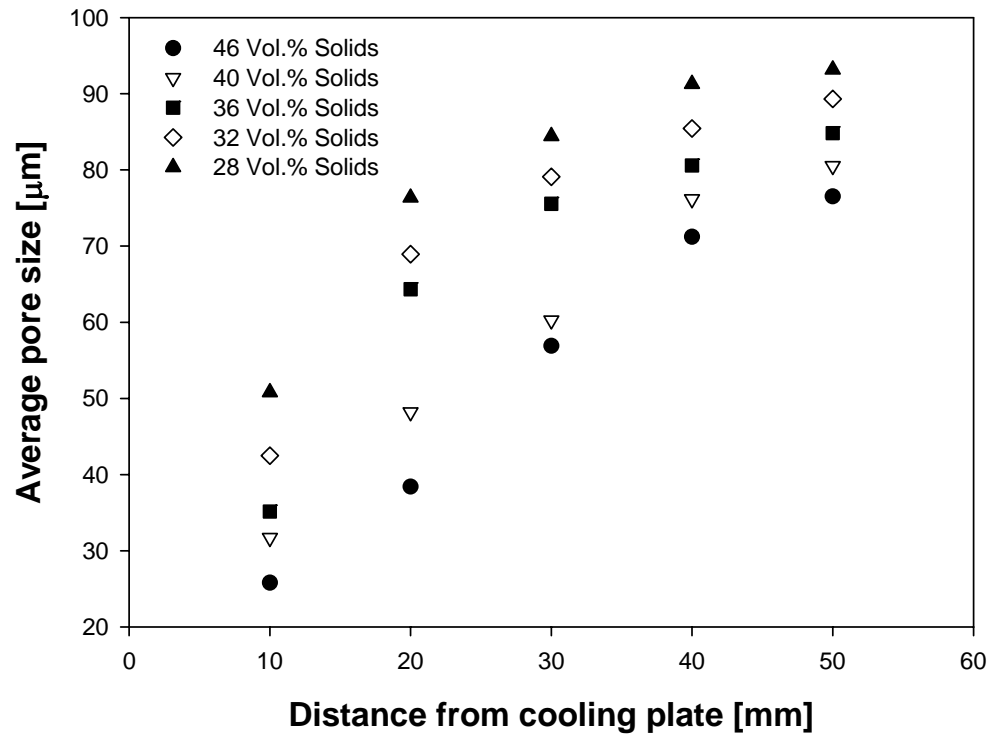


Fig. F.5: Macropores size distribution for various suspensions frozen at -20°C

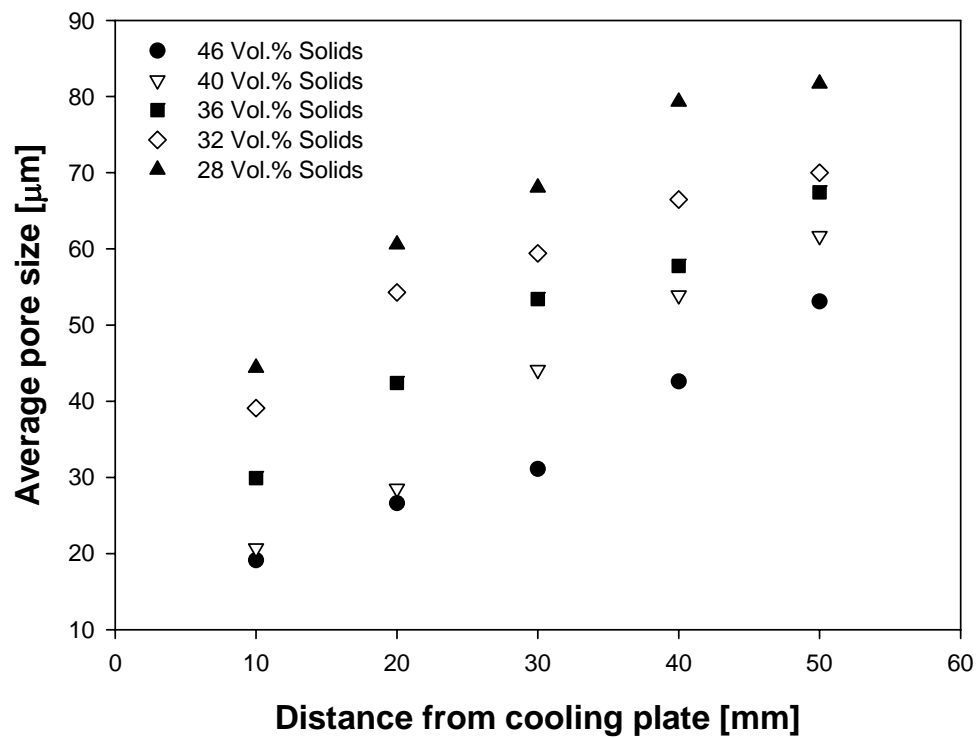


Fig. F.6: Macropores size distribution for various suspensions frozen at -30°C

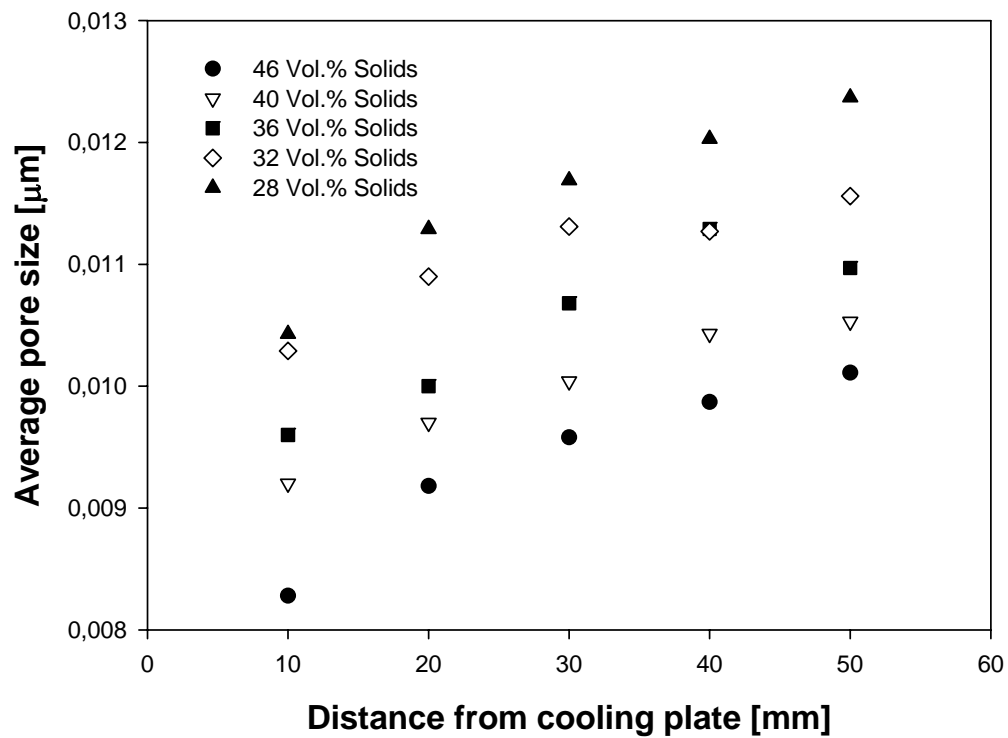


Fig. F.7: Mesopores size distribution for various suspensions frozen at -15°C

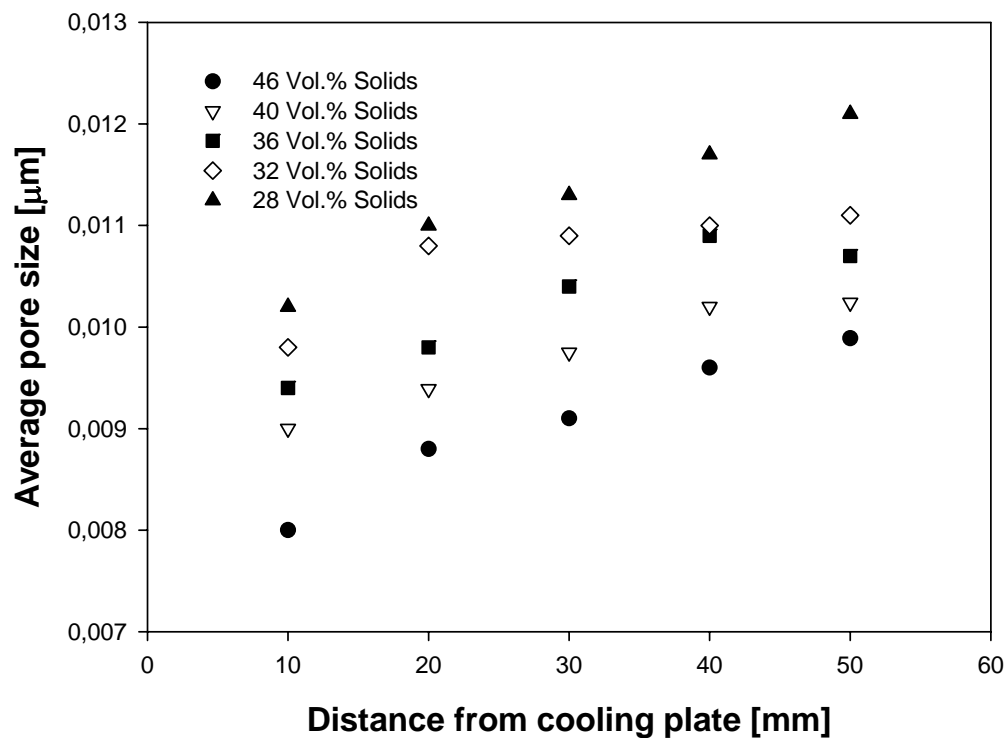


Fig. F.8: Mesopores size distribution for various suspensions frozen at -20°C

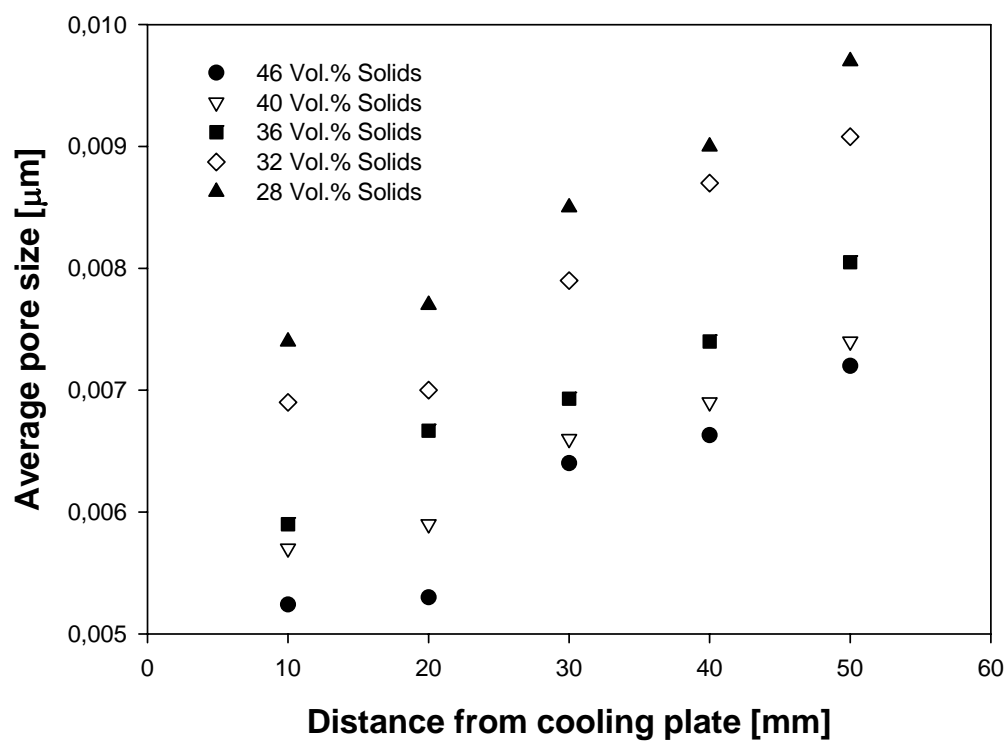


Fig. F.8: Mesopores size distribution for various suspensions frozen at -30°C

11 References

- [Ada97] A. W. Adamson,
Physical Chemistry of Surfaces, John Wiley & Sons
New York (1997).
- [And03] L. Andresen, D. Donchev, D. Koch, M. Kühn, G. Grathwohl,
J. Ulrich
4th European Congress of Chemical Engineering, Book 7, (2003),
Granada, Spain
- [Ara04] K. Araki, J.W. Halloran
J. Am. Ceram. Soc., 87 [10] (2004) 1859–1863
- [Bal98] A. R. Balkenende, H. J. A. P. van de Boogaard, M. Scholten, N. P.
Willard
Langmuir 14 (1998) 5907-5912
- [Bar03] M. W. Barsoum
Fundamentals of ceramics
MPG Books Ltd, Bodmin, Cornwall, IOP Publishing Ltd 2003
- [Bec35] R. Becker, W. Döring,
Kinetische Behandlung der Keimbildung in übersättigen Dämpfen
Annalen der Physik 24 (1935) 719-752
- [Bro02] L. Bronfenbrener, E. Korin
Chem. Engineering and Processing, 41 (2002) 357-363
- [Bru44] S. Brunauer
The Adsorption of gases and vapour
Oxford Univ. Press, London 1944
- [Bur51] W.K. Burton, N. Cabrera, F.C. Frank
Phil. Trans. Roy. Soc. A243, (1951) 299
- [Cha91] J.C. Chang, B.V. Velamakanni, Lange, Fred F.; Pearson, Dale S
J. Am. Cer. Soc. 74(9) (1991) 2201-2204.
- [Cro65] M. M. Cross
J. Colloid Interface Sci., 20 (1965) 417–437
- [Don02] D. Donchev, J. Ulrich
The controlled growth of ice crystals in ceramic slurries
Proceedings of 15th International Symposium on Industrial

-
- Crystallization, Sorrento, ed. A. Chianese, Chemical Engineering Transactions, AIDIC, Milano, 2002, 1071 – 1076
- [Don03] D. Donchev, L. Andresen, M. Kühn, D. Koch, G. Grathwohl, J. Ulrich
Proceeding, 4th European Congress of Chemical Engineering, Book 7, (2003), Granada, Spain
- [Don04] D. Donchev, J. Ulrich, L. Andresen, D. Koch, G. Grathwohl
Chem. Ing. Tech., 76 [11] (2004) 1688 – 1690
- [Don04a] Donchev D., J. Ulrich
11th International Workshop on Industrial Crystallization, ed. by Kwang-Joo Kim, Daeonsa, Daejeon, Korea (ROK), 2004, 350-358, ISBN 89-89637-23-6
- [Fel86] R.M. Felder, R.W. Rousseau
Elementary Principles of Chemical Process, 2nd ed., John Wiley & Sons. Inc. New York, 1986
- [Fle58] N. H. Fletcher,
J. Chem. Phys., 29, (1958) 572-576.
- [Fle62] N. H. Fletcher,
The Introduction of Rain clouds, Cambridge University Press, Cambridge (1962).
- [Fle69] N. H. Fletcher,
J. Atmos. Sci., 26, (1969) 1266-1271
- [For03] T.J. Fortin, K. Darla, L.T. Iraci, M.A. Tolbert,
Atmos. Chem. Phys. Discuss., 3 (2003) 867-894
- [Fuk01] T. Fukasawa, M. Ando, T. Ohji, S. Kanzaki,
J. Am. Ceram. Soc., 84 [1] (2001) 230-232
- [Fuk01a] T. Fukasawa, Z.-Y. Deng, M. Ando, T. Ohji, Y. Goto
J. Mat. Sci., 36 (2001) 2523-2527
- [Gar55] W.E. Garner,
Chemistry of solid state, Butterworths Scientific Publications, 1955
- [Gar90] J. Garside, A. Mersmann, J. Nyvlt
Measurement of crystal growth rates
European Federation of Chemical Engineering Working Party on Crystallization, 1990

- [Gib48] J.W. Gibbs,
Collected works. Band 1. Thermodynamics
Yale University Press, New Haven 1948
- [Gor01] B.Z. Gorbunov, A. Baklanov, N. Kakutkina, H.L. Windsor, R. Toumi
J. Aerosol Sci., 32 (2001) 199-215
- [Gor82] B. Z. Gorbunov and N.A. Kakutkina,
J. Aerosol Sci., 13, (1982) 21-28
- [Haa02] T. Haasner
Ph. D. Thesis, Beeinflussung der Keimbildung in der
Schichtkristallisation durch gezielte Oberflächenmodification
VDI Verlag GmbH Düsseldorf, ISBN 3-18-375903-0
- [Jon00] R. W. Jones,
Ind Ceram., 20 [2] (2000) 117–121
- [Jon02] A.G. Jones,
Crystallization Process Systems,
Butterworth-Heinemann, Oxford, 2002
- [Kha69] E. V., Khamskii
Crystallization from Solutions,
Consultants Bureau, Plenum Publishing Corp., New York. 1969
- [Kim01] K.-J. Kim, J. Ulrich
Powder Technology 121 (2001) 81-87
- [Koc03] D. Koch, L. Andresen, T. Schmedders, G. Grathwohl,
J. Sol–Gel Sci. Technol., 26 (2003) 149–152.
- [Kri59] I. M. Krieger, T. J. Dougherty
Trans. Soc. Rheol., 3 (1959) 137–152
- [Lan89] F. F. Lange (Da nameria statiatia I da dopalnia imenata)
J. Am. Ceram. Soc., 72 [1] (1989).3–15
- [Lau92] J. Laurie, C.M. Bagnall, B. Harris, R.W. Jones, R.G. Cooke, R.S.
Russell-Floyd, T.H. Wang, and F.W. Hammett,
J. Non-Crystalline Solids 147/148, (1992) 320–325
- [Lee98] T.D. Lee,
Ph.D. Thesis, Harvard University Cambridge, Massachusetts,
The Division of Engineering and Applied Sciences, 1998
- [Lew00] J.A. Lewis

-
- J. Am. Ceram. Soc., 83 [10] (2000), 2341-2359
- [Liu96] D.M. Liu
Porous Ceramic Materials: Fabrication, Characterization,
Applications, Aedermannsdorf, Trans. Tech Publ., 1996
- [Liu97] D.M. Liu, V. Dixit
Porous materials for tissue engineering
Uetikon- Zürich, Trans Tech Publications, 1997
- [Lop03] T.M. Lopez, D. Avnir and M. Aegerter
Emerging fields in sol-gel science and technology
IV International Materials research Congress (11th: 2002: Cancun,
Mexico)
Kluwer Academic Publishers, Norwell, Massachusetts, 2003
- [Low84] S. Lowell, J.E. Shields
Powder Surface Area and Porosity, 2nd ed.
Chapman and Hall, London, 1984
- [Mah78] W. Mahler
U.S. Pat. 4,122,041
- [Mah80] W. Mahler, M.F. Bechtold
Nature (London), 285 (1980) 27-28
- [Meg02] W van Megen,
J. Phys.:Condens. Matter, 14 (2002) 7699-7717
- [Mer01] A. Mersmann, C. Heyer, A. Eble,
Activated nucleation In: Crystallization Technology Handbook 2nd
ed., Marcel Decker, Inc., New York, 2001
- [Mer90] A. Mersmann
J. Crystal Growth, 102 (1990) 841-847
- [Mor99] S. Morissette and J. A. Lewis,
J. Am. Ceram. Soc., 82 [3] (1999).521–528
- [Mul01] J. W. Mullin,
Crystallization
4th Ed., Butterworth-Heinemann, Oxford, 2001
- [Mye01] A. S. Myerson
The Handbook of Industrial Crystallization, 2nd Ed., Butterworth-
Heinemann, Stoneham, 2001

-
- [Na03] B. Na, R.L. Webb
Int. J. Heat Mass Transfer, 46 (2003) 3797–3808
- [Net97] I. Nettleship, R. Sampathkumar
J. of Porous Mat. 4 (1997) 157–163
- [Neu95] M. Neumann
Vergleich statischer und dynamischer Schichtkristallisation und das Reinigungspotential der Diffusionswäsche, Ph. D Thesis, Universität Bremen, ISBN 3-931986-13-6, Papierflieger, Clausthal-Zellerfeld, 1996
- [Nov92] B. E. Novich, C. A. Sundback, R. W. Adams,
in Ceramic Transactions, Vol. 26, Forming Science and Technology for Ceramics. American Ceramic Society, Westerville, OH, 1992, pp. 157–64
- [Nýv85] J. Nývlt, O. Sohnel, M. Matuchova, M. Broul:
The kinetics of industrial crystallization
Elsevier, Amsterdam, 1985
- [Nýv77] J. Nývlt
Solid-Liquid Phase Equilibria, Publishing House of the Czechoslovak Academy of Science, Praha 1977
- [Oha73] M. Ohara, R. C. Reid:
Modeling crystal growth rates from solution
Prentice-Hall, Englewood Cliffs, 1973
- [Oma91] O. O. Omatete, M. A. Janney, and R. A. Strehlow,
Am. Ceram. Soc. Bull., 70 [10] (1991) 1641–1649
- [Ozk04] A. Ozkan
J. Colloid Interface Sci., 277 (2004) 437–442
- [Pad01] K. Padilla, V. Talanquer,
J. Chem. Phys., 114 (2001) 1319-1325
- [Per99] R.H. Perry, D.W. Green
Perry's Chemical Engineers' Handbook
The McGraw-Hill Companies Inc., 1999
- [Por02] Porotec
Mercury Intrusion Porosimetry Handbook. Pascal Series 140+440, 2002

-
- [Pus04] G. Pusch
In Ullmann's Encyclopedia of Industrial Chemistry
John Wiley & Sons, Inc.
- [Ram99] R. Ramachandra Rao, H.N. Roopa, T.S. Kannan
J. Eur. Cer Soc., 19 (1999) 2763-2771
- [Rav97] A. Ravaglioli, A. Krajewski
Implantable Porous Bioceramics in Porous Materials for Tissue
Engineering ed. D.M. Liu and V. Dixit
Trans Tech Publications, Switzerland, 1997
- [Ree88] J. S. Reed
Introduction to the Principles of Ceramic Processing
Wiley, New York, 1988.
- [Ric98] R.W. Rice
Porosity of ceramics
Marcel Dekker Inc., 1998
- [Rig01] Sean P. Rigby, R.S. Fletcher, S. N. Riley
J. of Colloid and Interface Sci. 240 (2001) 190–210
- [Ros78] R.G. Ross, P. Andersson, G. Backstrom
J. Chem. Phys., 68 (1978) 3967-3971
- [San00] A.J. Sanchez-Herencia, L. James, F.F. Lange
J. Eur. Cer. Soc. 20(9), (2000) 1297-1300
- [Sant00] W.N. Dos Santos
J. Mater. Sci., 35 (2000) 3977-3982
- [Seg89] D. Segal
Chemical synthesis of advanced ceramic materials
Cambridge University Press, 1989
- [Sha60] E.G. Shafrin, W.A. Zisman
J. Phys. Chem., 64 (1960) 519-524
- [Shö92] O. Shönel, J. Garside
Precipitation
Oxford: Butterworth-Heinemann, 1992
- [Sig00] W.M. Sigmund, N.S. Bell, L. Bergström
J. Am. Ceram. Soc., 83 [7] (200) 1557–1574
- [Smi] R. Smith-Johannsen

- U.S. Pat. 3,177,161
- [Smo87] V. E. Smorodin,
Sov. Phys. Dokl., 32, (1987) 405-407
- [Sof01] S. W. Sofie, F. Dogan
J. Am. Ceram. Soc., 84 [7] (2001) 1459–1464
- [Som00] K. Sommer
Size Enlargement
Ullmann's Encyclopedia of Industrial Chemistry, 2004
- [Sta98] M.J. Statham, F. Hammett, B. Harris, R.G. Cooke, R.M. Jordan, A.
Roche
J. Sol-Gel Sci. Tech. 13 (1998) 171–175
- [Str68] R. F. Strickland-Constable:
Kinetic and mechanisms of crystallization
Academic Press, London, 1968
- [Ter95] R.A. Terpstra, P.P.A.C. Pex, A.H. de Vries
Ceramic Processing,
Chapman & Hall, London, 1995, 196-197.
- [Ulr89] J. Ulrich
Crystal Res. Techn. 24 (1989) 3, 249 – 257
- [Vol39] M. Volmer,
Kinetik der Phasenbildung
Steinkopff, Leipzig 1939
- [YLee98] Y.L. Lee, W.S. Chou, L.H. Chen,
Surface Sci., 414 (1998) 363-373
- [You91] A. C. Young, O. O. Omatete, M. A. Janney, P. A. Menchhofer,
J. Am. Ceram. Soc., 74 [3] (1991) 612–618
- [Youn55] T. Young
Miscellaneous Works; ed. G. Peacock, Murray, London, 1855, 1-
55
- [Was22] E.W. Washburn, E.W. Bunting
J. Am. Ceram. Soc., 4 (1922) 983-989
- [Wea89] R.C. Weast ed.
Handbook of Chemistry and Physics
Boca Raton, FL: CRC Press, 1989

- [Wu71] S. Wu
J. Polym. Sci., C34 (1971) 19
- [Wu82] S.Wu
Polymer Interface and Adhesion
Marcel Dekker, New York, 1982
- [Wu99] W. Wu, G.H. Nancollas
Ad. Colloid Interface Sci., 79 (1999) 229-279
- [Zhu02] X. Zhu, D. Jiang, Sh. Tan
Mater. Res. Bulletin, 37 (2002) 541-553
- [Zis64] W.A. Zisman
ACS Adv. Chem. Ser., 43 (1964) 1-51

Erklärung

Ich erkläre, daß ich die vorliegende Dissertation selbständig und nur unter Verwendung der angegebenen Literatur und Hilfsmittel angefertigt habe. Diese Dissertation wurde bisher an keiner Universität oder Hochschule vorgelegt. Frühere Bewerbungen um den akademischen Grad eines Dr.-Ing. wurden von mir nicht vorgenommen.

Halle (Saale), den 25.04.2005

Danail Domchev

Curriculum Vitae

Personal data

Family name: Donchev
First name: Danail
Day of birth: 24. May 1974
Place of birth: Kazanlak, Bulgaria
Nationality: Bulgarian

Education

Sep. 1986 – July 1989: “Kiril i Metodii” middle school, Kazanlak, Bulgaria: Middle school

Sep. 1989 – July 1992: “Balgarska Roza” (Pharmaceutical materials and technology), high school, Kazanlak, Bulgaria: High school

Sep. 1992 – July 1997: “Asen Zlatarov” Bourgas Technical University, chemical engineering department, Bourgas, Bulgaria : Bachelor

Sep. 1997 – Nov.1999: “Asen Zlatarov” Bourgas Technical University, chemical engineering department, Bourgas, Bulgaria: Master of Science: Hydrodynamic in Fluidize-bed reactors (Otto von Guericke University, Magdeburg, Germany), (thesis)

Jan. 2001 – May 2005: Martin-Luther-Universität Halle-Wittenberg, Fachbereich Ingenieurwissenschaften, Institut für Verfahrenstechnik: (Thermal proceses)

Ph.D. study: Controlling Porosity and pore size distribution in green ceramic bodies via Freeze-casting